STRUCTURAL MECHANISMS OF SEMAPHORIN/PLEXIN SIGNALING

APPROVED BY SUPERVISORY COMMITTEE

Xuewu Zhang, Ph. D.

Luke Rice, Ph.D.

Michael Rosen, Ph.D.

Hongtao Yu, Ph.D.

DEDICATION

I would like to thank my mentor Xuewu, the members of my Graduate Committee and the Molecular Biophysics Graduate Program. I would also like to thank my parents, my wife Zhenyi and my daughter Angelina.

STRUCTURAL MECHANISMS OF SEMAPHORIN/PLEXIN SIGNALING

by

YUXIAO WANG

DISSERTATION

Presented to the Faculty of the Graduate School of Biomedical Sciences

The University of Texas Southwestern Medical Center at Dallas

In Partial Fulfillment of the Requirements

For the Degree of

DOCTOR OF PHILOSOPHY

The University of Texas Southwestern Medical Center at Dallas

Dallas, Texas

August, 2014

STRUCTURAL MECHANISMS OF SEMAPHORIN/PLEXIN SIGNALING

Publication No. _____

YUXIAO WANG, Ph.D.

The University of Texas Southwestern Medical Center at Dallas, 2014

XUEWU ZHANG, Ph.D.

Plexins are cell surface receptors that bind to their ligand semaphorins and transduce signals for regulating processes including neuronal development, angiogenesis and immune response. Deregulations of the plexin pathway are associated with cancers and neurodegenerative diseases. Signaling through plexins has been proposed to rely on their GTPase activating protein (GAP) activity for R-Ras and M-Ras. Activation of this GAP activity requires binding of semaphorin to the plexin extracellular region. However, the GAP activity of plexins eluded detection in several studies, and the mechanisms by which semaphorins activate plexins remained elusive. I discovered that plexins function as GAPs specific for Rap GTPases but not for R-Ras or M-Ras. The RapGAP activity of plexins is stimulated by binding of semaphorins, and is essential for the physiological functions of plexins. I further showed that induced-dimerization of plexin cytoplasmic region leads to activation of the GAP domain. The crystal structure of the active dimer of PlexinC1 was determined, revealing the structural basis for the dimerization-induced

allosteric activation of plexins. I also solved a structure of PlexinA4 cytoplasmic region, which suggested the existence of a pre-formed inhibitory dimer. Biochemical and cellular assay showed that although PlexinA4 indeed homodimerizes on cell surface, the pre-formed dimer I crystallized is likely to be physiologically irrelevant. To summarize, these findings define an essential pathway for semaphorin-plexin signaling, and reveal the structural mechanisms for the activation of plexins by semaphorins. We also show that plexins in cells exist as pre-formed dimers, the formation of which likely maintains the autoinhibited state of plexins.

TABLE OF CONTENTS

CHAPTER ONE Overview of semaphorin/plexin signaling 1

Semaphorins and plexins 1

Physiological functions of semaphorin and plexin 3

Intracellular signaling of plexins 5

Domain organization of plexin cytoplasmic region 6

The GAP domain of plexins and its substrates 8

Plexins recruits GEFs to activate RhoGTPases 9

The RBD of Plexins binds to RhoGTPases 11

Different plexin family members also activate specific pathways 12

Activation mechanisms of plexin 14

Mechanisms for the autoinhibition of plexin 14

Mechanisms for semaphorin induced activation of plexin 16

The role of RhoGTPases in plexin activation 18

Summary and key questions 18

CHAPTER TWO Plexins are GAPs for Rap and are activated by induced dimerization 22

Plexin cytoplasmic regions exhibit GAP activity to Rap but not R-Ras or M-Ras. 22

Dimerization stimulates the RapGAP activity of plexins$_{cyto}$. 23

Plexins use a non-canonical mechanism for catalyzing Rap GTP hydrolysis 26

Rac1 does not stimulate the RapGAP activity of plexins$_{cyto}$ in solution 28

RapGAP activity of full-length plexins in cells is stimulated by semaphorin 29

Rap inactivation is essential in plexin-mediated neuronal growth cone collapse 30

Discussions and future directions 31

Materials and methods 36

Protein expression and purification 36

In solution GAP activity assays 37

RalGDS pull-down assay for the RapGAP activity of FKBP-PlexinC1$_{cyto}$ in cells . 38

FRET-based RapGAP activity assays in cells 40

Neuron growth cone collapse assay 42

CHAPTER THREE Crystal structure of the active dimer of plexin 55

Screening of the coiled-coil-plexin$_{cyto}$ fusion constructs for optimal induction of the active dimer 55

Overall structure of the PlexinC1$_{cyto}$ active dimer 56

Interactions in the dimer interface 57

Dimerization induced conformational changes that lead to GAP activation. 58

Conformation of the RBD and GAP distal subdomain 61

Mutational analysis of the active dimer structure 62

Discussions and future directions 63

Materials and Methods 66
Protein Expression 66
In vitro GAP assays 66
Crystallization, structure determination and analyses 67
COS7 cell collapse assay 69

CHAPTER FOUR Crystal structure of a pre-formed inhibitory dimer of plexin . 86

Crystal structure of PlexinA4$_{cyto}$ reveals a pre-formed dimer mediated by a new conformation of the juxtamembrane helix 86
Crystal structure of GCN4 coiled-coil fused PlexinA4$_{cyto}$ shows the same inhibitory dimer 89
Examine the formation of the inhibitory dimer in solution 91
Use disulfide cross-linking to trap the inhibitory dimer 93
Use structural scaffolding to promote inhibitory dimer formation 94
Examine inhibitory dimer formation on lipid vesicles 96
Determine the functional significance of the inhibitory dimer structure 97
Determining the oligomerization state of plexin on cell surface 99
Discussions and future directions 100
Materials and methods 104
Protein expression and purification 104

Crystallization and structural determination of PlexinA4$_{cyto}$ and GCN4 coiled-coil fused PlexinA4$_{cyto}$ 105

Native PAGE of PlexinA4$_{cyto}$ 108

Analytical ultracentrifugation 108

Disulfide crosslinking assay 109

Lipid vesicle assay 109

COS7 cell collapse assay 110

Bibliography 131

PRIOR PUBLICATIONS

Y. Wang*, H. G. Pascoe*, C. A. Brautigam, H. He, X. Zhang, Structure basis for activation and non-canonical catalysis of the Rap GTPase activating protein domain of plexin. ***eLife*** (2013) **2**:e01279 (*co-first author)

Y. Wang*, H. He*, N. Srivastava, S. Vikarunnessa, Y.-b. Chen, J. Jiang, C. W. Cowan, X. Zhang. Plexins are GTPase-activating proteins for Rap and are activated by induced dimerization. ***Science Signaling*** (2012) **5**, ra6 (*co-first author)

Z. Zheng, Y. Wang, L. Wang, P. Gao, The combined effects of amino acid substitutions and indels on the evolution of structure within protein families. ***PLoS One*** (2010)5:e14316.

XM. Zhang, Y. Wang, L. Wang, G. Chen, W. Liu, P. Gao, Site-directed mutagenesis of manganese peroxidase from *Phanerochaete chrysosporium* in an in vitro expression system. ***Journal of Biotechnology*** (2009) **139**:176-178.

S. Wang, F. Xin, X. Liu, Y. Wang, Z. An, Q. Qi, PG Wang, N-terminal deletion of peptide:N-glycanase results in enhanced deglycosylation activity ***PLoS One*** (2009) **4**:e8335.

LIST OF FIGURES

Figure 1-1. Domain organizations of semaphorins and plexins. 19

Figure 1-2. Structural organization of plexin cytoplasmic region 20

Figure 1-3. Structures of plexin extracellular regions and their complexes with semaphorins. 21

Figure 2-1 Purified plexinscyto display GAP activity for Rap but not for R-Ras or M-Ras. 44

Figure 2-2. HPLC-based assay for the plexin RapGAP activity. 45

Figure 2-3 Effect of dimerization on the GAP activity of $plexins_{cyto}$. 46

Figure 2-4 The RapGAP activity of $plexins_{cyto}$ is stimulated by induced dimerization. 47

Figure 2-5 GST-RalGDS pull-down assays for the RapGAP activity of plexin in cells. 48

Figure 2-6 Mutational analysis of the RapGAP activity of $plexins_{cyto}$. 50

Figure 2-7 Binding of Rac1 does not affect the GAP activity of $plexins_{cyto}$ 51

Figure 2-8 Semaphorin activates the RapGAP activity of full-length PlexinB1 in cells. 52

Figure 2-9 The RapGAP activity of plexin is required for semaphorin induced neuronal growth cone collapse..... 53

Figure 2-10 A schematic model for the regulation of the RapGAP activity of plexin..... 54

Figure 3-1. Activation of the plexin GAP by the coiled-coil fusion..... 70

Figure 3-2. Design of the coiled-coil fusions of mouse PlexinA1$_{cyto}$ and zebrafish PlexinC1$_{cyto}$. 71

Figure 3-3. Structure of the active dimer of zebrafish CC(a)PlexinC1$_{cyto}$..... 72

Figure 3-4. Superimposition of the coiled-coil induced active dimer of PlexinC1$_{cyto}$ and the active dimer in the PlexinC1$_{cyto}$/Rap complex structure. 73

Figure 3-5. Conformational changes of the juxtamembrane helix induced by formation of the active dimer..... 74

Figure 3-6. Comparison of the conformations of helix 11 in the CC(a)PlexinC1$_{cyto}$ active dimer and that in the monomeric PlexinA3 structure..... 75

Figure 3-7. Active dimer formation opens the activation segment..... 76

Figure 3-8. Comparison of the activation segment conformations in monomer structures and in active dimer structures..... 77

Figure 3-9. Simulated annealing omit map of the activation segment in PlexinC1$_{cyto}$. 78

Figure 3-10. Sequence alignments of structural elements involved in the active dimer formation. 79

Figure 3-11. Structural flexibility of regions distal to the GAP active site. 80

Figure 3-12. Mutational analyses of the activation mechanism. 81

Figure 3-13. Schematic model for the activation of the plexin RapGAP by semaphorin-induced dimerization..... 82

Figure 3-14. A model of Rac1 bound plexin active dimer 83

Figure 4-1. Crystal structure of PlexinA4$_{cyto}$ pre-formed dimer 112

Figure 4-2. Interface of the pre-formed dimer of PlexinA4$_{cyto}$ 113

Figure 4-3. Conformational variation of the pre-formed dimer observed in the PlexinA4$_{cyto}$ crystal. 115

Figure 4-4. The GAP active sites are blocked in the inhibitory dimer of PlexinA4$_{cyto.}$ 116

Figure 4-5. A model for semaphorin induced conformational transition of plexin. 117

Figure 4-6. Crystal structure of GCN4 coiled-coil fused PlexinA4$_{cyto.}$ 118

Figure 4-7. Analysis of inhibitory dimer formation in solution..... 119

Figure 4-8. Analytical ultracentrifugation analysis of the oligomerization state of PlexinA4$_{cyto.}$ 120

Figure 4-9. Disulfide crosslinking of the inhibitory dimer 121

Figure 4-10. Use structural scaffold to stabilize the inhibitory dimer. 122

Figure 4-11. Examine inhibitory dimer formation on lipid membrane 123

Figure 4-12. Collapse assay of PlexinA4 wildtype and inhibitory dimer mutants 124

Figure 4-13. FCCS assay of PlexinA4 wildtype and inhibitory dimer mutants .. 126

Figure 4-14. A hypothetical model showing the state of plexin before and after semaphorin binding..... 127

Figure 4-15. Electrostatic interactions that anchors the kinked juxtamembrane helix on to the GAP domain..... 128

LIST OF TABLES

Table 3-1. Data collection and refinement statistics 84

Table 3-2. Protein concentrations and fitting methods used for determining k_{cat}/K_M of plexins 85

Table 4-1. Data collection and refinement statistics 129

Table 4-2. Buffer pH in crystallization condition of $plexins_{cyto}$ and the state of the juxtamembrane helix in the structures. 130

LIST OF DEFINITIONS

BSA	Bovine serum albumin
CFP	Cyan fluorescent protein
cGMP	Cyclic guanosine monophosphate
CRMP	Collapse response mediator protein
DH	Dbl homology
DMEM	Dulbecco's modified Eagle's medium
DOPC	1,2-Dioleoyl-sn-Glycero-3- Phosphocholine
DOPS	1,2-Dioleoyl-sn-Glycero-3-Phosphoserine
DTT	Dithiothreitol
EDTA	Ethylenediaminetetraacetic acid
FBS	Fetal bovine serum
FRET	Fluorescence resonance energy transfer
GAP	GTPases-activating protein
GCN4	General control protein 4
GEF	Guanine-nucleotide exchange factors
GDP	Guanosine-5'-diphosphate
GMP-PNP	5'-Guanylyl imidodiphosphate
GTP	Guanosine-5'-triphosphate
HGF	Hepatocyte Growth Factor

HPLC	High-performance liquid chromatography
Ig	Immunoglobulin
IPT domain	Ig-like, plexin, transcription factor domain
mGFP	Monomeric green fluorescent protein
MICAL	Molecule interacting with CasL
NGF	Nerve growth factor
OD	Optical density
PAGE	Polyacrylamide gel electrophoresis
PBS	Phosphate buffered saline
PEG	Polyethylene glycol
PH	Pleckstrin homology
$PI(4,5)P_2$	Phosphatidylinositol 4,5-bisphosphate
PIE-FCCS	Two-color pulsed-interleaved excitation fluorescence cross-correlation spectroscopy
PLC	Phospholipase C
PSI domain	Plexin-semaphorin-integrin domain
RBD	RhoGTPases-binding domain
RGS	Regulators of G protein signaling
RPM	Revolutions per minute
SAD	Single wavelength anomalous diffraction

SDS	Sodium dodecyl sulfate
SF	Scatter Factor
TCEP	Tris(2-carboxyethyl)phosphine
VEGF	Vascular endothelial growth factor
YFP	Yellow fluorescent protein

CHAPTER ONE

Overview of semaphorin/plexin signaling

Semaphorins and plexins

The intricate architecture of multicellular organisms is constructed from a single fertilized egg through precisely controlled developmental and morphogenetic processes. Semaphorins and plexins are ligand-receptor pairs that regulate the morphogenesis of the nervous and cardiovascular systems, two of the most complicated structures in the human body (Kruger et al., 2005; Tran et al., 2007). Semaphorin/plexin signaling is also involved in essential processes such as cell migration and immune response (Kikutani et al., 2007; Takamatsu and Kumanogoh, 2012; Tran et al., 2007). Abnormalities in the plexin pathways have been associated with cancer and neurodegenerative diseases (Gu and Giraudo, 2013; Tamagnone, 2012; Yaron and Zheng, 2007).

Semaphorins are a large family of secreted or membrane associated glycoproteins that are divided into eight classes based on their sequence similarities and domain organizations (Figure 1-1) (Tran et al., 2007; Yazdani and Terman, 2006). Class 1 and 2 semaphorins are present in invertebrates. Vertebrates express 20 different semaphorins that are grouped into class 3-7. Class V semaphorin only exists in viruses. Class 2, 3 and

V semaphorins are secreted proteins that can exert long-range effect across tissues, whereas the other semaphorins are located on the cell surface and activate signaling upon cell-cell contact. Class 3, 4 and 6 semaphorins contain protease cleavage sites in their extracellular regions, which increase their structural diversity. All semaphorins feature an N-terminal Sema domain responsible for binding of plexins (Antipenko et al., 2003; Love et al., 2003). The C-terminal portion of semaphorins usually contains a cysteine-rich plexin-semaphorin-integrin (PSI) domain followed by an Immunoglobulin-like (Ig-like) domain. Class 4, 5 and 6 semaphorins are transmembrane proteins with C-terminal cytosolic tails, allowing them to mediate bidirectional signaling (Toyofuku et al., 2004b). Semaphorins exist as constitutive dimers, stabilized by interactions between their Sema domains and often strengthened by inter-chain disulfide bridges between the PSI domains (Antipenko et al., 2003; Klostermann et al., 1998; Koppel and Raper, 1998; Love et al., 2003).

Plexins are a family of single transmembrane receptor proteins grouped into four classes (class A, B, C and D) (Figure 1-1) (Tran et al., 2007). Invertebrates express Plexins A and B, which serve as receptors for class 1 and 2 semaphorins, respectively. Vertebrates have 9 plexin family members (Plexin A1-A4, B1-B3, C1 and D1) that transduce signals for the 20 vertebrates semaphorins. Each plexin has distinct affinities towards different semaphorins, therefore generating a large number of possible ligand-receptor combinations to fulfill their roles in morphogenesis (Kruger et al., 2005; Tran et al., 2007). Plexins have a large, multi-domain extracellular region that contains an N-

terminal Sema domain followed by multiple PSI and Ig-like, plexin, transcription factor (IPT) domains. Although the Sema domains in plexins and semaphorins all adopt the seven-blade β-propeller fold which consists of seven four-stranded β sheet, their sequences diverge greatly and each contains unique insertions in the β-propeller (Gherardi et al., 2004). Interactions between semaphorins and plexins are mediated by direct engagement of their Sema domains. Binding of class 3 semaphorins to plexins also requires a co-receptor neuropilin (Fujisawa, 2002). The cytoplasmic region of plexin is highly conserved and always composed of three domains: a juxtamembrane segment, a RhoGTPase binding domain (RBD) and a GTPases-activating protein (GAP) domain (Figure 1-2) (He et al., 2009; Tong et al., 2009).

Physiological functions of semaphorin and plexin

To precisely establish neuronal connections, the growth and navigation of axons are controlled by a variety of mechanisms such as axon guidance signaling and receptor trafficking, etc. (O'donnell et al., 2009). The leading edge of a growing axon is the growth cone, a dynamic structure whose direction of growth is determined by signals from axon guidance cues (Lowery and Van Vactor, 2009). There are four families of classical cue molecules: netrins, semaphorins, ephrins and Slits (Guan and Rao, 2003). Netrins act to attract axon growth, whereas the other three cues are all repulsive. Semaphorins are the largest family of axon guidance molecules, initially characterized by their ability to strongly repel axon growth (Messersmith et al., 1995; Takahashi et al.,

1999). By expressing semaphorins in different locations, the tissues surrounding the neuronal projections define a pathway permissive for axon growth (Tran et al., 2007). In addition, semaphorins also inhibit axon branching and facilitate axon pruning, both of which are essential for the formation of a mature neuronal network (Tran et al., 2007). In certain situations semaphorins can also act as attractants for axon growth. For example, when intracellular cyclic guanosine monophosphate (cGMP) level is elevated, neuronal axons steer toward Sema3A rather than away from it (Song et al., 1998). Studies using genetic and biochemical analysis have established that plexins are the receptors mediating the neuronal pathfinding functions of semaphorins (Cheng et al., 2001; Nakamura et al., 2000; Rohm et al., 2000a; Takahashi et al., 1999; Tamagnone et al., 1999; Winberg et al., 1998).

The cardiovascular system is an extensively branched and organized network bearing similarity to the nervous system. Many axon guidance molecules, such as Slits, netrins and ephrins, also play roles in pattern formation of the vasculature system (Carmeliet, 2003). Class 3 semaphorins have been characterized by their roles in regulating angiogenesis, i.e. the formation of new blood vessels. Sema3A activates its receptor PlexinA1 in endothelial cells, causing reduced integrin activity to promote the sprouting of new blood vessels (Serini et al., 2003). Sema3E/PlexinD1 signaling, on the other hand, inhibits angiogenesis and causes the exclusion of blood vessels from somites (Gu et al., 2003). Plexins can also associate with vascular endothelial growth factor receptor (VEGFR), a well-characterized regulators of angiogenesis. PlexinA1 was shown

to bind to VEGFR2 and potentiate its activation by VEGF (Catalano et al., 2009; Toyofuku et al., 2004a). It is possible that neuropilins mediate the communication between plexin and VEGFR by serving as co-receptors for both of these receptors (Gu et al., 2003).

The role of semaphorin/plexin in immune regulation has recently started to be uncovered. The migration of immune cells and the establishment of cell-cell conjugation are critical for the progression of immune response. Sema4D is expressed in B cells and, through binding to the receptor CD72 on dendritic cells, enhances their interactions with B cells (Kumanogoh et al., 2000). Sema7A, a well-characterized immune semaphorin, is expressed on activated T-cells and binds to integrins on macrophages to stimulate the production of cytokines (Suzuki et al., 2007). Note that in the above cases semaphorins engage non-plexin receptors on immune cell surface. Canonical semaphorin/plexin signaling is also involved in immune regulation. PlexinA1, for example, is expressed in dendritic cells and binds to Sema6D on T-cells. The interaction promotes cell-cell association and also initiates signaling to regulate dendritic cell functions (Wong et al., 2003). The role of several other plexins expressed in immune cells, such as PlexinB1 and PlexinA4, still remains poorly understood and deserves further study.

Intracellular signaling of plexins

Semaphorin/plexin regulate a wide variety of physiological processes including axon guidance, angiogenesis and immune response, which all require the dynamic

remodeling of cell adhesion and the cytoskeleton. This allows semaphorin/plexin expressed in different tissues to generate diverse physiological outputs by regulating a common set of intracellular pathways, particularly Ras and Rho GTPases signaling. These GTPases are molecular switches that alternate between GTP and GDP bound forms. When loaded with GTP they activate downstream effectors to regulate cell adhesion and cytoskeleton dynamics, whereas the GDP-bound form remains quiescent (Hall and Lalli, 2010; Merajver and Usmani, 2005; Ridley, 2001). The activation state of small GTPases depends on the action of two families of regulator proteins: Guanine-nucleotide exchange factors (GEFs) and GAPs. GEFs act to enhance the exchange rate of the bound guanine nucleotide, effectively promoting the loading of GTP which has much higher intracellular concentration than GDP. GAPs inactivate small GTPases by stimulating the intrinsically slow GTP hydrolysis rate, thereby converting them to the GDP-bound inactive form.

Domain organization of plexin cytoplasmic region

Early studies based on homology analysis revealed that the cytoplasmic region of plexins contains two segments with sequence similarity to RasGAPs, interrupted by a ~200 residue insertion showing no obvious homology to known proteins (Figure 1-2A) (Hu et al., 2001; Rohm et al., 2000b). Also unique to the plexin family is a 40-residue juxtamembrane segment that connects the presumed GAP domain to the transmembrane helix (Figure 1-2A). Several structures of plexin cytoplasmic region have been solved

(mouse PlexinA1, PlexinA3, PlexinB1 and zebrafish PlexinC1) (Bell et al., 2011; He et al., 2009; Tong et al., 2009; Wang et al., 2012; Wang et al., 2013). These structures show that the two segments with RasGAP homology fold together to form an intact GAP domain with an overall fold virtually identical to canonical RasGAPs such as p120GAP. The insertion region in the GAP domain, which was shown to interact with several RhoGTPases and therefore named RBD, assumes ubiquitin-like fold and resides next to the GAP domain (Figure 1-2B). The GAP domain and RBD form a tight unibody strengthened by extensive hydrophobic interactions between them (He et al., 2009). In all the structures of plexin cytoplasmic regions the overall structure of the GAP-RBD unibody remains virtually unchanged. Mutations in the GAP-RBD interface severely affect the physiological function of plexins, suggesting that their intimate association is essential for the stability and/or the function of the protein (He et al., 2009).

The juxtamembrane segment adopts a helix-loop-helix-loop conformation and wraps around the GAP domain (Figure 1-2). In several structures the first helix in the juxtamembrane segment (refereed to as the juxtamembrane helix hereafter) assumes the conformation of a long helix with a kink in the middle and docks to one side of the GAP domain (He et al., 2009; Tong et al., 2009; Wang et al., 2012). In one of the PlexinB1 structures the juxtamembrane helix is not visible (Bell et al., 2011), suggesting that this helix is not tightly associated with the GAP domain. The segment following the juxtamembrane helix is incorporated into the GAP domain by extensive hydrophobic

interactions and adopts identical conformation in all the structures of plexin cytoplasmic region.

The GAP domain of plexins and its substrates

The GAP domain is highly conserved among all plexins. Mutating the invariant arginine residue in the GAP domain, which corresponds to the catalytic "arginine finger" in RasGAPs, abolishes plexin-mediated cell morphological changes (Oinuma et al., 2004a; Rohm et al., 2000b; Saito et al., 2009; Sakurai et al., 2010). Transgenic mice carrying the arginine finger mutated plexins phenocopied the plexin-null mutants (Worzfeld et al., 2014b). These data strongly support that the GAP domain and its catalytic activity are essential for the biological functions of plexins. However, the identity of the substrates for the GAP domain of plexin remained controversial. Several studies showed that plexins act as GAPs for the Ras homologues R-Ras and M-Ras (Oinuma et al., 2004a; Oinuma et al., 2004b; Saito et al., 2009; Toyofuku et al., 2005). This GAP activity requires the simultaneous binding of semaphorin and a RhoGTPase Rnd1 to the extracellular and cytoplasmic regions of plexin, respectively (Oinuma et al., 2004a). R-Ras inactivation by the plexin GAP may contribute to neuronal axon growth cone collapse via decreasing integrin-mediated adhesion (Oinuma et al., 2006). Intriguingly, while binding between plexins and R-Ras has been observed (Sakurai et al., 2010; Tong et al., 2009), detection of the RasGAP activity of plexin has proven to be challenging (He et al., 2009; Sakurai et al., 2010; Tong et al., 2009). In fact none of the

previous studies was able to demonstrate the GAP activity of plexins in vitro towards R-Ras/M-Ras using purified proteins. It has been suggested that plexins might inhibit R-Ras by binding and sequestering it from downstream effectors, rather than converting it to the GDP-bound inactive state (Sakurai et al., 2010). A recent study showed that genetic inactivation of R-Ras and M-Ras in mice failed to alleviate the developmental defects caused by arginine-finger mutation of the GAP domain of plexin (Worzfeld et al., 2014a). These results cast doubt on the claim that R-Ras/M-Ras are the substrates of the plexin GAP domain.

Plexins recruit GEFs to activate RhoGTPases

Both class A and class B plexins recruit RhoGEFs to induce the activation of RhoGTPases. Class A plexins bind to FARP1 and its homolog FARP2, both of which are multi-domain proteins containing a Dbl homology (DH) domain with RhoGEF activity (Toyofuku et al., 2005; Zhuang et al., 2009). FARP1 catalyzes GTP/GDP exchange for RhoA (Koyano et al., 2001), whereas the identity of the substrate for FARP2 remains controversial. Different groups have reported exclusive specificity of FARP2 for either Rac1 or Cdc42 (Fukuyama et al., 2005; Kubo et al., 2002; Miyamoto et al., 2003; Murata et al., 2006; Toyofuku et al., 2005). Our lab recently solved the crystal structure of a C-terminal fragment of FARP2, revealing a multi-layered autoinhibition mechanism in which the RhoGEF active site is blocked by the last helix in the DH domain and the second Pleckstrin homology (PH) domain (He et al., 2013). Previous studies showed that

semaphorin stimulation of plexin leads to the activation of FARPs, which then upregulate their substrate Rho GTPases to alter cytoskeleton dynamics (Toyofuku et al., 2005; Zhuang et al., 2009). Semaphorin was shown to activate FARP2 by causing its dissociation from PlexinA1 (Toyofuku et al., 2005). On the other hand, the interaction between FARP1 and PlexinA4 appears to be constitutive and not regulated by semaphorin (Zhuang et al., 2009). The activation mechanisms of FARPs and the regulation of the interactions between FARPs and plexins require further study (He et al., 2013).

Class B plexins all contain a C-terminal PDZ binding motif that binds to the PDZ domains of two closely related RhoA GEFs, LARG and PDZRhoGEF (Aurandt et al., 2002; Driessens et al., 2002; Hirotani et al., 2002; Swiercz et al., 2002). In addition to the PDZ domain and the RhoGEF catalytic domain, they also contain a regulators of G protein signaling (RGS) domain that binds to $G\alpha_{12/13}$ (Sternweis et al., 2007). In the apo state LARG/PDZRhoGEF adopt an autoinhibited conformation that has not been structurally characterized. Deletion of the RGS domain releases the autoinhibition, which could also be disrupted by the binding of Gα to RGS (Sternweis et al., 2007). The PDZ binding motif in PlexinB1 localizes LARG/PDZRhoGEF to the plasma membrane (Hirotani et al., 2002). Semaphorin stimulation is then required to activate their RhoGEF activity, leading to increased RhoA GTP level which facilitates growth cone retraction (Hirotani et al., 2002; Swiercz et al., 2002). How LARG/PDZRhoGEF are activated after their recruitment by plexins is still not clear.

The RBD of Plexins binds to RhoGTPases

Previous studies have identified several RhoGTPases, including Rac1, Rnd and RhoD, that directly associate with plexins in their GTP bound active state. Rac1 has been shown to bind to the RBD of class A and B plexins (Driessens et al., 2001; Rohm et al., 2000b; Turner et al., 2004). This interaction seems to stabilize PlexinB1 on the cell membrane and enhance its affinity for Sema4D (Vikis et al., 2002). It was also suggested that PlexinB1 binds and sequesters Rac1-GTP from its downstream effector PAK, leading to disassembly of actin cytoskeleton structures (Hu et al., 2001; Vikis et al., 2002). This sequestration model is unlikely to apply to class A plexins, which recruit and activate FARPs to cause an increase of Rac-GTP level (Toyofuku et al., 2005). In addition, active Rac1 was shown to be required for PlexinA1 mediated COS7 cell collapse (Turner et al., 2004). The precise role of Rac1 in plexin signaling still requires elaboration.

Rnd1 is a constitutively active RhoGTPase that, when overexpressed in fibroblasts, causes cells to detach from the extracellular substrates and round up, possibly through its ability to bind and activate p190RhoGAP (Nobes et al., 1998; Wennerberg et al., 2003). Rnd1 was initially suggested to act synergistically with semaphorin in triggering the activation of the GAP activity of PlexinB1 (Oinuma et al., 2004a). A homologue of Rnd1, Rnd2, was shown to specifically interact with PlexinD1 and promotes its activation (Uesugi et al., 2009). One study found that Rnd1 can also drive

constitutive activation of PlexinA1 in the absence of semaphorin (Zanata et al., 2002). Together these results suggest that Rnd1 functions as an upstream activator of plexin. Structural studies revealed that Rnd1 interacts with the plexin RBD in the same mode as that of Rac1, raising the question whether Rac1 and Rnd1 function redundantly or in competition with each other (Bell et al., 2011; Tong et al., 2009). It remains unknown if the pathways downstream of Rnd are affected by their recruitment by plexins.

RhoD is another RhoGTPase that was suggested to bind to the RBD of class A and class B plexin (Zanata et al., 2002). RhoD seems to bind to the same interface on RBD as that of Rac1/Rnd but with a lower affinity (Tong et al., 2007). Intriguingly, overexpression of RhoD strongly inhibits Sema3A/PlexinA1 mediated COS7 cell collapse, an effect that cannot be antagonized by overexpression of Rnd1 (Zanata et al., 2002). Therefore the inhibition of plexin signaling by RhoD is unlikely to be solely due to its competition with Rnd1 for binding of plexin RBD.

Different plexin family members also activate specific pathways

In addition to the above discussed common themes in plexin signaling, different plexin family members also recruit distinct downstream players. For example, class A plexins interact with molecule interacting with CasL (MICAL), which contains an N-terminal flavoprotein monooxygenase domain (Hung and Terman, 2011; Terman et al., 2002). In *Drosophila*, loss of MICAL causes similar defects as deletion of Plexin A (Terman et al., 2002). The activation of the enzymatic activity of MICAL requires the

binding of semaphorin to plexin (Schmidt et al., 2008). Another plexin-interacting protein collapse response mediator protein (CRMP) is also involved in the activation of MICAL (Schmidt et al., 2008). The mechanism by which MICAL mediates plexin signaling was revealed by a study demonstrating that MICAL directly binds F-actin and catalyzes the oxidation of a methionine in the polymerization interface, resulting in actin depolymerization and axon growth cone collapse (Hung et al., 2011).

Class B plexins have been suggested to associate with receptor tyrosine kinases. For example, PlexinB1 interact with the receptor tyrosine kinases Met, which normally mediates Scatter Factor 1 (SF1)/ Hepatocyte Growth Factor (HGF) signaling. Binding of PlexinB1 to Met allows Sema4D, the ligand for PlexinB1, to trigger the activation of Met and cause tyrosine phosphorylation of both Met and PlexinB1 (Conrotto et al., 2005; Giordano et al., 2002). Although the downstream signaling events are still not clear, activation of Met is known to promote invasive growth of epithelial cells and contribute to tumor metastasis (Boccaccio and Comoglio, 2006), indicating a potential role of Sema4D/PlexinB1 in cancer progression (Giordano et al., 2002).

The specific signaling branches downstream of PlexinC1 and PlexinD1 are starting to be uncovered. PlexinD1, for example, was shown to signal through the small GTPase Arf6 (Sakurai et al., 2010; Sakurai et al., 2011). Sema3E binding of PlexinD1 was suggested to causes transient elevation of phosphatidylinositol 4,5-bisphosphate ($PI(4,5)P_2$) level on plasma membrane, which is recognized by the PH domain of guanine nucleotide exchange protein 100 (GEF100) (Sakurai et al., 2011). Arf6 activation by

GEF100 was proposed to causes internalization of integrin and disassembly of focal adhesion, leading to axon growth cone collapse (Sakurai et al., 2011). Another study using image-based RNAi screening identified SH3BP1, a GAP for Rac1, to mediate Sema3E/PlexinD1 induced cell morphological changes (Tata et al., 2014). PlexinD1 was suggested to bind and activate the GAP activity of SH3BP1 upon Sema3E stimulation, causing rapid decrease of Rac1-GTP level and disassembly of F-actin network (Tata et al., 2014). It is unclear if these pathways operate in parallel or are exclusively activated in certain tissue types.

From the above discussion it is apparent that the recruitment and activation of the downstream signaling molecules often depend on binding of semaphorins to plexins. To fully understand the signal transduction processes, it is essential to investigate what is the basal and activated states of plexin, and how semaphorin binding alters the conformation of plexin to initiate downstream signaling.

Activation mechanisms of plexin

Mechanisms for the autoinhibition of plexin

The state of plexins prior to semaphorin binding is not well understood. Structural comparison of PlexinA3 with p120GAP/Ras complex indicates that the GAP active site of plexin was too narrow for the binding of substrates. It was proposed that the GAP domain of plexin intrinsically assumes an autoinhibited conformation (He et al., 2009). In

addition, multiple lines of evidence indicate that plexin may exist as pre-formed inhibitory dimers. Deletion of the extracellular Sema domain was shown to render PlexinA1 constitutively active, suggesting that Sema domains is required for maintaining the autoinhibited state of plexin (Takahashi and Strittmatter, 2001). The crystal structure of a fragment of PlexinA2 extracellular region (residues 38-561) showed that the Sema domain of PlexinA2 forms a symmetrical head-on dimer (Nogi et al., 2010). The dimer interface involves the third blade of the β-propeller, which is also responsible for binding of semaphorin. A model was then proposed that the pre-formed inhibitory dimer of Sema domain is disrupted by semaphorin, resulting in activation of plexins (Figure 1-3) (Nogi et al., 2010). The dimerization affinity of Sema domain, however, is estimated to be extremely low, and the crystal structure of a longer fragment of PlexinA2 extracellular region (35-703) solved by a different group does not contain such head-on dimer (Janssen et al., 2010). Crystal structures of PlexinB1 and PlexinC1 extracellular region also do not seem to support that they exist as pre-formed oligomers (Janssen et al., 2010; Liu et al., 2010). The cytoplasmic region of plexin was suggested to homodimerize as well based on a crystal structure of PlexinB1 RBD, which forms dimers in the crystal mediated by a conserved short β-hairpin (Tong et al., 2007). However, this hairpin was shown to fold into the core interface between RBD and GAP domain in the full-length plexin cytoplasmic region structures, suggesting that the RBD dimer is unlikely to form unless the extensive intramolecular GAP-RBD interactions are lost (He et al., 2009).

Mechanisms for semaphorin induced activation of plexin

The Sema domain in semaphorins has been well-documented to homodimerize in a side-by-side fashion (Antipenko et al., 2003; Janssen et al., 2010; Liu et al., 2010; Love et al., 2003; Nogi et al., 2010). The Sema domain mediated dimerization is relatively weak and often strengthened by inter-chain disulfide bridges formed between the cysteine-rich PSI domains that always follow the Sema domain (Gherardi et al., 2004). Several studies showed that mutating the cysteine that stabilize semaphorin dimerization strongly diminishes their ability to trigger plexin activation, suggesting that the monomeric form of semaphorin is inactive (Klostermann et al., 1998; Koppel and Raper, 1998). Antibody induced clustering of the extracellular region of plexins mimics semaphorin binding and triggers activation of plexin cytoplasmic region (Oinuma et al., 2004a; Oinuma et al., 2004b). In addition, replacing the extracellular region of plexin with that of the TrkA receptor allows the chimeric protein to be activated by the TrkA ligand nerve growth factor (NGF), which is known to induce the dimerization of TrkA extracellular region (Perrot et al., 2002). Collectively these results suggest that semaphorin binds to plexin extracellular region to induce their dimerization, which leads to the initiation of intracellular signaling.

Several crystal structures of plexin extracellular region in complex with semaphorin have been determined (PlexinA2/Sema6A, PlexinB1/Sema4D and PlexinC1/Sema7A) (Janssen et al., 2010; Liu et al., 2010; Nogi et al., 2010). Despite the sequence divergence between different classes of plexins and semaphorins, these

structures superimpose well and the binding mode of semaphorin/plexin remains unchanged (Figure 1-3A). These structures revealed that one semaphorin dimer indeed engages two copies of plexin extracellular region simultaneously. The Sema domains in semaphorin and plexin interact with each other through the third blade of their β-propeller in an orthogonal fashion (Figure 1-3A). The two copies of plexin extracellular region in the heterotetramer remain separated with their C-termini pointing away from each other (Figure 1-3A). All of the structures are solved with truncated plexin extracellular regions missing multiple PSI and IPT domains connecting the Sema domain to the transmembrane region. Therefore they provided little clue with regard to the state and conformation of the plexin cytoplasmic region after ligand binding (Figure 1-3C). The distance between the C-termini of the two plexin extracellular region could potentially be bridged by the missing membrane proximal domains, allowing intimate interactions between the transmembrane and cytoplasmic regions (Janssen et al., 2010; Nogi et al., 2010). On the other hand, these structures do not exclude the possibility that in the semaphorin/plexin complex, the cytoplasmic regions from the two plexin monomers remain separated. This would be consistent with a mechanism in which the cytoplasmic region of plexin forms a pre-formed inhibitory dimer, and is activated by semaphorin-induced separation of this dimer (Antipenko et al., 2003; Tong et al., 2007). This ambiguity could be resolved by a structure of full-length plexin bound to semaphorin, which may be difficult to obtain due to the large size of plexin and intrinsic flexibility between the multiple domains.

The role of RhoGTPases in plexin activation

As described previously, the RhoGTPase Rnd1 and Rac1 were suggested to also promote plexin activation. A recent study showed that mutating the RhoGTPases binding interface does not affect plexin mediated COS7 cell collapse (Bell et al., 2011), therefore RhoGTPases are unlikely to be essential for activation of plexin as suggested previously (Oinuma et al., 2004a). The crystal structures of PlexinB1 in the apo state and in complex with Rac1 have been solved, which revealed no conformational change after Rac1 binding (Bell et al., 2011; Tong et al., 2009). A model of plexin activation involving oligomerization mediated by the RBD/RhoGTPase interaction was proposed (Bell et al., 2011), but existence of this oligomeric structure in solution or on the cell surface has not been established (Siebold and Jones, 2013).

Summary and key questions

Semaphorin/plexin signaling is essential for a spectrum of essential physiological processes. Although it has been widely accepted that plexins function as GAPs for small GTPases, the downstream substrate of plexin remained controversial and elusive. In addition, it is not clear how plexins remain inactive prior to semaphorin binding, and how semaphorin triggers activation of the cytoplasmic region of plexin for signal transduction. The mechanisms by which RhoGTPase Rac1 and Rnd1 regulate plexin activation are also unknown. My thesis work is focused on addressing these key questions.

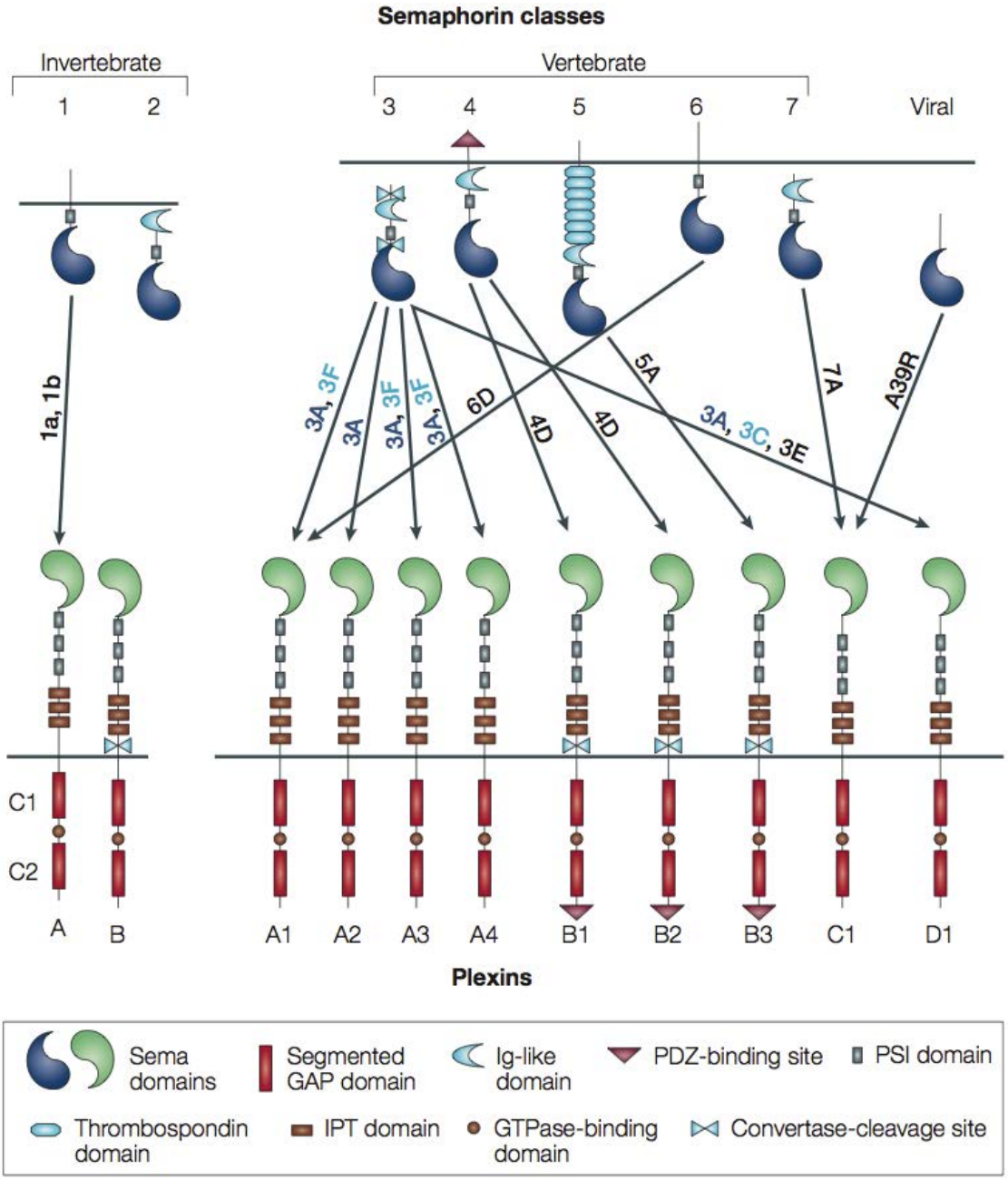

Figure 1-1. Domain organizations of semaphorins and plexins.

Arrows indicate interactions between semaphorins and plexins. The figure is from Kruger et al., 2005.

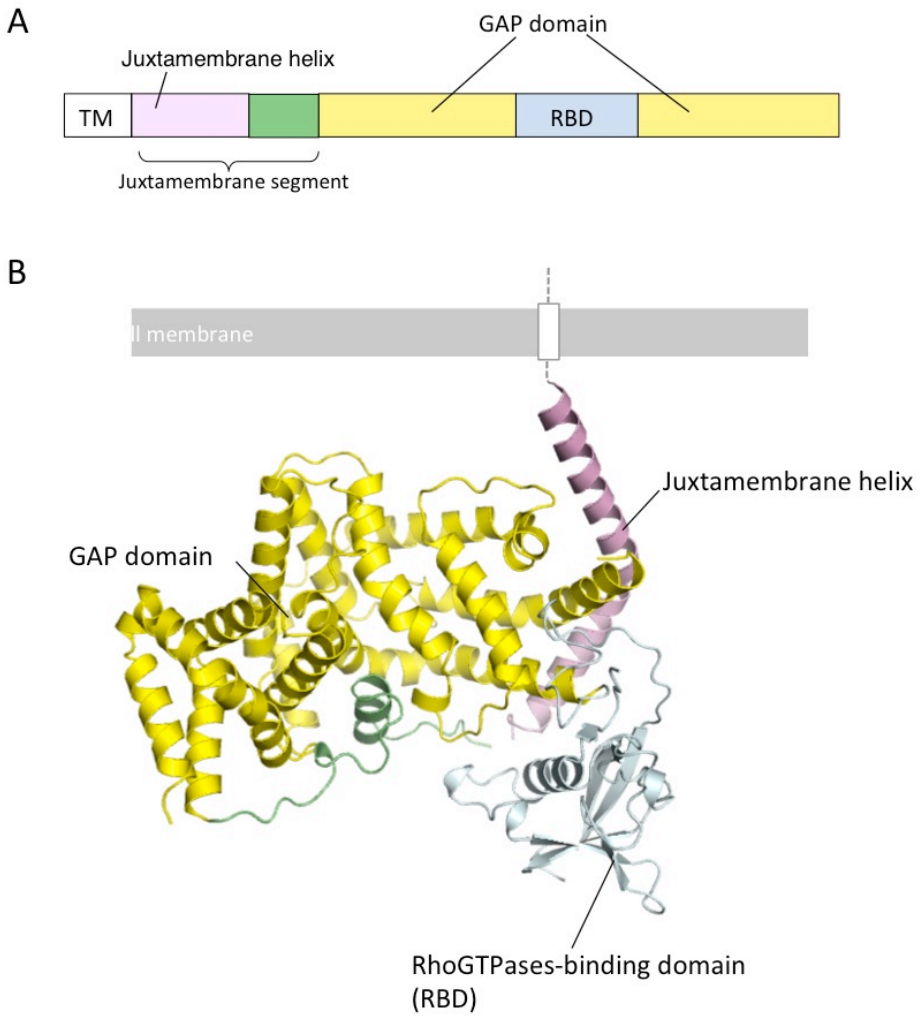

Figure 1-2. Structural organization of plexin cytoplasmic region

(A) Domain organization of plexin cytoplasmic region. The regions showing RasGAP homology are labeled GAP domain.

(B) Crystal structure of PlexinA3 cytoplasmic region. There are 4 residues missing in the structure that connect the transmembrane helix to the N-terminus of the juxtamembrane helix.

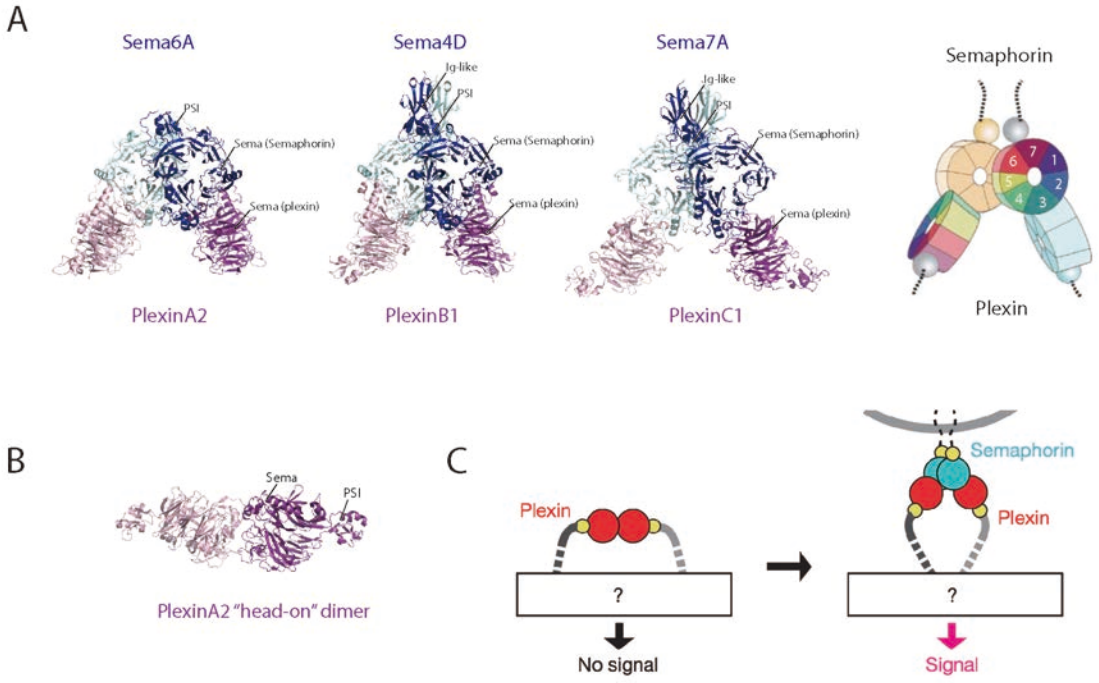

Figure 1-3. Structures of plexin extracellular regions and their complexes with semaphorins.

(A) Structures of semaphorin/plexin complexes. The structures were superimposed based on semaphorin and presented in the same view. The two monomers in a semaphorin dimer are colored light/dark blue, whereas the two copies of plexin extracellular region are colored light/dark purple. Cartoon representation of the binding between the Sema domains in semaphorin and plexin are shown on the right (modified from Nogi et al., 2010). The seven blades in the β-propeller are labeled 1-7.

(B) Structure of the pre-formed dimer of PlexinA2 Sema domain reported by Nogi et al., 2010.

(C) A model presented by Nogi et al showing plexin switches from a pre-formed inhibitory dimer to a semaphorin induced active dimer. Note that the states of the plexin cytoplasmic region before and after semaphorin binding were unknown and therefore not drawn. This figure is from Nogi et al., 2010.

CHAPTER TWO

Plexins are GAPs for Rap and are activated by induced dimerization

Plexin cytoplasmic regions exhibit GAP activity to Rap but not R-Ras or M-Ras.

To thoroughly investigate the GAP activity of plexin family members, we purified the cytoplasmic regions (referred to as $Plexins_{cyto}$) of Plexins A1-A4, B1, C1 and D1. The GAP activity of these proteins towards purified, GTP-loaded R-Ras and M-Ras was measured by using a continuous photometric assay (Webb and Hunter, 1992). At 10 μM concentration, none of the $Plexin_{cyto}$ proteins accelerated GTP hydrolysis of either R-Ras or M-Ras, whereas dramatic acceleration was observed when the GAP domain of p120GAP at 0.05 μM was used as a positive control (Figure 2-1, A and B).

In the RasGAP family, SynGAP and three proteins of the GAP1 group exhibit dual specificity towards both Ras and Rap (Kupzig et al., 2006; Pena et al., 2008). The high degree of structural similarity of the plexin GAP domain to that of SynGAP (He et al., 2009) led us to speculate whether plexins also possess GAP activity towards Rap. Rap1B and Rap2A, two of the five known members in the Rap subfamily, were used as substrates to measure the GAP activity of $Plexins_{cyto}$. The photometric assays showed that all the $Plexin_{cyto}$ proteins at 10 μM concentration accelerated GTP hydrolysis of both Rap1B and Rap2A (Figure 2-1, C and D). These results were confirmed by an HPLC-based assay that assesses the ratio of GTP and GDP bound to Rap after incubation with

plexins (Figure 2-2). Among the plexins we tested, PlexinC1$_{cyto}$ displayed the highest activity (first order rate constant k = 0.013 s^{-1} for Rap1B). Class A plexins were much less active (k =1.4~1.6 x10^{-4} s^{-1} for Rap1B), but still higher than the intrinsic activity of Rap (Rap1B: k = 9.1 x 10^{-5} s^{-1}).

Dimerization stimulates the RapGAP activity of plexins$_{cyto}$.

Plexins$_{cyto}$ are predominantly monomeric in solution (Figure 2-3B) (He et al., 2009). To test whether their RapGAP activity is regulated by dimerization, we fused PlexinA1$_{cyto}$ to the C-terminus of a modified FKBP, which can be induced to homodimerize upon binding to a bivalent compound AP20187 (referred to as the dimerizer) (Clackson et al., 1998). We placed FKBP at the N-terminus rather than the C-terminus of Plexin$_{cyto}$, because this topology is likely to better mimic semaphorin-induced dimerization of full-length plexins. A flexible linker (3 or 9 residues) is included between FKBP and Plexin$_{cyto}$ to avoid imposing tight restraints on the distance and orientation between the two Plexin$_{cyto}$ molecules in the induced dimer (Figure 2-3A). These proteins are referred to as FKBP-L3-PlexinA1$_{cyto}$ and FKBP-L9-PlexinA1$_{cyto}$, respectively.

Similar to native PlexinA1$_{cyto}$, these FKBP-PlexinA1$_{cyto}$ fusion proteins were predominantly monomeric in solution (Figure 2-4A). Their RapGAP activities were also indistinguishable from that of the native protein (Figure 2-3B). As expected, adding the dimerizer induced robust dimerization of the FKBP-PlexinA1$_{cyto}$ fusions (Figure 2-4A). Strikingly, dimerized FKBP-PlexinA1$_{cyto}$ proteins showed much higher RapGAP activity

(Figure 2-3B). The dimerizer did not alter the activity of native PlexinA1$_{cyto}$ (Figure 2-3B), supporting that the stimulated activities of the FKBP-PlexinA1$_{cyto}$ proteins are due specifically to formation of an active dimer. To test the generality of this dimerization-driven activation mechanism, we constructed a FKBP fusion of PlexinC1$_{cyto}$ with the 3-residue linker. Despite the rather high basal activity of monomeric PlexinC1$_{cyto}$ (Figure 2-1C), three-fold activation was observed for dimerized FKBP-L3-PlexinC1$_{cyto}$ (Figure 2-4C). We also tested the dimerization-induced activation of FKBP-L3-PlexinC1$_{cyto}$ in cells by using a GST-RalGDS pull-down assay (Zwartkruis et al., 1998). Although severe degradation of the protein after AP20187 treatment obscured the expected increase of RapGAP activity, the basal activity of PlexinC1 was readily detected by this cell-based assay (Figure 2-5).

FKBP-L3-PlexinA1$_{cyto}$ was activated by dimerization to higher levels (4-fold) than FKBP-L9-PlexinA1$_{cyto}$ (3-fold) (Figure 2-3B), indicating that closer proximity of the two Plexin$_{cyto}$ monomers favors formation of the active dimer. To further explore the effect of the inter-monomer distance on plexin activation, we fused the PlexinA1$_{cyto}$ to the C-terminus of the coiled-coil dimerization motif of General control protein 4 (GCN4) to enforce constitutive dimerization on plexins (O'Shea et al., 1991). The distance between the two C-termini in the GCN4 coiled-coil helix dimer is ~7 Å (PDB ID: 2ZTA), much smaller than that in the FKBP dimer (~16Å) (PDB ID: 1BL4). Thus the coiled-coil is capable of bringing the two Plexin$_{cyto}$ N-termini much closer. We also included a flexible linker of various lengths (1, 4 and 7 residues) between the coiled-coil and

PlexinA1$_{cyto}$, allowing a wider range of inter-monomer distance to be sampled. The 1-residue linker essentially restrains the two N-termini in Plexin$_{cyto}$ within the range of direct contacts, whereas the 7-residue linker allows more than 40 Å distance between the two (assuming ~3 Å span per linker residue, 7 x 3 x 2 = 42 Å).

The coiled-coil indeed induced robust dimerization of PlexinA1$_{cyto}$ (Figure 2-4). These coiled-coil plexin dimers are all more active than the dimerized FKBP-PlexinA1$_{cyto}$ fusions (Figure 2-3B). The one with the 4-residue linker (referred to as CC-L4-plexinA1$_{cyto}$) displays the highest RapGAP activity ($k = 3.9 \times 10^{-3}$ s^{-1} for Rap1B), which is 28-fold and 7-fold higher than the native protein and FKBP-L3-PlexinA1$_{cyto}$, respectively. In contrast, none of the dimerized FKBP- and coiled-coil-PlexinA1$_{cyto}$ stimulated GTP hydrolysis for either R-Ras or M-Ras under similar conditions (Figure 2-3, C and D).

We also generated constructs of coiled-coil fusions of plexins A2-A4, B1, C1 and D1, and were able to purify soluble proteins and confirm formation of the dimers for CC-L4-plexinA2 and A4. They both displayed higher RapGAP activity than their respective native proteins (Figure 2-4D). The degree of activation varied among different plexin family members, which may be due to differences in their intrinsic catalytic capacity and/or the degree of active dimer formation induced by the coiled-coil.

These results together suggest that the RapGAP activity of monomeric plexins is autoinhibited, and it can be activated by formation of the active dimer. Previous studies have suggested that SynGAP and other dual specificity GAPs interact with Rap in a

binding mode similar to that of the p120GAP/Ras complex (Pena et al., 2008; Sot et al., 2010). Assuming the same Rap binding mode for plexins, the Rap binding sites in monomeric PlexinA3 and B1 structures are clearly more closed than that in SynGAP (He et al., 2009; Tong et al., 2009). This might prevent Rap binding and serve as the autoinhibition mechanism. Higher activity of the coiled-coil-plexin$_{cyto}$ dimers compared to the FKBP-plexin$_{cyto}$ dimers suggests that close proximity of the two juxtamembrane segments in plexin monomers promotes formation of the active dimer. These findings support that semaphorin activates plexin by inducing dimerization of the plexin cytoplasmic region, as opposed to separation of a pre-formed inhibitory dimer.

Plexins use a non-canonical mechanism for catalyzing Rap GTP hydrolysis

Although Rap and Ras are close homologues, their respective canonical GAPs are structurally unrelated and use different catalytic mechanisms. RasGAPs such as p120GAP catalyze GTP hydrolysis for Ras/R-Ras/M-Ras by using an arginine finger residue (Scheffzek et al., 1997), which neutralizes the developing negative charge of the leaving g-phosphate group in GTP. The arginine residue also stabilizes Gln61 in the switch II region of Ras, which orients a nucleophilic water molecule for catalysis. Rap lacks the ability to position the nucleophilic water because it contains a threonine residue at the equivalent position (Thr61). Canonical RapGAPs facilitate Rap GTP hydrolysis by providing an asparagine residue ("Asn thumb"), which fulfills the catalytic role for Gln61 in Ras (Scrima et al., 2008).

The dual specificity GAPs such as SynGAP can act as RapGAPs without such an "Asn thumb" (Kupzig et al., 2009; Sot et al., 2010). They are structurally related to RasGAPs and also possess the arginine finger. This arginine residue is required for catalyzing GTP hydrolysis for Rap, although its precise role is unknown (Sot et al., 2010). A recent study has shown that mutating Gln63 in Rap to either alanine (Q63A) or glutamate (Q63E) renders Rap insensitive to the dual specificity GAPs, but only slightly affects GTP hydrolysis catalyzed by canonical RapGAPs (Sot et al., 2010). These observations have led to the model that the dual specificity GAPs induce a conformational change in switch II of Rap, which pulls Gln63 into the active site to play the catalytic role of Gln61 in Ras (Sot et al., 2010).

The structural similarity of plexins to SynGAP indicates that they use the same alternative mechanism for catalyzing GTP hydrolysis for Rap. To test this, we measured the activity of plexins towards the Rap1B Q63E and Q63A mutants. Both of these two mutations strongly inhibited GTP hydrolysis catalyzed by either monomeric or dimeric plexins (Figure 2-6A and B). In addition, we constructed the Rap G12V mutant, which is also sensitive to the canonical RapGAPs but not to SynGAP (Pena et al., 2008). This mutation severely impaired plexin-catalyzed GTP hydrolysis. Similar to other dual specificity GAPs, mutating the arginine finger residue in plexin (Arg1429 in PlexinA1) renders both monomeric and dimeric plexins$_{cyto}$ catalytically dead (Figure 2-6C).

Rac1 does not stimulate the RapGAP activity of plexins$_{cyto}$ in solution

The crystal structure of PlexinA1 in complex with Rac1 was solved by Huawei He in our lab. The overall structure is identical with the PlexinB1/Rac1 complex, showing that Rac1 does not induce conformational changes in plexin (Bell et al., 2011; Wang et al., 2012). To validate the structural observations, we tested whether Rac1 modulates the RapGAP activity of plexin$_{cyto}$. The experiments were designed to measure the effect of the plexin-Rac interaction as shown in the structure in the present study and previous structures (Tong et al., 2009), but not the new potential secondary interaction in the PlexinB1-Rac1 structure, which is weak and does not form stably in solution (Bell et al., 2011). We used PlexinB1$_{cyto}$ to test the effect of Rac1 on plexin monomers because it has relatively high basal activity and its binding to Rac1 has been well characterized (Bell et al., 2011; Tong et al., 2007; Tong et al., 2009). To ensure sufficient binding between Rac1 and plexin in the assay, the concentration of GTP-loaded Rac1 Q61L was 10-fold higher than that of PlexinB1$_{cyto}$ and ~2-5-fold higher than the dissociation constant (K_d) value (~20-43 μM) (Bell et al., 2011; Tong et al., 2009). Rac1 did not alter the RapGAP activity of PlexinB1$_{cyto}$ (Figure 2-7D) or the activities of the FKBP or coiled-coil dimer of PlexinA1$_{cyto}$ (Figure 2-7E). These results together with the crystal structure demonstrate that Rac1 does not directly contribute to activation of the RapGAP activity of plexin in solution. This likely holds true for the other plexin-interacting RhoGTPases, which bind to plexin in the same mode with similar affinities (Tong et al., 2007; Tong et al., 2009).

Biochemical assays have suggested that induced clustering of RhoGTPase-bound plexins$_{cyto}$ elicits their GAP activity to R-Ras (Oinuma et al., 2004b; Toyofuku et al., 2005). We used R-Ras or M-Ras as the substrate in GAP assays and found that dimerized plexins$_{cyto}$ remained inactive to both R-Ras and M-Ras in the presence of Rac1(GTP) (Figure 2-7, F and G).

RapGAP activity of full-length plexins in cells is stimulated by semaphorin

To examine whether full-length plexins function as RapGAPs when activated by their semaphorin ligands, we employed the Raichu-Rap reporter system to monitor the activity of Rap in living cells (Mochizuki et al., 2001). In this system, an increase in the level of GTP-bound Raichu-Rap leads to stronger fluorescence resonance energy transfer (FRET) between the reporter fluorescent proteins CFP and YFP, and vice versa. We chose PlexinB1 for these assays because its activation by the Sema4D ligand has been well characterized, and unlike the interaction between some class A plexins and class 3 semaphorins its interaction with Sema4D does not require the presence of neuropilin as the co-receptor (Kruger et al., 2005; Tran et al., 2007).

COS7 cells cotransfected with full-length PlexinB1 and the Raichu-Rap reporter were stimulated with Sema4D and subjected to time-lapse FRET imaging. The Raichu-Rap protein is not localized exclusively at the cell membrane where plexin is activated by semaphorin (Mochizuki et al., 2001; Ohba et al., 2003), consequently plexin could only act on a fraction of Raichu-Rap in the cell. In particular, we observed strong fluorescence

signals in the perinuclear region of the cell, consistent with previous reports that a large amount of Rap resides on the Golgi apparatus and late endosomes (Beranger et al., 1991; Nomura et al., 2004; Pizon et al., 1994). This pool of Rap is not accessible to plexin and therefore excluded from the FRET analyses. The result shows that the mean FRET value of the peripheral regions of cells transfected with wild-type PlexinB1 and Raichu-Rap decreased within 5 minutes after Sema4D treatment (Figure 2-8). PlexinB1 bearing the arginine finger mutation R1677A, which inactivates the RapGAP activity, failed to cause FRET decrease of Raichu-Rap (Figure 2-8). In addition, cells transfected with the Raichu-Rap construct bearing the plexin-resistant Q63E mutations exhibited no FRET decrease after Sema4D treatment (Figure 2-8). We also performed the same FRET assays using the Raichu reporter for R-Ras. FRET levels of cells expressing Raichu-R-Ras and PlexinB1 did not decrease after Sema4D treatment (Figure 2-8).

These results suggest that plexins act as Rap-specific GAPs in cells as they do in solution. Semaphorin stimulates this activity, likely by inducing dimerization of the plexin cytoplasmic regions in a mode similar to that in the FKBP and coiled-coil dimerization systems, in which the juxtamembrane helices in the two plexin monomers are brought close to each other.

Rap inactivation is essential in plexin-mediated neuronal growth cone collapse

To determine whether the plexin RapGAP activity is required for semaphorin-induced repulsive axon guidance, I collaborated with Nishi Srivastava in Christopher W.

Cowan lab. She cultured primary rat cortical neurons, which express PlexinA1 and its co-receptor Neuropilin1 endogenously (Chen et al., 2008; Murakami et al., 2001), and analyzed Sema3A-induced growth cone collapse. Sema3A promotes growth cone repulsion through the PlexinA1/Neuropilin1 holo-receptor complex (Tran et al., 2007). Under basal conditions, addition of Sema3A to the culture medium induced a robust collapse (~70%) of the growth cones by 1 hour (Figure 2-9, A and B). If the plexin RapGAP activity is important for semaphorin-induced growth cone repulsion, expression of Rap1B (Q63E), which is resistant to plexins but remains sensitive to canonical RapGAPs (Sot et al., 2010), would reduce or block Sema3A-induced growth cone collapse. The results revealed that ectopically expressed Rap1B (Q63E) inhibited Sema3A-induced growth cone collapse in a DNA concentration-dependent manner when compared to vector only-transfected neurons (Figure 2-9, A and B). These findings indicate that inactivation of Rap by the plexin RapGAP plays an essential role in semaphorin-induced growth cone collapse. Consistently, mutating the arginine finger in plexin, which abrogates its RapGAP activity as demonstrated above, has been shown to abolish plexin-induced cell morphological changes by several previous studies (Oinuma et al., 2004a; Rohm et al., 2000b; Saito et al., 2009; Sakurai et al., 2010)

Discussions and future directions

Identification of the RasGAP domain in plexins over a decade ago raised the critical question which Ras family member they act on for signal transduction (Hu et al.,

2001; Rohm et al., 2000b). We show here that plexins, while structurally homologous to the RasGAPs, possess GAP activity specific for Rap. It appears that the RasGAP fold has evolved a spectrum of specificity for the Ras family members. While p120GAP and many others containing the RasGAP fold are only active to the Ras/M-Ras/R-Ras group, SynGAP and some GAP1 proteins are dual specific GAPs that can also act on Rap. Plexins likely reside at the other end of the spectrum, as they are active towards Rap but not Ras/R-Ras/M-Ras under the conditions that we have examined. Our mutational analysis suggests that plexin catalyzes Rap GTP hydrolysis by using the alternative mechanism proposed recently for the dual specific GAPs (Sot et al., 2010). While plexins may also display GAP activity towards R-Ras and M-Ras as reported earlier under certain conditions, it is more likely that they inactivate R-Ras and M-Ras through an indirect mechanism or by sequestering them from their downstream effectors (Sakurai et al., 2010).

Our growth cone collapse assays with the Rap Q63E mutant together with previous analyses of the arginine finger mutants of plexins suggest that inactivation of Rap by the plexin RapGAP is essential for plexin-mediated neuronal growth cone collapse and other changes in cell morphology (Oinuma et al., 2004a; Rohm et al., 2000b; Saito et al., 2009; Sakurai et al., 2010). This inactivation of Rap is likely limited to the plasma membrane regions where plexin is activated by semaphorin. The RapGAP activity of plexins as shown by our kinetic assays is very low when compared to other RapGAPs (Brinkmann et al., 2002). This localized, low level of RapGAP activity may

allow plexin to trigger localized cell morphological changes without perturbing other functions of Rap inside the cells such as vesicular transport (Gloerich and Bos, 2011). The EphA4 receptor has also been shown to induce growth cone collapse through inactivating Rap, although EphA4 itself does not possess GAP activity and does so by recruiting a canonical RapGAP named spine-associated RapGAP (Richter et al., 2007). Conversely, activation of Rap by the Rap-specific guanine nucleotide exchange factor Epac leads to axon growth (Murray and Shewan, 2008; Murray et al., 2009). It appears that multiple signaling pathways converge on Rap, and its activity plays a key role in determining whether the axon undergoes collapse or outgrowth. This is consistent with several studies showing that active Rap promotes neurite outgrowth by regulating cell adhesion and cytoskeleton dynamics through integrin and RhoA, respectively (Jeon et al., 2010; Richter et al., 2007; Yamada et al., 2005).

The three recent structural studies of the plexin ectodomains elucidate the binding mode between plexin and semaphorin, but have not addressed how this binding triggers activation of the plexin cytoplasmic region (Janssen et al., 2010; Liu et al., 2010; Nogi et al., 2010). We show that the RapGAP activity of purified plexin cytoplasmic region can be activated by dimerization and the levels of activation increases as the two monomers are brought closer, strongly favoring an activation mechanism that involves formation of an activating dimer (Figure 2-10). Given that the GAP activity does not modify plexins themselves, plexins cannot employ an activation mechanism similar to that used by most receptor tyrosine kinases in which two kinases activate each other by cross

phosphorylation (Schlessinger, 2000). Instead, activation of the plexin GAP is likely achieved by a specific inter-monomer interaction that triggers a conformational change in the GAP domain (Figure 2-10). A recent study has suggested that the dual-specificity GAP CAPRI is also regulated by dimerization (Dai et al., 2011). The dimerization mode and the conformational change required for activation await structural analyses of dimeric plexins and related GAPs.

This activation mechanism involving the active dimer does not rule out the possibility of a preformed, inactive dimer of plexin on the cell surface (Antipenko et al., 2003; Tong et al., 2007). In this case, semaphorin binding would trigger the switch from the inactive to the active dimer. The "head-on" dimer of PlexinA2 extracellular region reported recently is of particular interest in this regard (Nogi et al., 2010). The two C-termini in this dimer point to opposite directions, which may impose spatial and orientational restraints that prevent formation of the active dimer of the cytoplasmic region.

The role of the RBD-binding RhoGTPases is another intriguing issue in plexin signaling. Our biochemical analyses suggest that the RhoGTPases are not involved directly in the dimerization-driven activation mechanism of plexin. Given that RhoGTPases, plexins and Rap are all associated with the plasma membrane, RhoGTPases may contribute to plexin activation in the context of the membrane surface. Binding of RhoGTPases may help restrain the plexin cytoplasmic region in the orientation that favors formation of the active dimer or increase the accessibility of the

GAP active site to Rap. Alternatively, RhoGTPases may destabilize the inhibitory dimer of plexin formed on the cell surface as discussed above and shift the equilibrium towards the active state. Moreover, the RBD-RhoGTPase interaction has been suggested to sequester RhoGTPases from their downstream effectors, thereby contributing to signaling without altering the activation state of plexins (Vikis et al., 2002).

Materials and methods

Protein expression and purification

The coding sequence for the cytoplasmic domain of mouse PlexinA1 (residues 1269-1894), A2 (1264-1894), A3 (residues 1247-1872), A4 (1263-1893), C1 (residues 975-1571), D1 (residues: 1297-1916) (provided by Dr. Masahiko Taniguchi) and human PlexinB1 (1515-2315) were amplified by PCR. These cDNAs were sub-cloned into either a modified pET28 vector (Novagen) that contains a recognition site for the human rhinovirus C3 protease following the His_6-tag (His-tagged), or another modified pET28 vector that expresses the target protein with an N-terminal His_6-Sumo tandem tag (His-sumo-tagged). The constructs of FKBP-$plexins_{cyto}$ with either one of the two linkers (3-residue linker: GSG; 9-residue linker: GSSGSGSSG) were generated by PCR by using the coding sequence for FKBP in the pC_4-F_v1E plasmid (ARIAD) and those of plexins. The GCN4 coiled-coil sequence (VKQLEDKVEELLSKNAHLENEVARLKKLV) with three different linkers (1-residue linker: G; 4 residue linker: GSSG; 7-residue linker: GSSGSSG) were fused with $plexins_{cyto}$ by PCR and subcloned into the same expression vectors. Mutants of plexins were generated by Quickchange (Stratagene). Expression and purification of these proteins were conducted as described previously (He et al., 2009). The oligomerization states of the proteins were assessed by gel filtration chromatography using Superdex 200 10/300 GL columns (GE healthcare).

The GAP domain of p120GAP (residues 714-1047) was expressed by using the His-tagged vector in the bacteria strain BL21(DE3) and purified with a 1 ml Histrap

column (GE Healthcare) followed by ion exchange chromatography (1 ml resource Q, GE Healthcare). The small GTPases including Rac1 (residues 2-177), Rap1B (residues 2-167), Rap2A (residues 2-167), R-Ras (residues 22-201) and M-Ras (residues 10-178) were all expressed and purified through similar procedures. Mutations were generated by Quickchange. Guanine nucleotide exchange was performed by incubating the purified small GTPases with GTP or the nonhydrolyzable analogue guanylyl imidodiphosphate (GMP-PNP) at 40-fold excess in the presence of 4 mM EDTA on ice for 2 hours. The reaction was terminated by 10 mM $MgCl_2$, and excess nucleotide was removed by gel filtration using a Superdex 75 10/300 GL column (GE Healthcare).

In solution GAP activity assays

The photometric GAP assays were performed as described with minor modifications (Webb and Hunter, 1992). Briefly, GTP-loaded small GTPases were added to the reaction solution containing 50 mM Tris-HCl pH 7.6, 20 mM NaCl, 2 mM $MgCl_2$, 10% glycerol, 4 unit/ml purine nucleoside phosphorylase (Sigma) and 200 μM 7-methyl-6-thioguanosine (Berry & Associates). The final concentration of all the small GTPases in the reactions was 50 μM. The absorbance at 360 nm was monitored continuously in a 1 cm path-length cuvette. In these conditions, an increase of 1 O.D. unit was calibrated to be equivalent to release of 95 μM inorganic phosphate from the GTP hydrolysis reaction

After 20-30 s of baseline reading with small GTPases in the reaction solution, plexins (10 μM) or p120GAP (0.05 μM) was added and mixed, and GAP-catalyzed

reactions were monitored for 400 s in total. For assays involving dimerized FKBP-plexins$_{cyto}$, 10 μM FKBP-plexins$_{cyto}$ were first incubated with 5 μM AP20187 at room temperature for 5 min. Then 50 μM small GTPase was added and mixed to start the assay. To test the effect of Rac1 on the GAP activity of plexins$_{cyto}$, 100 μM GTP-loaded Rac1 (Q61L) was incubated with 10 μM plexins$_{cyto}$ at room temperature for 5 min before the assay. The data were fit to the single exponential decay model to obtain the rate constants k using the program Prism5.

The HPLC-based GAP assay was performed similar to described in (Biddlecome et al., 1996). Briefly, aliquots of Rap were heat denatured to release the bound guanine nucleotides. Denatured proteins were removed by centrifugation and following ultrafiltration using a 10 kD cut-off concentrator (Amicon). The nucleotide containing flow-through was loaded onto an anion exchange column (AX300,100 x 4.6mm, SynChropak), and eluted with a buffer gradient of KH_2PO_4 (pH 7.0) from 0 mM to 700 mM. Elution of the nucleotides was monitored by the absorbance at 254 nm. Standard elution profiles of GTP and GDP were obtained by running analytical grade GTP and GDP from Sigma on the same column.

RalGDS pull-down assay for the RapGAP activity of FKBP-PlexinC1$_{cyto}$ in cells

The FKBP-L3-PlexinC1$_{cyto}$ in the pIRES-EGFP2 vector (Clontech) expressed in cells failed to reduce the abundance of GTP-bound Rap by this assay, likely due to

cytosolic localization of the protein which cannot act efficiently on the Rap substrate localized on the membrane surface (Bos et al., 2007). FKBP-PlexinC1$_{cyto}$ was therefore targeted to the membrane by including the myristoylation signal sequence from the kinase Yes (residue 1-11: MGCIKSKENKS) at the N-terminus (Figure 2-5A). A C-terminal Myc-tag was also included for detection by Western blot. The assay was performed as described previously (Zwartkruis et al., 1998). Briefly, HEK293T cells in 6-well plates were transfected with Myr-FKBP-PlexinC1$_{cyto}$ alone or together with Myc-tagged Rap1B in pcDNA3.1 (Invitrogen) using Fugene HD (Promega). Twenty-four hours after transfection, cells were washed once in PBS and treated with 100 nM AP20187. Cells were washed with cold PBS and then lysed in the lysis buffer (50 mM HEPES, pH 7.3, 200 mM NaCl, 2 mM $MgCl_2$, 1% Triton X100, 5% glycerol, 2 mM DTT with a protease inhibitor cocktail (Roche)). The lysates were cleared by centrifugation, and the supernatant was incubated with 5 μl pre-equilibrated GST beads bound to 5 μg purified GST-RalGDS at 4ºC for 45 min. GST-beads were washed 4 times and the bound GTP-loaded Rap were eluted with the SDS-PAGE sample buffer (50 mM Tris-HCl, pH 6.8, 1% SDS, 10% glycerol, 5% ß-mercaptoethanol, 0.02% bromophenol blue) and boiled for 1 min before SDS-PAGE and Western blot analyses with an anti-Myc antibody (Cell Signaling) for transfected Myc-Rap1B or an anti-Rap1 antibody (BD Transduction) for endogenous Rap1. Loading amounts were normalized by the total protein concentrations as determined with the Bio-Rad protein assay. A fraction of the lysates

was analyzed by Western blot directly to probe the total amounts of Rap and Myr-FKBP-PlexinC1$_{cyto}$.

FRET-based RapGAP activity assays in cells

Full-length VSV-tagged PlexinB1 in pcDNA3 (Invitrogen) was obtained from Dr. Kun-liang Guan at UCSD. The Raichu-Rap and Raich-R-Ras constructs were provided by Dr. Michiyuki Matsuda at Kyoto University. Various mutations of these constructs were generated by Quickchange.

COS7 cells (~1.0 x 10^5) in Dulbecco's modified Eagle's medium (DMEM) with 10% fetal bovine serum (FBS) were plated onto 35mm glass bottom dishes (MatTek). Cells were transfected with different combinations of the plexin constructs and Raichu reporters on the next day with Fugene6 (Roche) following the manufacturer's instruction with a Fugene: plexin: Raichu ratio of 15:4:1. Two days after transfection, cells were washed with 1 ml phosphate buffered saline (PBS) and then supplied with 600 μl DMEM/F-12(1:1) medium (GIBCO) containing 25 mM HEPES but without serum or phenol red. Live imaging was performed on a DeltaVisionRT microscope equipped with a 37°C chamber and a CoolSNAP HQ CCD camera. Images were acquired using a 436/10 excitation filter together with 465/30 or 535/30 emission filters for the CFP or YFP channel, respectively. Cells with net fluorescent signal intensities over one hundred for both channels were chosen for FRET measurements. For each dish, 4-6 cells were

imaged using a 40x/1.35 oil lens and 10% neutral density filter. Images were first acquired for 2-3 min to ensure stability of the focus and fluorescence signals. Cells were then treated with Sema4D at the final concentration of ~5 nM, followed by refocusing and subsequent image acquisition. All the acquisitions were performed at 20-s interval for 6 min, with the exposure time set to 400 ms. Images were processed with the program ImageJ (Abramoff et al., 2004).

After background subtraction, an intensity threshold was chosen to define the boundary of the cell. Pixels outside of this region were set to zero intensity. For each pixel the intensity ratio between the YFP (FRET acceptor) and CFP (FRET donor) channels was calculated and taken as the FRET value (Nakamura and Matsuda, 2009). FRET images were pseudo-colored according to the FRET values. For quantification of the FRET data for each transfection combination, all the cells in each group (8-12 cells) that remained in focus during the imaging process were included. For each cell, we randomly selected 2-4 regions in the peripheral areas of the cell for quantification. Strong fluorescence signals were observed in the perinuclear regions, which likely represent Raichu-Rap localized on perinuclear membrane compartments (Ohba et al., 2003). This pool of Raichu-Rap is not accessible to plexin and was therefore excluded from the FRET analyses. The mean FRET values of the regions of interest were calculated using ImageJ. The changes in the mean FRET values with respect to that of the first time point were plotted as a function of time.

Neuron growth cone collapse assay

Dissociated rat cortical neurons were generated from E18 embryos using standard methods (Cowan et al., 2005). Dissociated neurons were cultured on poly-D-lysine- and laminin-coated glass coverslips in Neurobasal medium (Invitrogen) plus B27 supplement (Invitrogen), penicillin/streptomycin and glutamine. After dissociation in papain, and before plating, the neurons were cotransfected with pcDNA3.1-Rap1B (Q63E) or vector control together with a plasmid expressing mCherry using Lipofectamine 2000. The total amount of DNA transfected was held at 2 mg, and the titrated amount of Rap1B plasmid was balanced with empty vector (pcDNA3.1). Two days after plating (100,000 neurons/well in a 24-well plate), neurons were stimulated with Sema3A at 7.5 nM or conditioned media for 1 hour at 37°C and 5% CO_2. The neurons were then fixed in PBS supplemented with 4% paraformaldehyde and 2% sucrose for 8 min, F-actin was visualized using partial permeabilization and phalloidin-Alexa-554 (Invitrogen) as described (Cowan et al., 2005). Transfected neurons were identified by the mCherry fluorescent signal. The relative percentage of collapsed growth cones was determined under experimenter-blinded conditions using standard criteria as described (Cowan et al., 2005). Over 450 growth cones were counted for each experimental condition. Two-way ANOVA showed a significant interaction between Rap1B (Q63E) transfection and semaphorin 3A stimulation ($F_{2,12}$=287.2, $p<0.0001$). Simple main effects were determined by multiple one-way ANOVA and independent samples t-tests. One-way ANOVA of the stimulated group alone showed a significant effect of Rap1B (Q63E) transfection

($F_{2,6}$=337.2, p<0.0001). Bonferroni post hoc analyses showed significant differences between vector-only and 0.5 μg Rap1B (Q63E) transfection (p<0.001), as well as between vector-only and 1.0 μg Rap1B (Q63E) transfection (p<0.001). One-way ANOVA of the unstimulated group alone also showed that Rap1B (Q63E) transfection affected growth cone collapse ($F_{2,6}$=10.17, p<0.05); Bonferroni analysis indicated this effect was significant between vector and 0.5 μg Rap1B (Q63E) (p<0.05). Individual t-tests performed at each level of Rap1B (Q63E) transfection showed that semaphorin stimulation significantly induced growth cone collapse when cells were transfected either with vector (t_4=33.09, p<0.0001) or 0.5 μg Rap1B (Q63E) (t_4=35.36, p<0.0001).

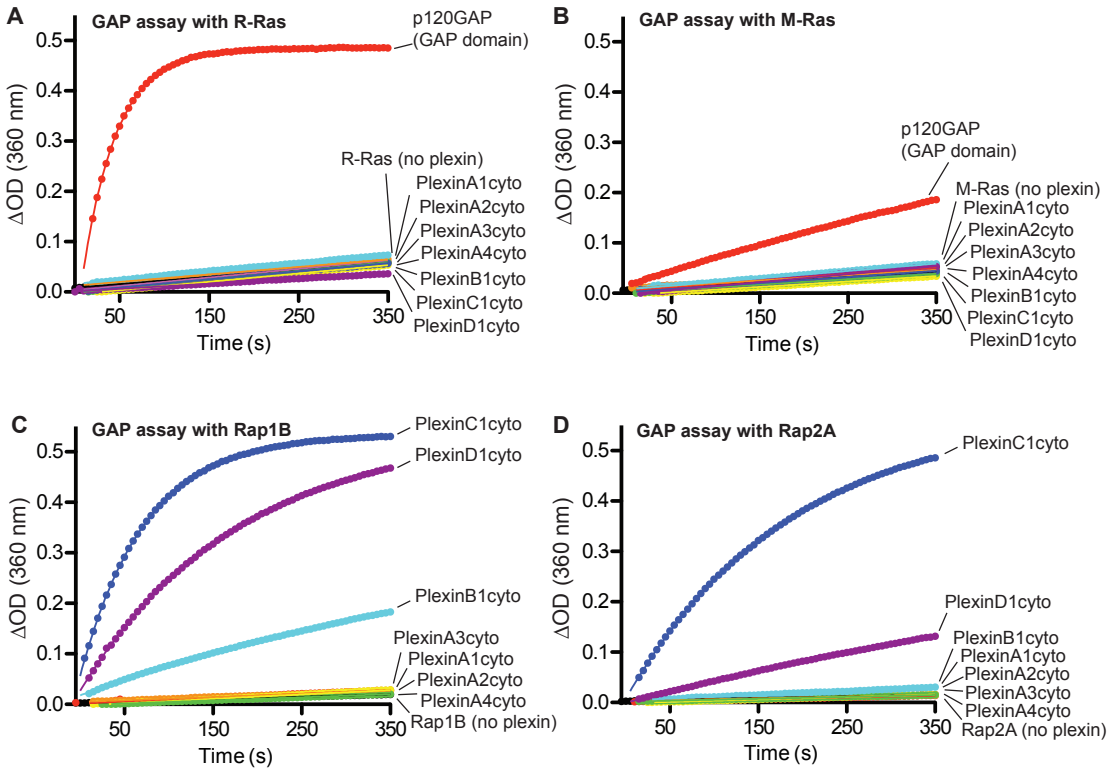

Figure 2-1 Purified plexinscyto display GAP activity for Rap but not for R-Ras or M-Ras.

(A to D) None of the tested plexins$_{cyto}$ accelerate GTP hydrolysis for R-Ras (A) or M-Ras (B). Plexins$_{cyto}$ show GAP activity towards both Rap1B (C) and Rap2A (D). Data shown are representative of at least 3 independent experiments.

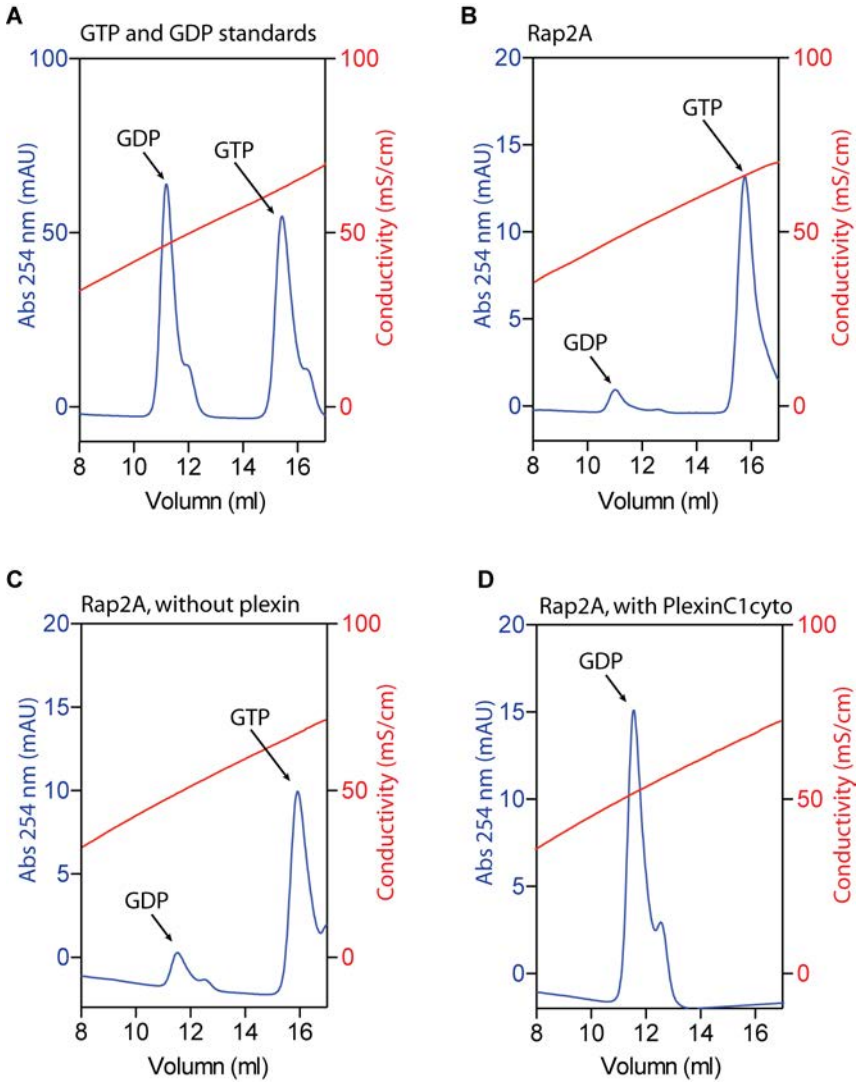

Figure 2-2. HPLC-based assay for the plexin RapGAP activity.

(**A**) Anion exchange chromatogram of GDP and GTP standards. GDP and GTP are eluted at conductivities of ~40 mS/cm and ~60 mS/cm, respectively.

(**B**) Rap2A purified from *E. Coli.* is ~90% GTP bound, perhaps due to its low intrinsic GTPase activity.

(**C**) Incubation of Rap2A at room temperature for 30 min does not change the GTP/GDP ratio.

(**D**) Incubation of Rap2A in the presence of $PlexinC1_{cyto}$ at room temperature for 30 min leads to complete hydrolysis of bound GTP to GDP.

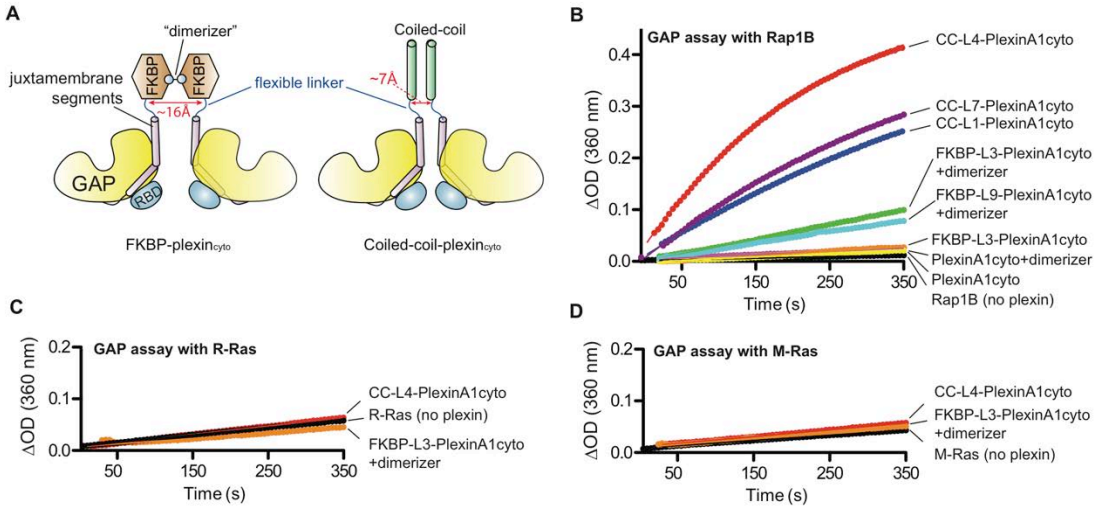

Figure 2-3 Effect of dimerization on the GAP activity of plexins$_{cyto}$.

(**A**) Schematic diagrams of the FKBP or coiled-coil plexin$_{cyto}$ fusions to enable induced or constitutive dimerization.

(**B**) The RapGAP activity of PlexinA1$_{cyto}$ is stimulated by dimerization. "+dimerizer" indicates pre-incubation of the FKBP fusions with the dimerizer.

(**C** to **D**) CC-L4-PlexinA1$_{cyto}$ and dimerized FKBP-PlexinA1$_{cyto}$ do not show GAP activity for R-Ras (C) or M-Ras (D).

Data shown are representative of at least 3 independent experiments.

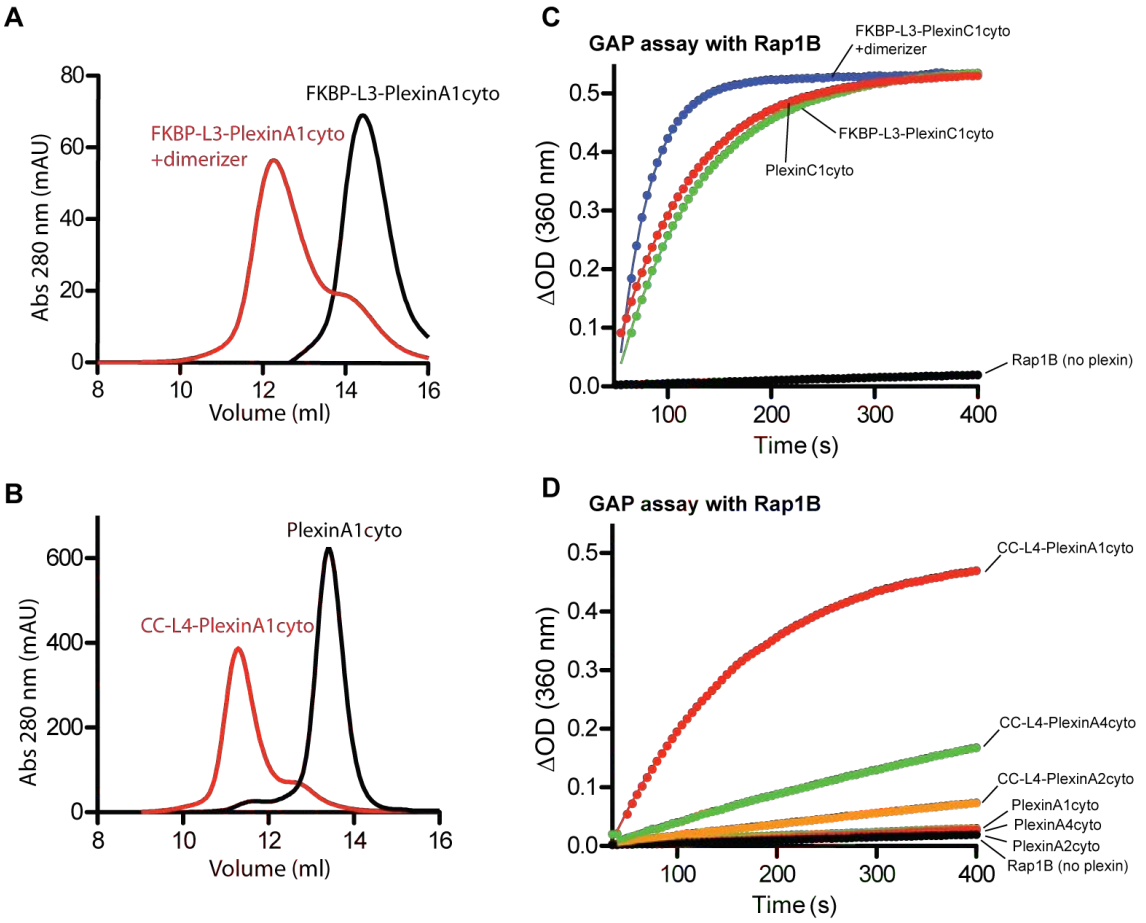

Figure 2-4 The RapGAP activity of plexins$_{cyto}$ is stimulated by induced dimerization.

(**A**) Gel filtration profiles of FKBP-L3-PlexinA1$_{cyto}$ with or without the dimerizer AP20187. (**B**) Gel filtration profiles of native PlexinA1$_{cyto}$ and CC-L4-PlexinA1$_{cyto}$. The results in (A) and (B) show that PlexinA1$_{cyto}$ is predominantly monomeric in solution, but can be induced to dimerize through the FKBP/AP20187 system or the coiled-coil dimerizer. The peak positions in (A) and (B) are not comparable because different columns were used.

(**C**) Stimulation of the RapGAP activity of FKBP-L3-PlexinC1$_{cyto}$ by dimerization.

(**D**) Coiled-coil enforced dimerization increases the RapGAP activity for PlexinA1$_{cyto}$, PlexinA2$_{cyto}$, and PlexinA4$_{cyto}$. CC-L4-PlexinA1$_{cyto}$ displays the highest degree of activation (28-fold). CC-L4-PlexinA2$_{cyto}$ and CC-L4-PlexinA4$_{cyto}$ are 3-fold and 8-fold more active than their respective native proteins. The GAP assay conditions are the same as in Fig. 1. Data shown are representative of at least 3 independent experiments.

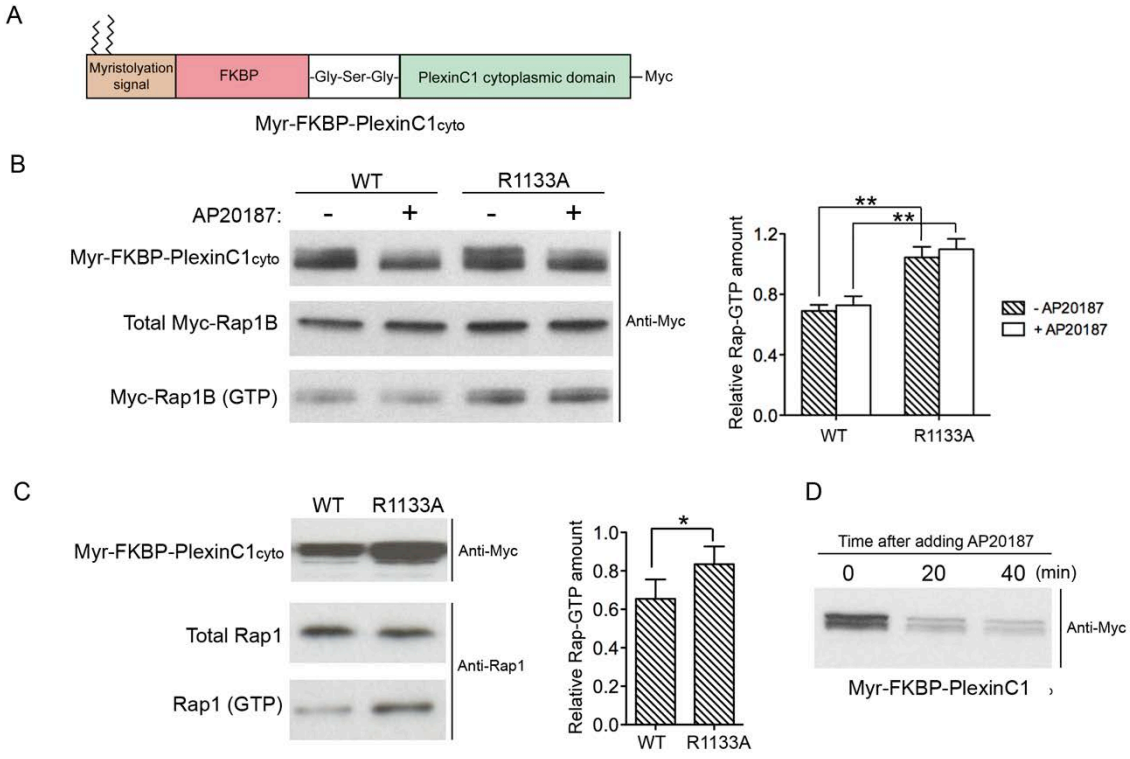

Figure 2-5 GST-RalGDS pull-down assays for the RapGAP activity of plexin in cells.

(**A**) Diagram of the construct of the membrane-localized FKBP-L3-PlexinC1$_{cyto}$ (named Myr-FKBP-PlexinC1$_{cyto}$). The myristoylation signal from the kinase Yes (residues 1-11) was fused to the N-terminus of FKBP-L3-PlexinC1$_{cyto}$ to target the protein to both plasma membrane and intracellular membranes.

(**B**) GST-RalGDS pull-down assays for transfected Myc-tagged Rap. Myc-tagged Rap1B was cotransfected with either the wild-type (WT) or the catalytically dead mutant (R1133A) of Myr-FKBP-PlexinC1$_{cyto}$ into HEK293T cells. The GST-RalGDS pull-down assay was employed to determine the amount of GTP-bound Myc-Rap1B, which was normalized to the amount of total Myc-Rap1B to calculate the relative Rap-GTP amount. Cells expressing wild-type PlexinC1 show significantly lower amounts of GTP-bound Rap1B compared with those expressing the R1133A mutant ($p<0.01$ by two-way ANOVA followed by Bonferroni post-hoc test, n = 5 experiments). Stimulation with AP20187 (the dimerizer) did not cause significant change in the amounts of GTP-bound Rap1B ($F_{1,16}=0.54$, $p=0.47$ by two-way ANOVA, n = 5 experiments). This lack of change could be because AP20187 treatment caused rapid loss of the plexin protein [shown in both (B) and (D)], and the ~3-fold increase in the RapGAP activity of FKBP-PlexinC1$_{cyto}$

as shown by our in solution assays (fig. S2C) is offset by the loss of the plexin protein. Western blots were quantified using ImageJ. Error bar: standard error of the mean. Asterisks (**) indicate statistical significance ($p<0.01$).

(**C**) GST-RalGDS pull-down assays for endogenous Rap1 in HEK293T cells. The pull-down experiments and data analysis were performed as in (B), and an anti-Rap1 antibody (BD Transduction) was used for probing endogenous Rap1. Cells expressing the wild-type PlexinC1 have decreased amounts of GTP-bound endogenous Rap1 compared to those expressing the R1133A mutant. Error bar: standard error of the mean. Western blots were quantified using ImageJ. Asterisk (*) indicates statistical significance ($p<0.05$ by Student's t-test, $n = 5$ experiments).

(**D**) Loss of the expressed Myr-FKBP-PlexinC1$_{cyto}$ protein after AP20187 stimulation. The lower band likely corresponds to the N-terminally partially degraded protein because the Myc-tag is at the C-terminus. The rapid loss of the protein after AP20187 treatment is likely due to degradation as well, the mechanism of which is not understood at present.

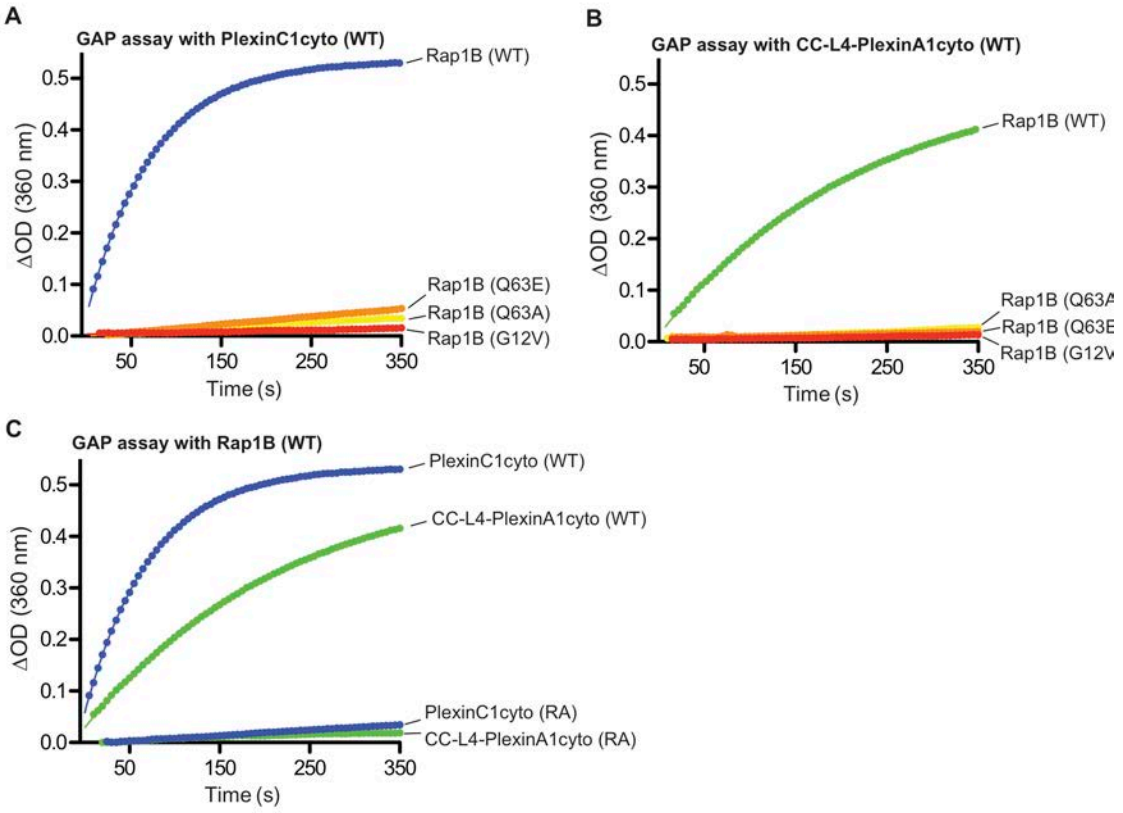

Figure 2-6 Mutational analysis of the RapGAP activity of plexins$_{cyto}$.

(**A** to **B**) The G12V, Q63A or Q63E mutation in Rap1B inhibits GTP hydrolysis catalyzed by PlexinC1$_{cyto}$ (A) or CC-L4-PlexinA1$_{cyto}$ (B).

(**C**) Mutation of the arginine finger (RA) abolishes the RapGAP activity of both PlexinC1$_{cyto}$ and CC-L4-PlexinA1$_{cyto}$.

Data shown are representative of at least 3 independent experiments.

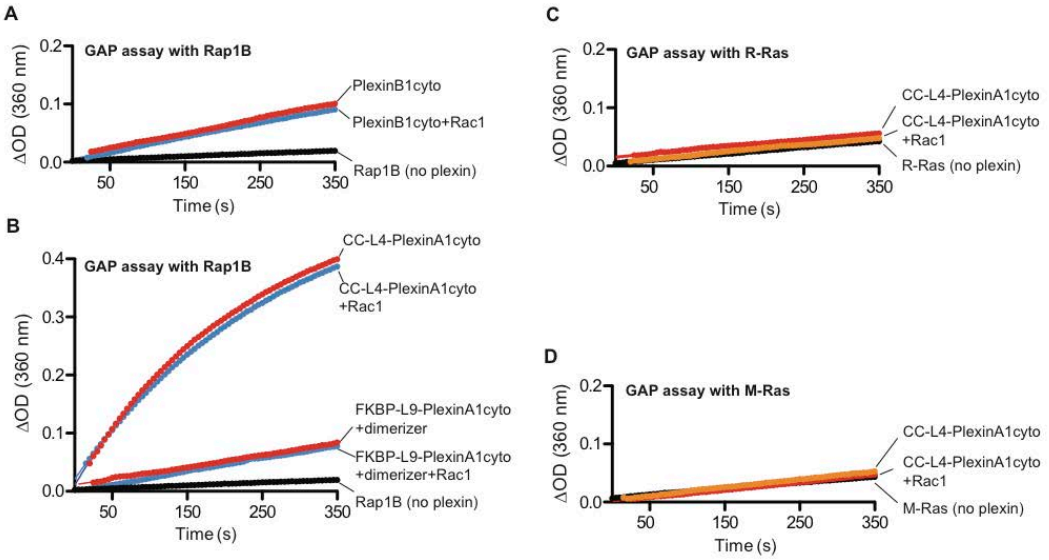

Figure 2-7 Binding of Rac1 does not affect the GAP activity of plexins$_{cyto}$

(**A**) Active Rac1 does not affect the RapGAP activity of PlexinB1$_{cyto}$. For GAP assays with Rac1, plexin proteins were incubated with GTP-loaded Rac1(Q61L) before the assays.

(**B**) Active Rac1 does not affect the RapGAP activity of dimeric PlexinA1$_{cyto}$.

(**C** to **D**) CC-L4-PlexinA1$_{cyto}$ in the presence of Rac1 remains inactive towards R-Ras (C) and M-Ras (D).

Data shown are representative of at least 3 independent experiments.

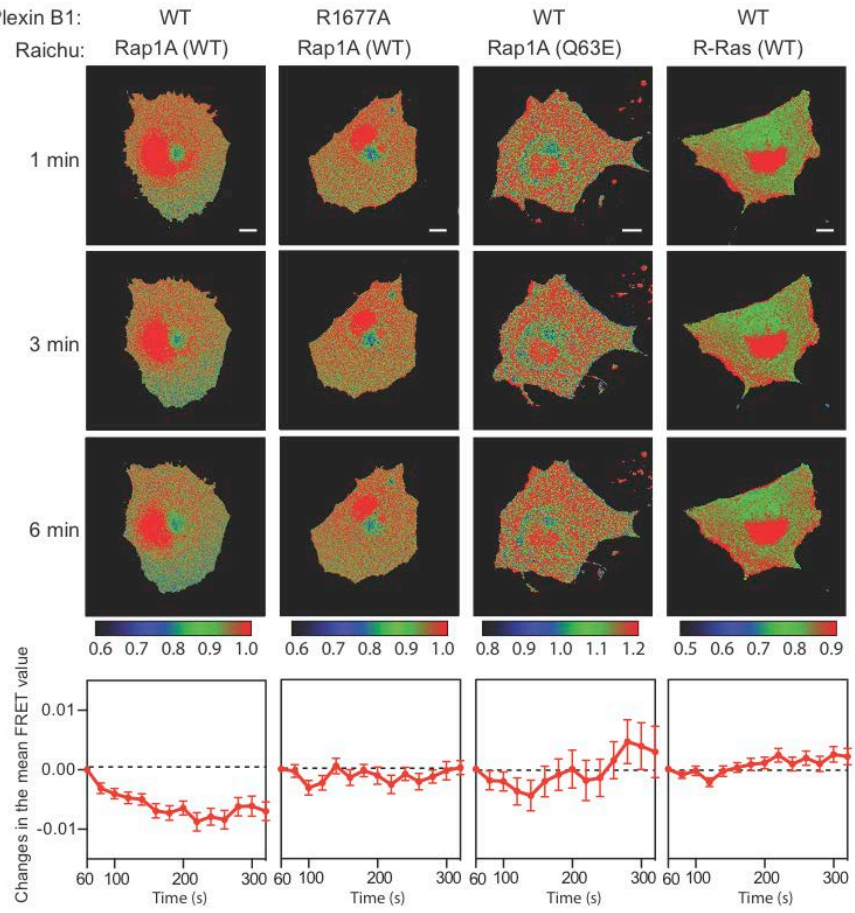

Figure 2-8 Semaphorin activates the RapGAP activity of full-length PlexinB1 in cells.

FRET images were recorded after semaphorin treatment of the cells transfected with the combinations of plasmids as indicated at the top panel. Each column contains three time-lapse images of one representative cell for each transfection combination. Scale bars: 10 μm. The images are pseudo-colored based on the FRET value of each pixel. The calibration bars for the coloring schemes are shown below each column. In the bottom panels, the changes in the mean FRET value of all the imaged cells in each group are plotted as a function of time. The plots are combined data from at least 3 independent experiments (n = 8~12 cells). Error bars represent standard error of the mean.

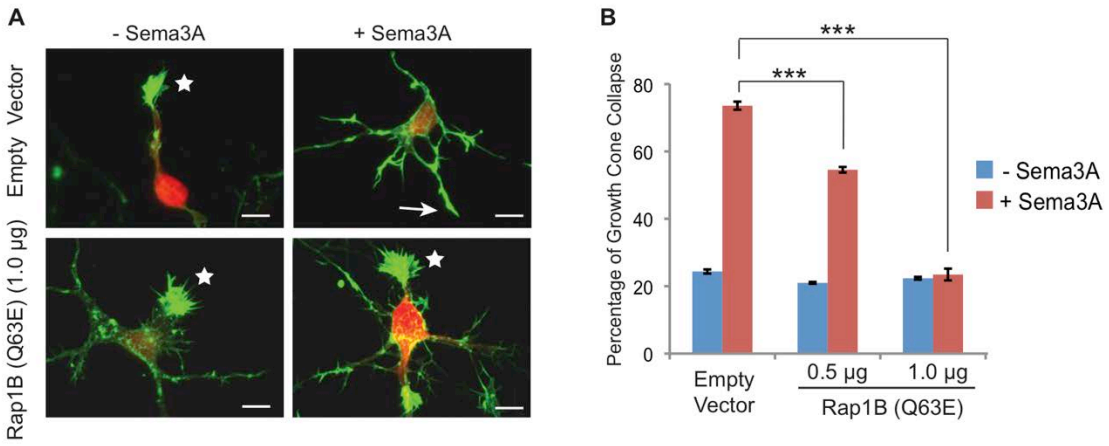

Figure 2-9 The RapGAP activity of plexin is required for semaphorin induced neuronal growth cone collapse.

(A) Representative images of semaphorin-induced growth cone collapse of rat cortical neurons. Growth cone morphology was visualized by staining of F-actin with Alexa-554 conjugated phalloidin (green). Transfected neurons were identified based on the mCherry fluorescence signal (red). Uncollapsed and collapsed growth cones are indicated by stars and arrows, respectively. Scale bars: 10 µm.

(B) Quantification of growth cone collapse of the neurons that are transfected with empty vector or various amounts of Rap1B Q63E mutant. Error bars represent standard error of the mean. Asterisks (***) indicate significant differences ($p<0.001$) determined by analysis of variance (ANOVA) followed by Bonferroni post-tests.

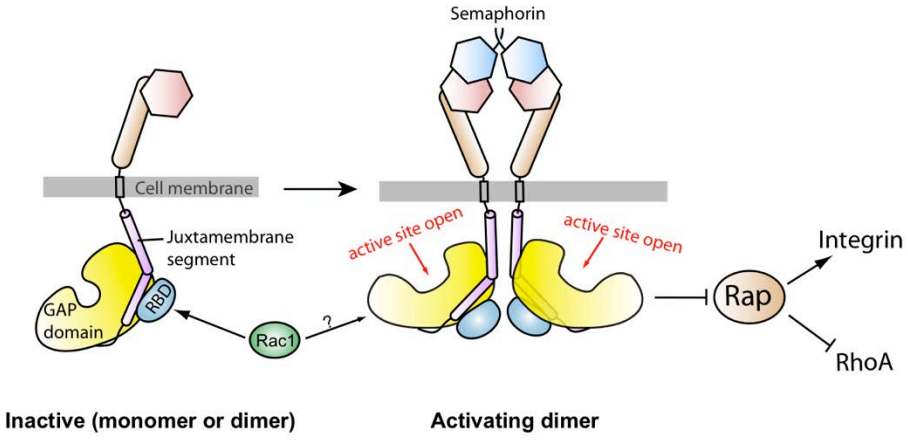

Figure 2-10 A schematic model for the regulation of the RapGAP activity of plexin.

Prior to semaphorin binding, plexin is an inactive monomer or dimer, in which the RapGAP activity is autoinhibited. Semaphorin-induced dimerization of the plexin extracellular region promotes formation of the activating dimer of the cytoplasmic region, which converts the GAP domain to the active state through an allosteric mechanism. Rac1 or other activator RhoGTPases are not involved in this allosteric activation process, and their roles in plexin activation are not clear. Plexin inactivates Rap to promote neuronal growth cone collapse and other changes in cell morphology, which may rely on the ability of Rap to regulate cell adhesion and cytoskeleton dynamics through integrin and RhoA, respectively.

CHAPTER THREE

Crystal structure of the active dimer of plexin

Screening of the coiled-coil-plexin$_{cyto}$ fusion constructs for optimal induction of the active dimer

Our previous study has shown that the RapGAP activity of the cytoplasmic region of plexins (plexins$_{cyto}$) can be activated by fusing it to the coiled-coil motif of GCN4 through a flexible linker of various lengths (Wang et al., 2012). To elucidate the structural basis for the dimerization-driven activation, we carried out extensive crystallization trials of these coiled-coil induced dimers of plexins$_{cyto}$. These efforts have all failed, presumably due to the flexibility of the linker. We therefore removed the linker and directly fused the coiled-coil with the juxtamembrane helix (the N-terminal helix in the juxtamembrane segment) of plexin$_{cyto}$ (Figure 3-1A). Assuming the coiled-coil motif and the juxtamembrane helix of plexin merge into a continuous helix, varying the relative register between them by adding or removing residues at the junction can result in dramatically different relative orientations between the two plexin monomers in the induced dimer. Without knowing the ideal arrangement of the two monomers for active dimer formation, we systematically tested fusing plexin$_{cyto}$ to each of the seven unique positions on the heptad repeat of the coiled-coil (Figure 3-1A). We used mouse PlexinA1$_{cyto}$ as a model system for the screening experiments, because it displayed the

highest level of activation by the coiled-coil induced dimerization in our previous study (Wang et al., 2012). We chose Ala1272, located near the N-terminus of the juxtamembrane helix in PlexinA1$_{cyto}$, as the reference for naming the fusion constructs. These constructs are referred to as CC(x)PlexinA1$_{cyto}$, in which "x" indicates the position of Ala1272 in PlexinA1 on the heptad repeat (Figure 3-2).

GAP activity assays showed that all these dimer constructs are substantially more active than the monomer (Figure 3-1B). Remarkably, CC(a)PlexinA1$_{cyto}$, CC(d)PlexinA1$_{cyto}$ and CC(g)PlexinA1$_{cyto}$, which confer in general similar inter-monomer orientations, achieve much higher activation levels than CC(b)PlexinA1$_{cyto}$, CC(c)PlexinA1$_{cyto}$, CC(e)PlexinA1$_{cyto}$ and CC(f)PlexinA1$_{cyto}$ (Figure 3-1B). The same trend of activation levels was also observed for the coiled-coil fusions of zebrafish PlexinC1$_{cyto}$ (Figure 3-1C and Figure 3-2). These results further support the notion that a specific association mode between the two plexin monomers is required for optimal dimerization-induced activation (Wang et al., 2012).

Overall structure of the PlexinC1$_{cyto}$ active dimer

We crystallized the highly active zebrafish CC(a)PlexinC1$_{cyto}$ and determined the structure at 3.3 Å resolution (Table 1). The two plexin monomers in the asymmetric unit form a symmetric side-by-side dimer (Figure 3-3A). The two juxtamembrane helices are oriented approximately in parallel, extending well beyond the main body of the proteins and integrating into the C-termini of the coiled-coil moiety. On the plasma membrane,

this configuration of the plexin dimer orients the active sites of both GAP domains toward the membrane surface and leaves sufficient space for binding of the membrane anchored Rap substrate. The same active dimer is also seen in the structure of the complex between Rap and PlexinC1$_{cyto}$ without the coiled-coil fusion solved by Heath Pascoe in the lab (Wang et al., 2013) (Figure 3-4), supporting that it represents the active state of plexins and is not a coiled-coil induced artifact.

The coiled-coil dimer in the CC(a)PlexinC1$_{cyto}$ structure is nearly identical to the isolated coiled-coil structures reported previously (O'Shea et al., 1991). Extending down from the coiled-coil moiety, the N-terminal portion of the juxtamembrane helix (residues 553-566) does not mediate any inter-molecular interactions. This part of the juxtamembrane helix likely has some flexibility to compensate for deletion or insertion of one residue at the junction between the coiled-coil and the juxtamembrane helix, allowing several constructs to induce the active dimer and achieve similarly high activation levels (Figure 3-1, B and C). Further deletion or insertion at the junction probably cannot be accommodated without severe distortion of the juxtamembrane helix, explaining the much lower activation levels of those constructs (Figure 3-1, B and C).

Interactions in the dimer interface

The dimer interface is formed by the juxtamembrane helix and one side of the GAP domain, burying a total of ~3500 Å^2 surface area (Figure 3-3A-C). The RBDs in the two monomers are far away from each other and not involved in dimer formation. The

center of the dimer interface is a 4-helix bundle structure comprised of the C-terminal portion of the juxtamembrane helix (residues 567-584) and the N-terminal portion of helix 11 in the GAP domain (residues 929-943) from each monomer (Figure 3-3C). The core of the 4-helix bundle is dominated by hydrophobic interactions, involving residues Ile571, Ile575, Phe579 and Leu582 from the juxtamembrane helix and Met933, Ile936 and Leu939 from helix 11 (Figure 3-3C). The core interface is supported by peripheral electrostatic interactions mediated by Arg572, Arg576 and Asp581 from the juxtamembrane helix and Glu770, Glu932, and Lys937 from the GAP domain (Figure 3-3B). A loop-helix segment (residues 1038-1058) between helix 15 and 17 in the GAP domain of each monomer wraps around the C-terminal portion of the 4-helix bundle. The interactions involve Leu1045, Lys1047, Leu1054, Leu1055, and Lys1058 in the loop-helix segment and Phe579, Gln583, Thr584 and Leu939 from the 4-helix bundle (Figure 3-3B). We call the loop-helix element "the activation segment" since it functionally resembles the activation segment in protein kinases and plays a major role in regulating the GAP activity (see below) (Huse and Kuriyan, 2002).

Dimerization induced conformational changes that lead to GAP activation.

Comparisons of the dimer structure with previously determined structures of plexins$_{cyto}$ reveal several substantial conformational differences (Bell et al., 2011; He et al., 2009; Tong et al., 2009; Wang et al., 2012). The most striking difference is in the juxtamembrane helix (Figure 3-5A). Except in one of the PlexinB1 structures where it is

disordered (Bell et al., 2011), the juxtamembrane helix in all other previous structures adopts a kinked conformation, with both the N- and C-terminal halves interacting with the GAP domain (He et al., 2009; Tong et al., 2009; Wang et al., 2012). In the active dimer structure, the last 2 turns in the juxtamembrane helix (residues 584-591, corresponding to residues 1281-1288 in mouse PlexinA3) convert to an extended loop. This loop and the following segment use Asp588, Leu589, Asp591 and Val593 to make a distinct set of intra-molecular interactions with the GAP domain (Figure 3-5B). The remaining N-terminal helical portion (residues 553-584) adopts a straight conformation and rotates by ~90º in relation to the inactive structures (Figure 3-5A) to mediate the formation of the 4-helix bundle at the center of the dimer interface (Figure 3-3, B and C). Helix 11 undergoes a small tilt to accommodate the juxtamembrane helix from the dimer partner, and the top part (residues 929-934) adopts a 3_{10} helix like conformation to pack Met933 against the hydrophobic core of the 4-helix bundle (Figure 3-6 and Figure 3-3C)

The conformational changes in the juxtamembrane helix and helix 11 are coupled to changes in the activation segment. In all the previously reported structures of $plexins_{cyto}$, the highly conserved helical portion of the activation segment adopts essentially the same "closed" conformation (Figure 3-8A and Figure 3-10C). An asparagine residue in the helix (Asn1774 in mouse PlexinA3) is invariably hydrogen bonded with a conserved aspartate (Asp1758 in PlexinA3) in helix 15. A proline residue (Pro1772 in PlexinA3) at the N-terminus of the helix acts as a lid that covers the asparagine and blocks its access to the incoming Rap substrate (Figure 3-7A). Docking

Rap to PlexinA3 based on the PlexinC1/Rap complex structure results in a number of clashes between Rap and the activation segment (Figure 3-7B). The proline "lid" (Pro1772) sterically clashes with Tyr40 in Rap, while the carbonyl oxygen on the sidechain of Asn1774 makes an unfavorable contact with the sidechain of Asp38 in Rap (Figure 3-7B). The loop portion of the activation segment appears to be rather flexible, as it displays high B-factors in PlexinA3 (PDB ID: 3IG3) and the PlexinB1/Rac1 complex (PDB ID: 3SU8) and is partially disordered in apo-PlexinB1 (PDB ID: 3HM6) and the PlexinA1/Rac1 complex (PDB ID: 3RYT) (Bell et al., 2011; He et al., 2009; Tong et al., 2009; Wang et al., 2012) (Figure 3-8A). The loop likely samples many conformations, some of which may impose additional hindrance on Rap binding.

In contrast, the activation segment in the active dimer adopts an open conformation and shifts away from the GAP active site (Figure 3-7A and Figure 3-9). This shift appears to be induced by the interactions between the activation segment and the 4-helix bundle in the dimer interface (Figure 3-7A). The outward shift pulls Asn1052 (Asn1774 in PlexinA3) away from Asp1036 (Asp1758 in PlexinA3), precluding hydrogen bond formation. Pro1050 in the dimer structure also moves outward by ~3 Å compared to Pro1772 in PlexinA3 (Figure 3-7A). The activation segment in the structure of the PlexinC1/Rap complex adopts a similar open conformation (Figure 3-8B), with Pro1050, Asn1052 and Lys1053 making critical interactions with Rap. Therefore, a major mechanism in the dimerization-induced activation of plexins appears to be the outward shift of the activation segment, which opens the otherwise inaccessible active site to

allow Rap binding and catalysis of GTP hydrolysis (Figure 3-7, B and C). The activation segment in the PlexinC1/Rap complex appears to be slightly more closed than that in the coiled-coil-induced PlexinC1 dimer (Figure 3-8B), bringing Pro1050 against the Tyr40 of Rap for Van der Waals interactions. The Asn1052 sidechain conformation is also slightly shifted in order to form hydrogen bonds with residues in Rap. These differences indicate that the active dimer promotes a conformation of the GAP domain that is more open than required for accommodating Rap. Binding of Rap induces a slight closure of the active site for optimal interactions and catalysis of GTP hydrolysis.

Conformation of the RBD and GAP distal subdomain

The RBD in the active dimer does not undergo any notable conformational changes, although its orientation relative to the GAP domain is shifted compared to the previous structures (Figure 3-11). The juxtaposition between the RBD and the GAP is also different in the PlexinC1/Rap complex structure where plexin forms the same active dimer (Figure 3-11). Given these observations and the fact the RBD is not involved in the dimer interface or Rap binding, the differences likely reflect the flexibility between the RBD and the GAP domain and are not relevant to the activation mechanism. The subdomain composed of the first three and the last two helices in the GAP domain also shows some conformational differences that are likely due to flexibility (Figure 3-11). This subdomain in p120GAP is dispensable for the GAP activity (Scheffzek et al., 1997).

Mutational analysis of the active dimer structure

We performed extensive mutational analyses to test the activation mechanism revealed by the PlexinC1 dimer structure. Arg576, Asp581, Asp588, Val593 and Met933 are involved in the dimer interface or intra-molecular interactions that stabilize the new conformation of the juxtamembrane segment (Figure 3-3, B and C and Figure 3-5B). In the inactive monomer structures, residues at these positions are surface exposed and do not make any interactions (Figure 3-10, A and B). We made the R576E, D581K, D588K, V593E and M933E single mutations in CC(a)PlexinC1$_{cyto}$. The GAP assay showed that R576E, D581K, D588K and M933E strongly impaired dimerization-induced activation (Figure 3-12A). The deleterious effect of V593E on GAP activation is weaker but clearly observable at a lower plexin concentration (Figure 3-12C). To test the coupling between the dimerization and the conformation of the activation segment, we designed several mutations, including Q583A, T584A, L1045A, K1047A, L1054A, to disrupt the interactions between the activation segment and the juxtamembrane helix from the dimer partner (Figure 3-7A). The GAP assay showed that while K1047A modestly decreased dimerization-induced GAP activation, L1054A, L1045A and T584A greatly reduced the activation (Figure 3-12, B and C).

We further examined the activation mechanism by using a functional assay for plexins, which assesses their ability to induce COS7 cell collapse upon semaphorin stimulation (Takahashi et al., 1999). Since the ligand for zebrafish PlexinC1 was not available, mouse PlexinA3 and its ligand Sema3F were used in the collapse assays (He et

al., 2009). The K1273E, E1278R, E1285R and M1290E mutations of mouse PlexinA3, corresponding to R576E, D581K, D588K and V593E of zebrafish PlexinC1 respectively, all significantly impaired plexin-mediated COS7 cell collapse (Figure 3-12, D and E). A previous study identified a large panel of mutations that abolished PlexinB1-mediated COS7 cell collapse (Bell et al., 2011). These mutations were designed to test the model of plexin activation by Rac1-induced oligomerization. The results are also consistent with the activation mechanism shown here, as most of the mutated resides are conserved in zebrafish PlexinC1 and are involved in formation of the active dimer (Figure 3-10, B and C). In addition, mutations of highly conserved residues in the dimer interface have been identified in cancer patients, including R2040W in PlexinB1 (Gui et al., 2011) (corresponding to Lys1058 in zebrafish PlexinC1) and R1680Q/W in PlexinA2 (Network, 2012) (corresponding to Lys937 in zebrafish PlexinC1). Both of these mutations likely prevent formation of the active dimer of plexins.

Discussions and future directions

Most of the residues involved in stabilizing the active dimer are conserved across the plexin family from different species (Figure 3-10A-C), supporting that all plexins use this mechanism for activation. This study together with the previous structures of the plexin extracellular regions (Janssen et al., 2012; Janssen et al., 2010; Liu et al., 2010; Nogi et al., 2010) establishes a framework for understanding how the semaphorin-bound plexin extracellular region triggers activation of the cytoplasmic GAP domain for signal

transduction (Figure 3-13). Conformational changes similar to that undertaken by the plexin GAP domain may serve as On/Off switches for other structurally related GAPs such as CAPRI, which is also activated by dimerization (Dai et al., 2011). In addition to activation of the GAP, the active dimer-induced structural rearrangements may underlie the activation state-selective binding of plexins by signal transducers such as FARP2 (FERM, RhoGEF and pleckstrin homology protein 2) and MICAL (molecule interacting with CasL) (Schmidt et al., 2008; Toyofuku et al., 2005). The structures of the several extracellular membrane-proximal domains and the transmembrane helix of plexins have not been determined. Our data suggest that, upon semaphorin-induced dimerization, these domains are arranged precisely to ensure the proper juxtaposition of the juxtamembrane helix for inducing the formation of the active dimer of the cytoplasmic domain (Figure 3-13). Future work on these domains in the active dimeric state will fill in the missing links, leading to a complete structural model of semaphorin-activated plexin.

RhoGTPases including Rac1 and Rnd1 are suggested to be involved in activation of plexins, the mechanisms of which have remained a mystery. Docking Rac1 to the RBDs of the active dimer structure based on the known plexin/Rac1 complex shows that Rac1 can interact with the active dimer without any steric hindrance (Figure 3-14). In addition, this model places several positively charged residues in Rac1 against the cytosolic side of the plasma membrane (Figure 3-14), which is enriched in negatively charged lipids such as phosphatidylserine and Phosphatidylinositol 4,5-bisphosphate. We speculate that Rac1 may bind to the RBDs in the active dimer and, through electrostatic

interactions with the membrane, stabilize the active dimer conformation and thereby promoting the activation of plexin. This model could be tested by future studies using in vitro reconstituted lipid vesicle or bilayers.

Materials and Methods

Protein Expression

The human Rap1B construct (residues 2-167) in a modified pET28 vector (Novagen) that encodes a N-terminal His_6-tag and a recognition site for the human rhinovirus C3 protease has been described previously (Wang et al., 2012). The proteins were expressed in the bacteria strain BL21 (DE3) and purified as described previously (Wang et al., 2012). The coding region for the zebrafish $PlexinC1_{cyto}$ (residues 552-1147) was synthesized (GenScript) based on the gene bank entry XM685667.4. The GCN4 coiled-coil domain was fused to the N-terminus of the $PlexinC1_{cyto}$ by PCR. The fusion was subcloned into another modified pET28 vector containing a N-terminal tandem His_6-SUMO-tag (Wang et al., 2012). Quikchange (Stratagene) was used to alter the residues at the junction between the coiled-coil and PlexinC1. The coiled-coil fusion constructs of mouse $PlexinA1_{cyto}$ were cloned by using similar procedures. Mutants of coiled-coil PlexinC1 were generated by Quikchange reactions (Stratagene). The protein were expressed in the bacteria strain ArcticExpress (Stratagene) and purified as described previously (He et al., 2009; Wang et al., 2012). The His_6-SUMO-tag was removed by treatment with the SUMO-specific protease Ulp1.

In vitro GAP assays

For analyzing various structure-based mutations of CC(a)PlexinC1, the single turnover GAP assay was used (Wang et al., 2012; Webb and Hunter, 1992). The

concentration of PlexinC1 in the assays shown in Figure 3-12C was 0.25 μM. In all other assays, the concentration of PlexinC1 was 2 μM. The concentration of Rap1B-GTP was 120 μM. For determining the activation levels of the CC(x)Plexins$_{cyto}$ constructs, the initial reaction rate V_0 was measured at different Rap-GTP concentrations ([S]) (Table 2). Fitting the data to the Michaelis-Menten equation ($V_0 = (V_{max} [S])/ (K_M + [S])$) suggested that the Rap-GTP concentrations used (25-150 μM) were far below K_M (> 1 mM). For plexin constructs exhibiting low GAP activity, V_0 was determined by linear fitting of the initial period of the reaction (5~8 minutes) when less then 10% of Rap-GTP had been hydrolyzed. After subtraction of the baseline rate from reaction without plexin, the k_{cat}/K_M value of each construct was estimated by fitting the data to the equation $V_0 = (k_{cat}/K_M) [E][S]$ (when $[S] << K_M$), where [E] is the total plexin concentration. For plexin constructs with high GAP activity, single turn-over reaction curves measured at different Rap-GTP concentrations were baseline-subtracted and simultaneously fitted to the single exponential equation: $A(t) = (A_{max} - A_{min}) (1- \exp (-kt)) + A_{min}$, where $k = (k_{cat}/K_M)[E]$. In the fitting k was treated as a global parameter. The plexin and Rap concentrations and the analysis methods used are listed in Table 2.

Crystallization, structure determination and analyses

Mouse CC(d)PlexinA1, CC(g)PlexinA1, zebrafish CC(d)PlexinC1 and CC(a)PlexinC1 were subjected to crystallization trials. CC(a)PlexinC1$_{cyto}$ at 8 mg/ml crystallized initially at 20° C in 0.1M Bicine, pH 9.0, 20% PEG 6,000 in sitting-drop 96-

well plates. Larger crystals were grown by sitting-drop vapor diffusion at 20° C in 0.1M Bis-Tris propane, pH 9.1, 21% PEG 6,000. Crystals were cryo-protected using the crystallization solution supplemented with 25% glycerol and flash cooled in liquid nitrogen. Diffraction data were collected at 100 K on beamline 19ID at the Advanced Photon Source (Argonne National Laboratory). Data were indexed, integrated and scaled by using HKL2000 (Otwinowski and Minor, 1997). A 3.3 Å dataset in the $P2_12_12_1$ space group was collected. The structure of the GAP domain of mouse PlexinA3 (PDB ID: 3IG3) was used as the molecular replacement search model using the Phaser module in the Phenix package (Adams et al., 2002; Mccoy et al., 2007). Model building and iterative refinement was carried out using the Phenix and Coot programs (Adams et al., 2002; Emsley and Cowtan, 2004). MolProbity was used for comprehensive validation of the final model (Chen et al., 2010). The detailed statistics of data collection and refinement are included in Table 1. All the structural superimpositions shown in the figures were based on helices 13, 14 and 15 in the plexin GAP domain, because they are at the center of the GAP active site and adopt highly similar conformations in all the plexin structures. Molecular surface area was calculated using the get_area function in PyMOL (the PyMOL Molecular Graphics System, Schrodinger). Structure figures were generated in PyMOL. Sequence alignments were rendered by using ESPript (Gouet et al., 1999).

COS7 cell collapse assay

The COS7 cell collapse assay using full-length mouse PlexinA3 was performed as described previously (He et al., 2009). Mutants of PlexinA3 corresponding to those of zebrafish PlexinC1$_{cyto}$ tested in the GAP assay were designed based on a sequence alignment of the two proteins. COS7 cells were plated on 6-well plates one day before transfection at 1.0 x 10^5 cells/well. For each well, 1 μg of PlexinA3 and 0.5 μg of Neuropilin2 plasmids were transfected using FuGENE 6 (Promega) according to the manufacture's instructions. Two days after transfections, cells were treated with 5 nM alkaline phosphatase-tagged Sema3F for 25 minutes at 37ºC. Cells were then washed, fixed and stained with BCIP/NBT alkaline phosphatase substrate (Sigma) after heat inactivation of endogenous phosphatase at 65ºC for 1 hour. Transfection, treatment, imaging and counting of cells were performed in a blind fashion. Representative images of cells are shown in Figure 3-12E.

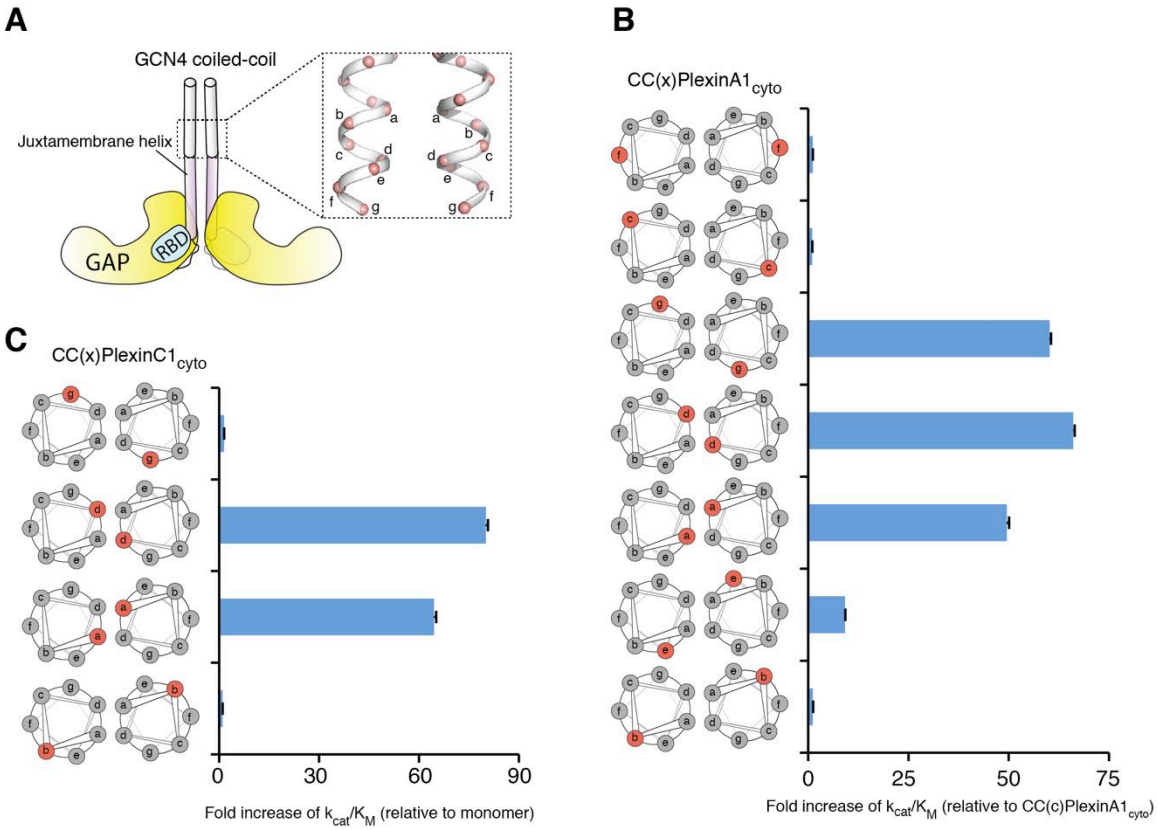

Figure 3-1. Activation of the plexin GAP by the coiled-coil fusion.

(**A**) Diagram of coiled-coil fusions of plexin$_{cyto}$.

(**B**) GAP activity of the coiled-coil fusions of mouse PlexinA1$_{cyto}$. The red color on the helical wheel diagrams indicates the position of Ala1272 in PlexinA1 on the heptad repeat of the coiled-coil, which corresponds to the "x" in CC(x)Plexin$_{cyto}$. Activity of monomeric PlexinA1$_{cyto}$ is too low to be measured reliably, therefore the fold increase of k_{cat}/K_M is calculated relative to CC(c)PlexinA1$_{cyto}$, which is the least active among the dimers but approximately 10-fold more active than the monomer.

(**C**) GAP activity of the coiled-coil fusions of zebrafish PlexinC1$_{cyto}$. The red color on the helical wheel diagrams indicates the position of Gln553 in zebrafish PlexinC1 on the heptad repeat of the coiled-coil. In both (**B**) and (**C**) error bars represent standard error of the k_{cat}/K_M.

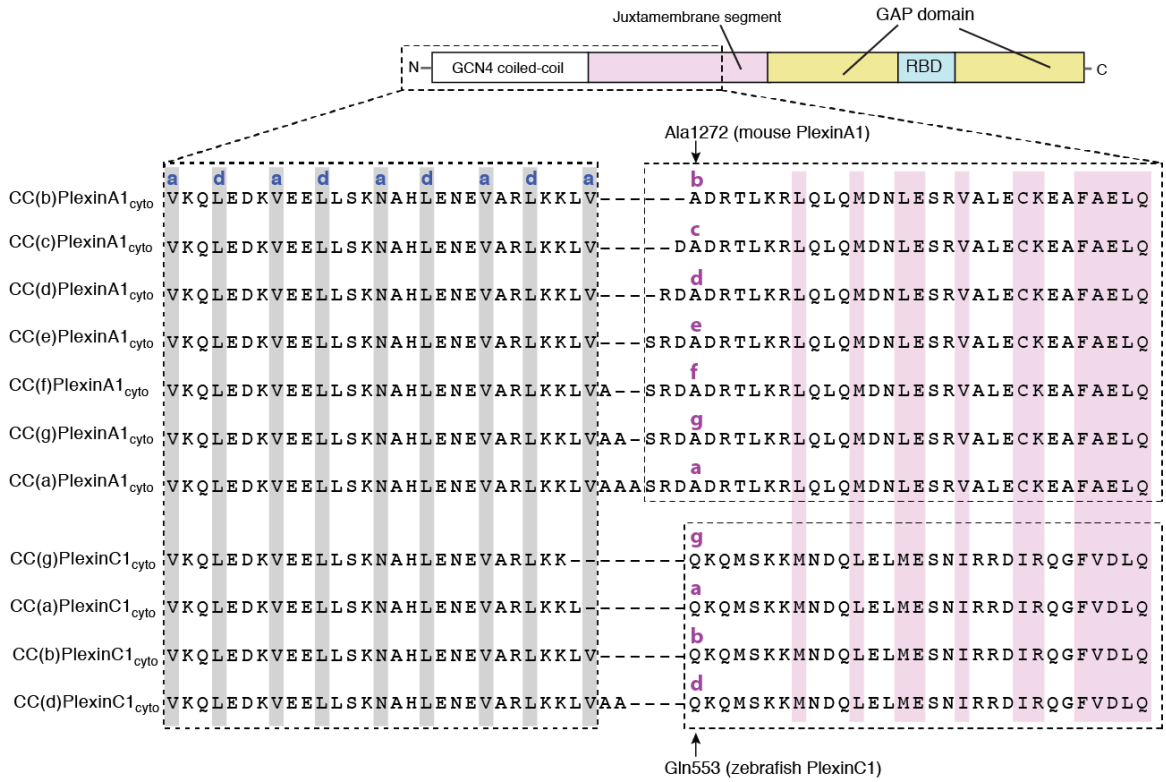

Figure 3-2. Design of the coiled-coil fusions of mouse PlexinA1$_{cyto}$ and zebrafish PlexinC1$_{cyto}$.

The "a" and "d" positions in the coiled-coil sequence that mediate the dimer formation are highlighted in gray. The sequences of the juxtamembrane segments from mouse PlexinA1$_{cyto}$ and zebrafish PlexinC1$_{cyto}$ are aligned. Residues at the active dimer interface are highlighted in pink. The positions of Ala1272 in mouse PlexinA1 and Gln553 in zebrafish PlexinC1 on the heptad repeat are labeled and designated as the "x" in "CC(x)Plexin$_{cyto}$".

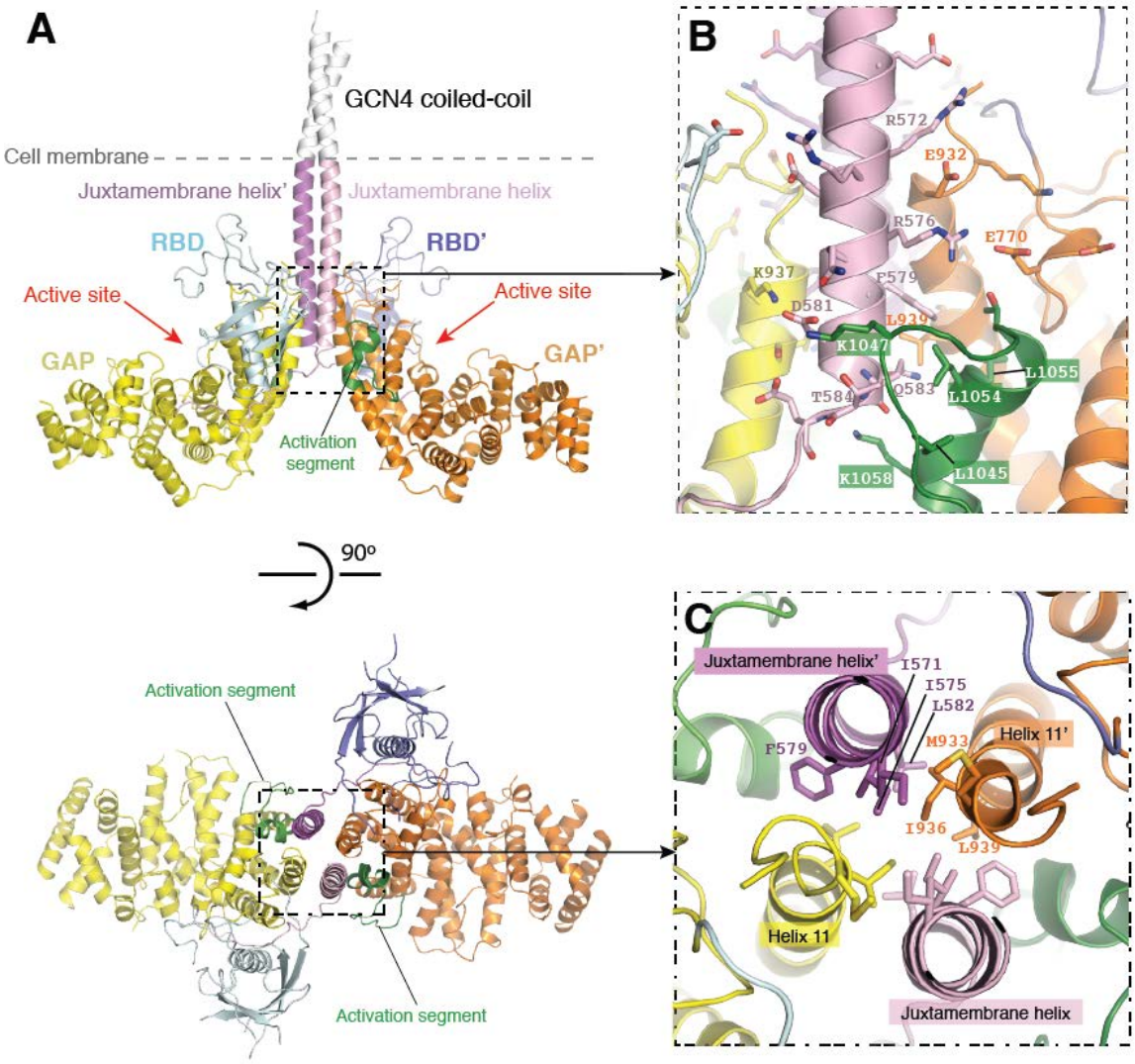

Figure 3-3. Structure of the active dimer of zebrafish CC(a)PlexinC1$_{cyto}$.

(**A**) Overall structure. In the bottom panel the coiled-coil moiety is removed for clarity.
(**B**) Interactions at the periphery of the dimer interface.
(**C**) Hydrophobic core of the dimer interface. Only residues on one monomer are labeled for clarity.

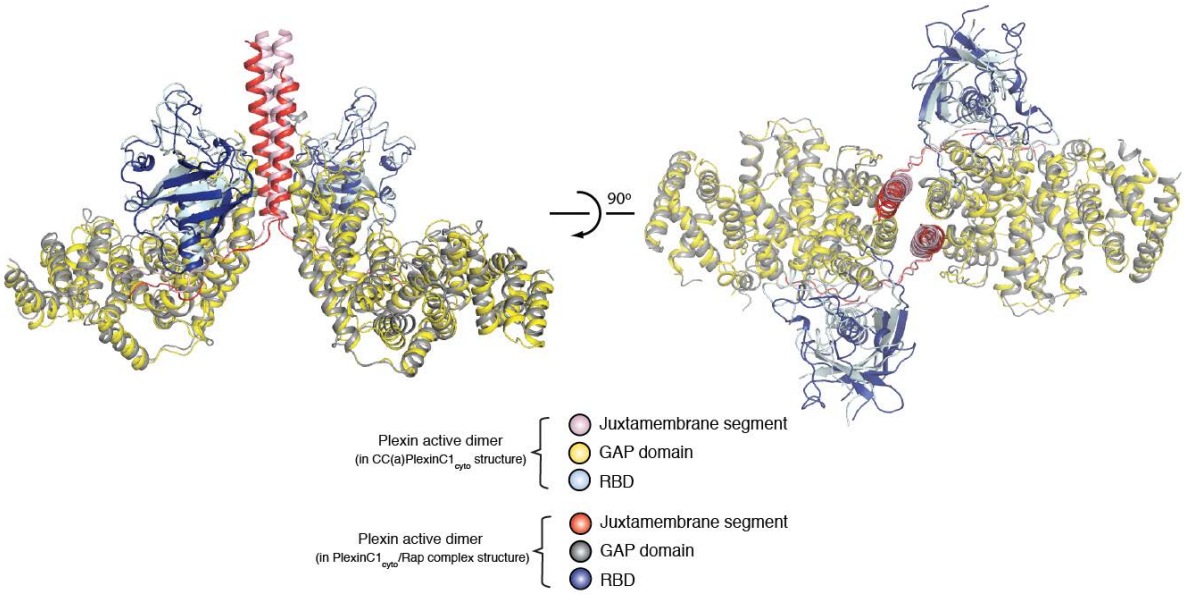

Figure 3-4. Superimposition of the coiled-coil induced active dimer of PlexinC1$_{cyto}$ and the active dimer in the PlexinC1$_{cyto}$/Rap complex structure.

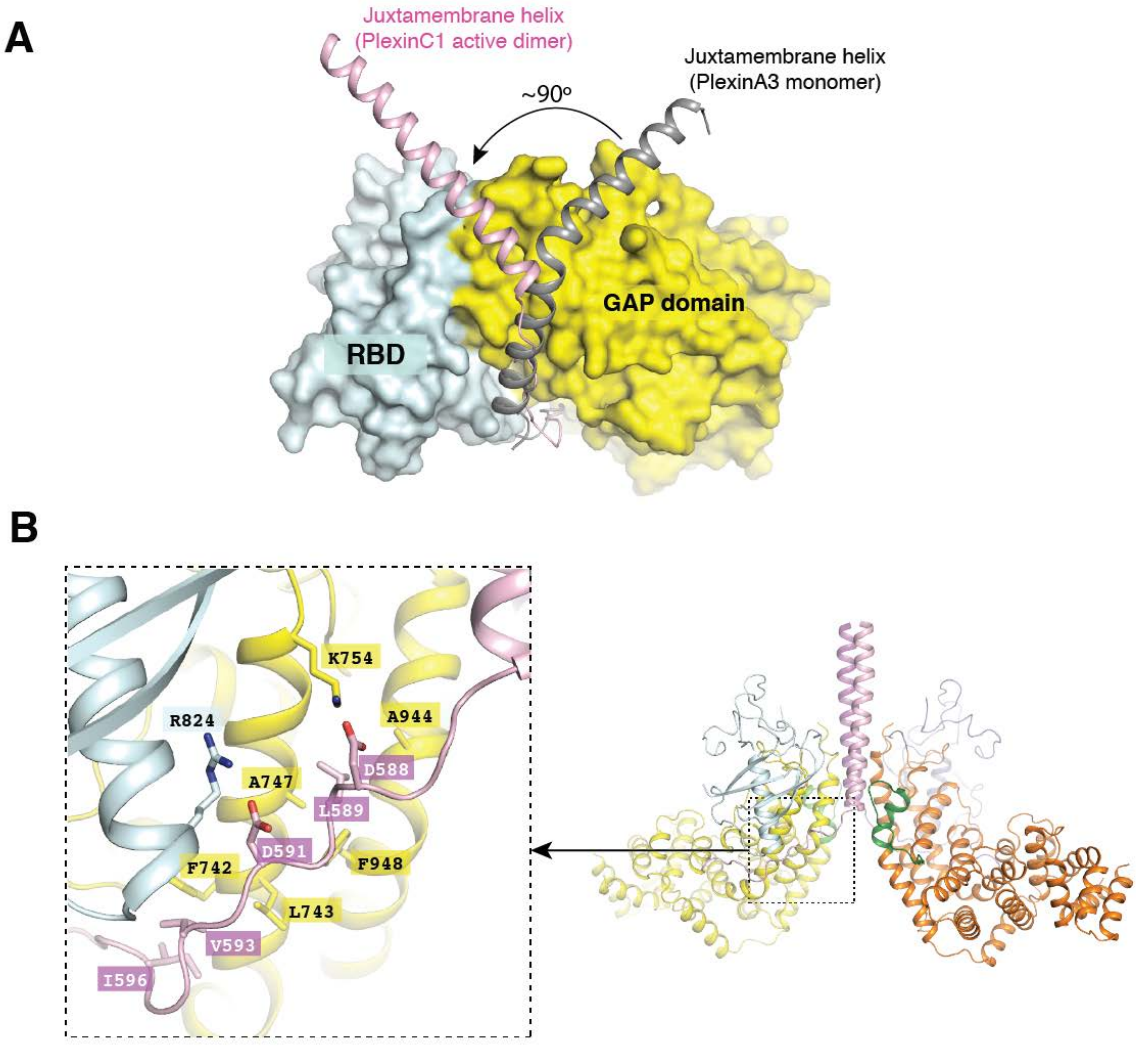

Figure 3-5. Conformational changes of the juxtamembrane helix induced by formation of the active dimer.

(**A**) Conformational changes of the juxtamembrane helix. One monomer in the PlexinC1$_{cyto}$ active dimer is superimposed onto the monomeric PlexinA3$_{cyto}$ structure (PDB code: 3IG3). The GAP domain and RBD of PlexinC1$_{cyto}$ are shown in the surface representation.

(**B**) Intra-molecular interactions made by the extended portion of the juxtamembrane segment.

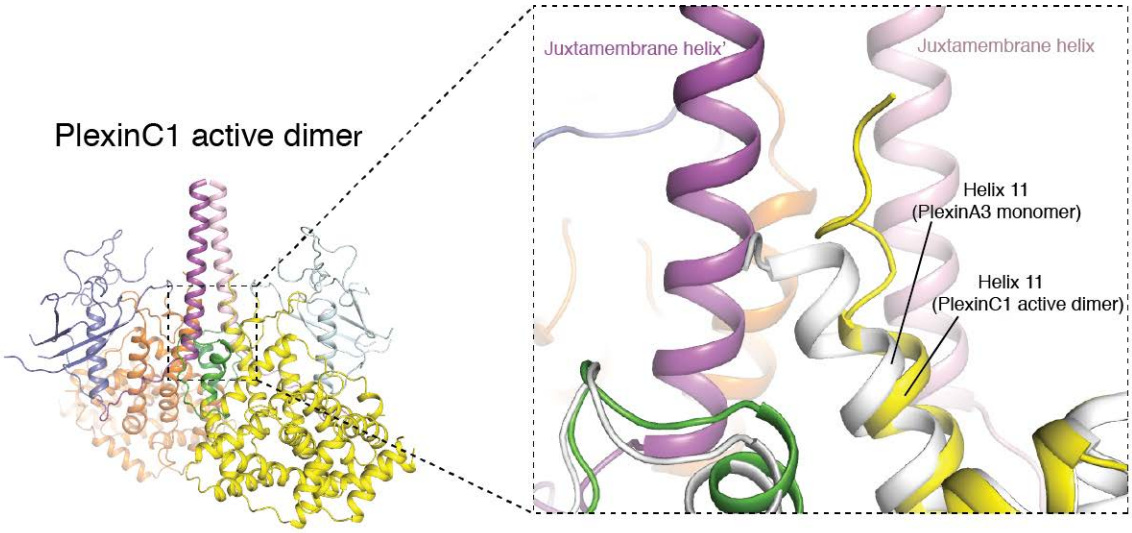

Figure 3-6. Comparison of the conformations of helix 11 in the CC(a)PlexinC1$_{cyto}$ active dimer and that in the monomeric PlexinA3 structure.

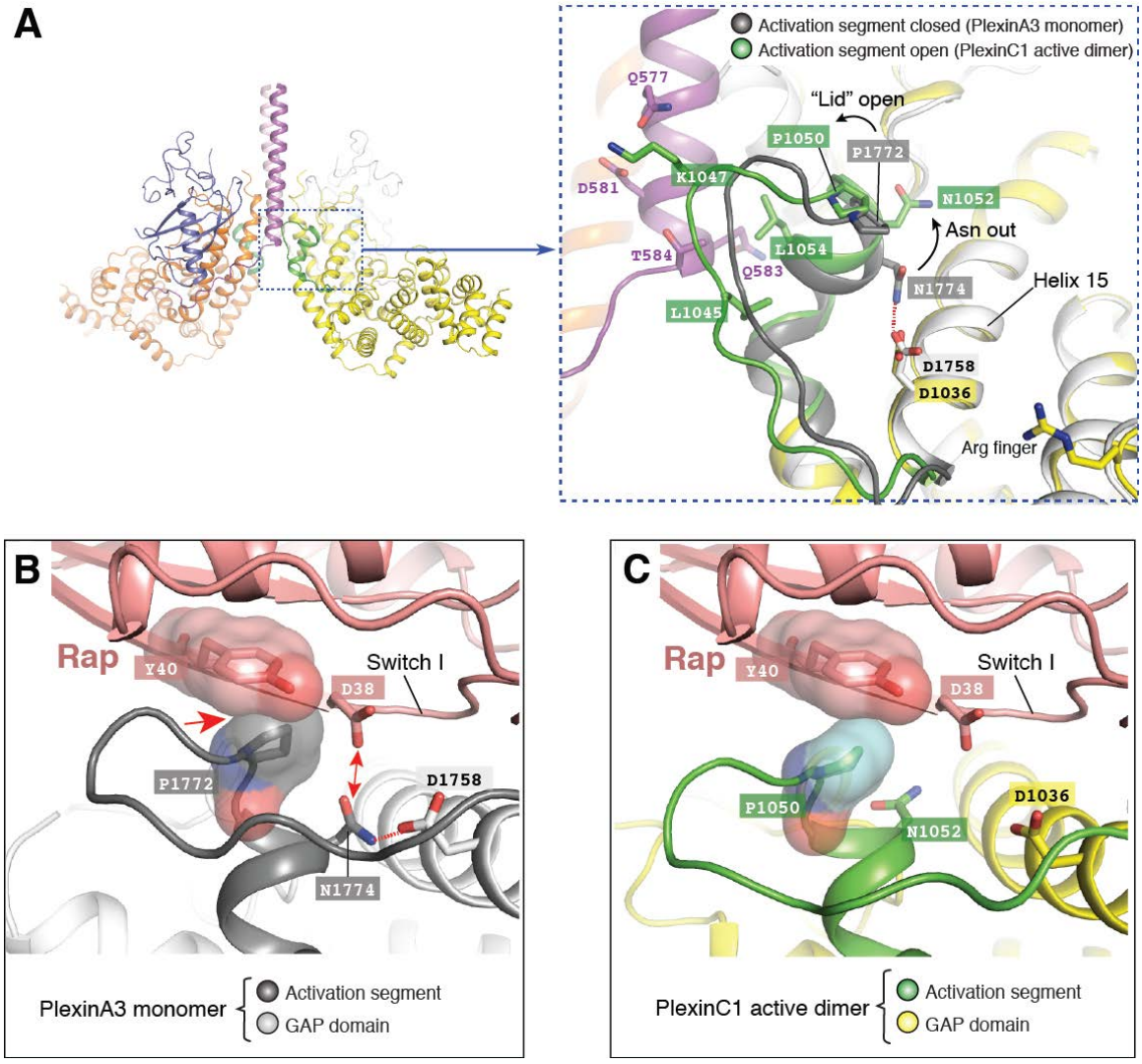

Figure 3-7. Active dimer formation opens the activation segment.

(**A**) Comparison of the activation segment in the active dimer structure and in the inactive PlexinA3$_{cyto}$ structure. Conformational changes important for GAP activation are indicated. Red dashed line: hydrogen bond.

(**B**) Docking of Rap to PlexinA3 based on the PlexinC1/Rap complex structure. Steric clashes and unfavorable interactions are indicated by red arrows.

(**C**) Docking of Rap to PlexinC1 in the coiled-coil induced active dimer.

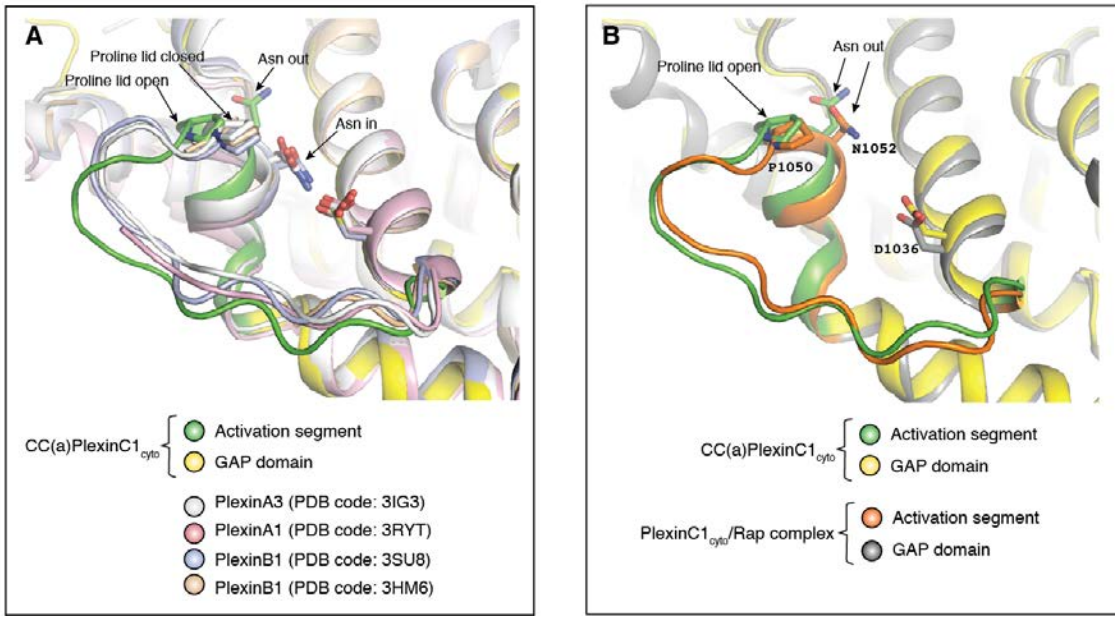

Figure 3-8. Comparison of the activation segment conformations in monomer structures and in active dimer structures.

(**A**) Comparison of the activation segment conformation in the CC(a)PlexinC1$_{cyto}$ active dimer structure with those in the previously determined plexin structures.

(**B**) Comparison of the activation segment conformation in the CC(a)PlexinC1$_{cyto}$ active dimer with that in the PlexinC1$_{cyto}$/Rap complex.

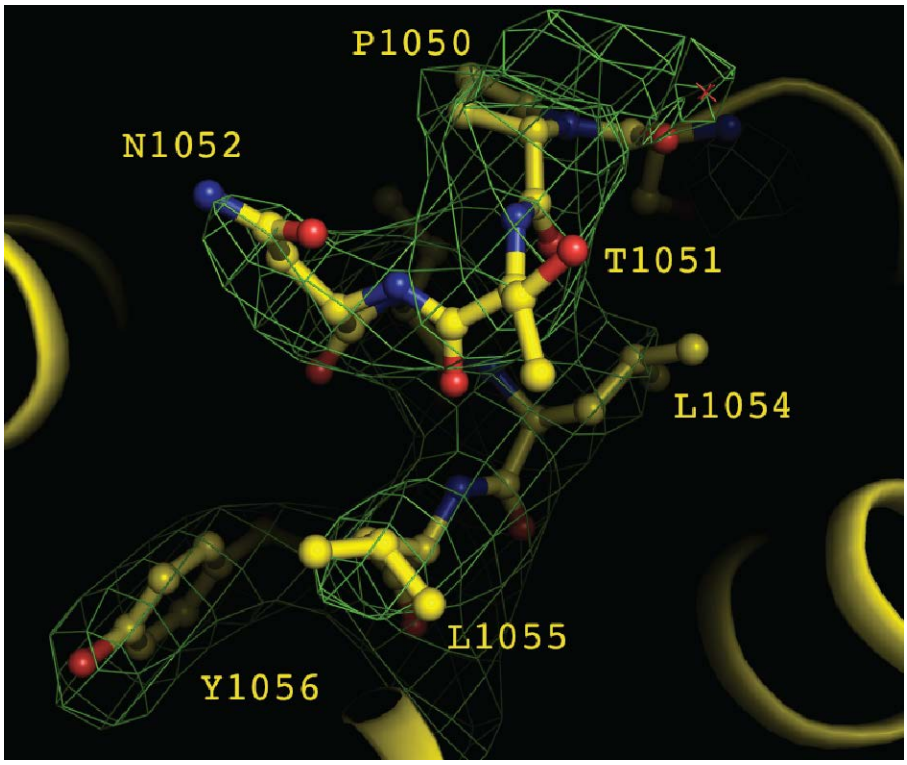

Figure 3-9. Simulated annealing omit map of the activation segment in PlexinC1$_{cyto}$.

A Sigma-A weighted simulated annealing omit map was calculated in Phenix by using the model with residues 1050-1056 in one of PlexinC1 molecules removed. The map is contoured at 3σ in green, with the final model of the structure superimposed.

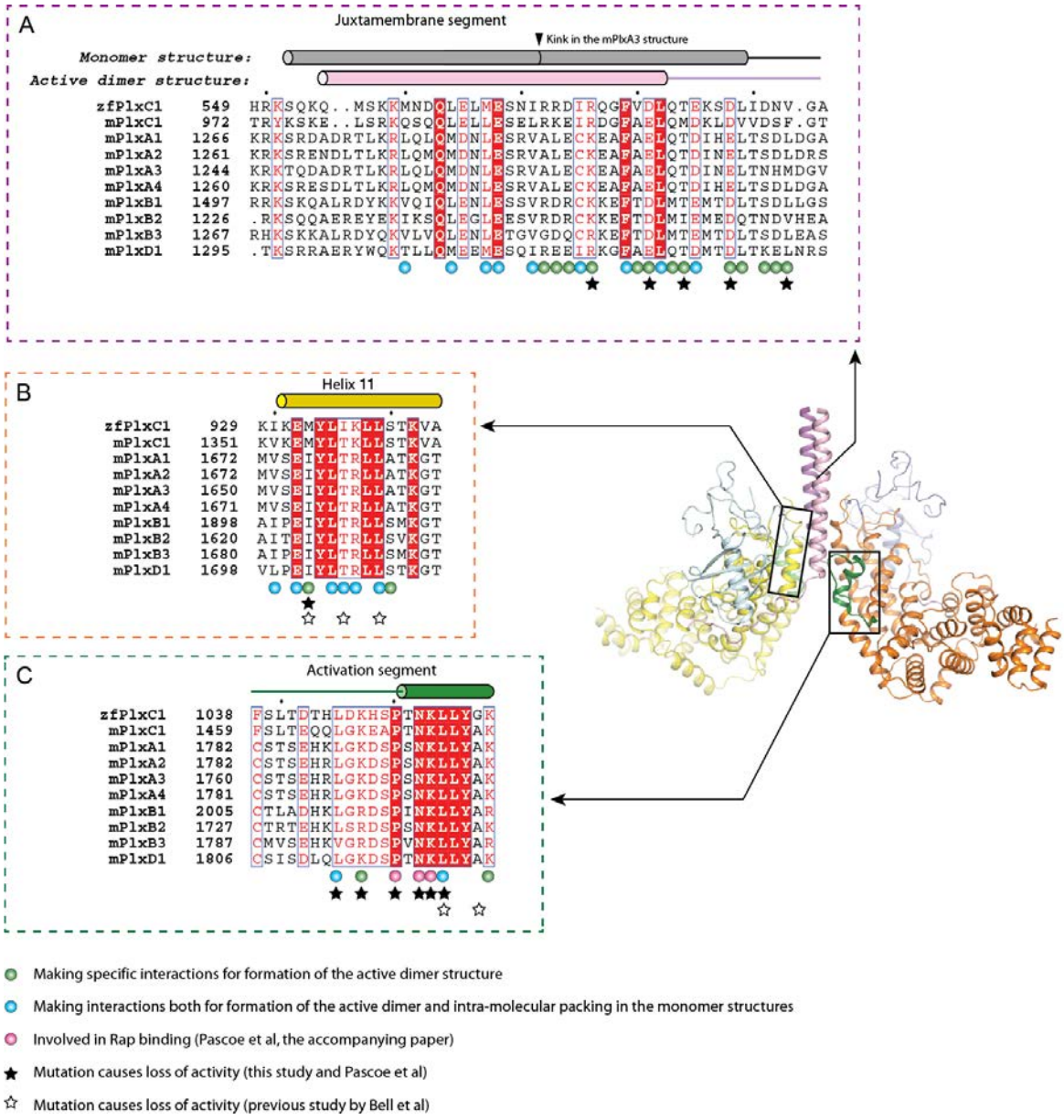

Figure 3-10. Sequence alignments of structural elements involved in the active dimer formation.

(**A**) Sequence alignment of the juxtamembrane segment.
(**B**) Sequence alignment of helix 11 in the GAP domain.
(**C**) Sequence alignment of the activation segment. zf: zebrafish; m: mouse.

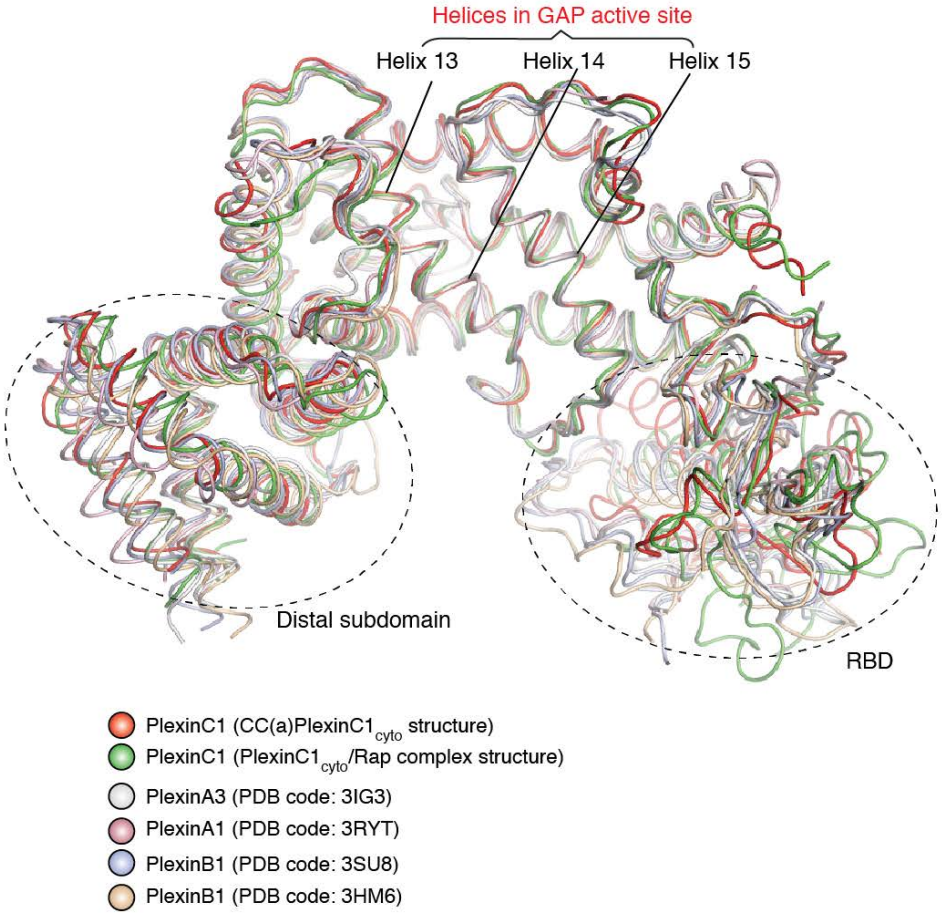

Figure 3-11. Structural flexibility of regions distal to the GAP active site.

Helices around the GAP active site in various structures of plexins in different activation states adopt highly similar conformations. In contrast, the RBD and the distal subdomain composed of the first three and last two helices in the GAP domain (highlighted by circles) show a variety of conformations and orientations relative to the GAP domain core, indicating higher structural flexibility of these regions.

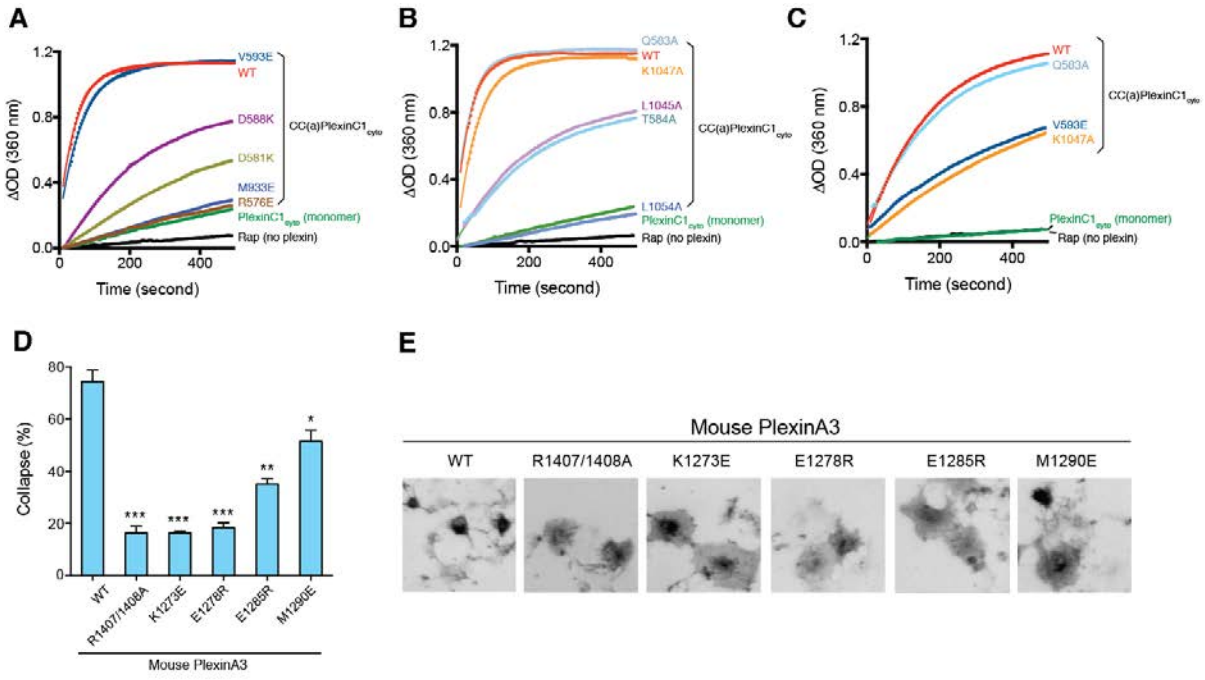

Figure 3-12. Mutational analyses of the activation mechanism.

(**A**-**C**) Mutational analyses of the activation mechanism using the GAP activity assay. Residues mutated in (**A**) are involved in stabilizing the active dimer, whereas residues in (**B**) couple the dimer formation to the opening of the activation segment. In (**A**) and (**B**) plexin concentration is 2 μM. (**C**) GAP assays for Q583A, V593E and K1047A mutants of CC(a)PlexinC1$_{cyto}$ at a lower concentration (0.25 μM). The Rap concentration is 120 μM for all the GAP assays. Data shown are representative of three replicate experiments.

(**D**) Mutational analyses of the activation mechanism using the COS7 cell collapse assay. Error bars represent standard error of the mean from three independent experiments. At least 150 cells were counted for each sample in each experiment. Statistical significance between wild type and each mutant is determined by two-tailed Student's t-test (* $p<0.05$; ** $p<0.01$; *** $p<0.001$). (**E**) Representative images of the COS7 cell collapse assays. Collapsed cells are indicated by red arrowheads.

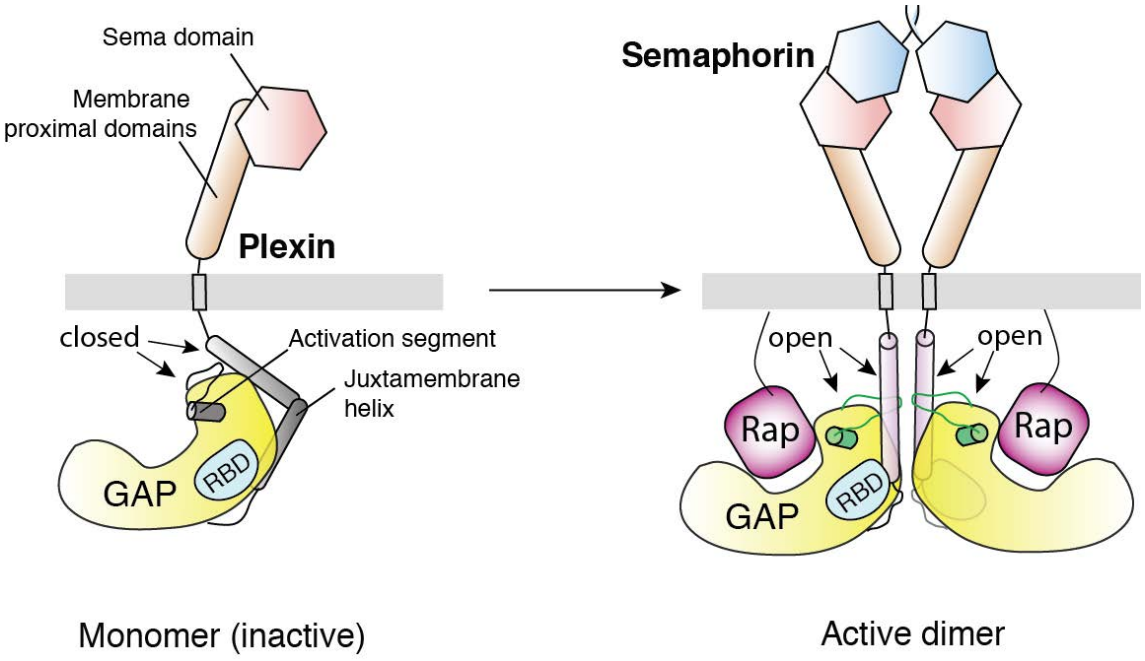

Figure 3-13. Schematic model for the activation of the plexin RapGAP by semaphorin-induced dimerization.

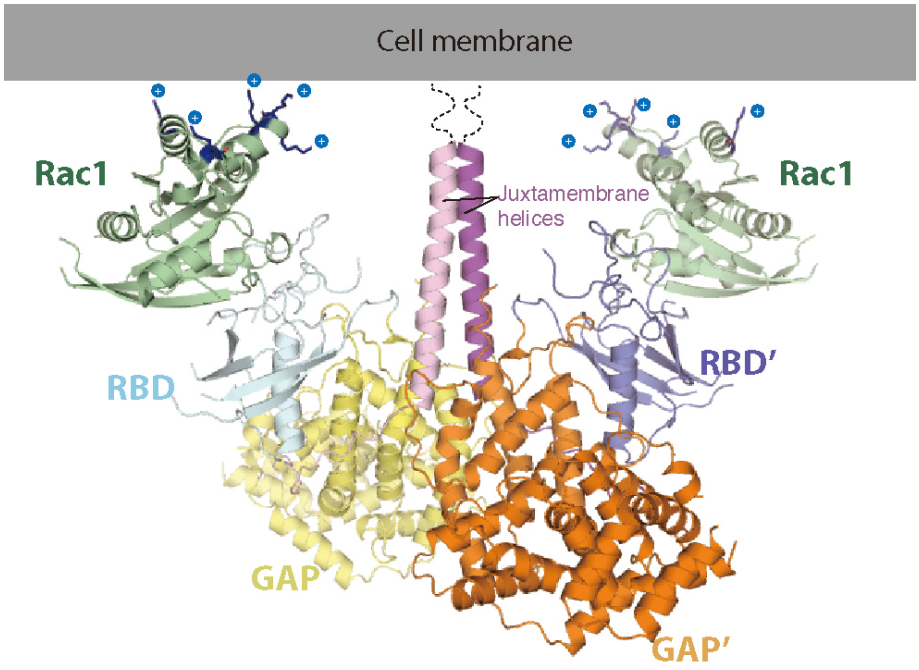

Figure 3-14. A model of Rac1 bound plexin active dimer

The model is made by superimposing the PlexinA1/Rac1 structure (PDB: 3RYT) and the PlexinC1 active dimer structure based on their RBD. Positively charged residues facing the plasma membrane are marked by "+". Dashed line: 6 residues not present in the structure.

Table 3-1. Data collection and refinement statistics

Data collection	
Space group	$P2_12_12_1$
Cell dimensions	
a, *b*, *c* (Å)	53.2, 146.1, 209.6
α, β, γ (°)	90, 90, 90
Resolution (Å)	50.0-3.30(3.36-3.30)*
R_{sym} (%)	11.1(86.8)
$I/\sigma I$	19.7(1.4)
Completeness (%)	95.8(79.5)
Redundancy	10.4(4.3)
Refinement	
Resolution (Å)	3.30
No. reflections	19840
R_{work}/ R_{free} (%)	22.2/28.3
No. atoms	8,888
Protein	8,871
Ligand/ion	0
Water	17
B-factors	
Protein	98.5
Ligand/ion	-
Water	45.3
R.m.s deviations	
Bond lengths (Å)	0.005
Bond angles (º)	0.848
Ramachandran plot	
Favored (%)	91.6
Allowed (%)	8.2
Disallowed (%)	0.2

*Highest resolution shell is shown in parenthesis.

Table 3-2. Protein concentrations and fitting methods used for determining k_{cat}/K_M of plexins

Plexin construct	Plexin concentration* (μM)	Rap-GTP concentrations (μM)	Data fitting method**
CC(a)PlexinA1$_{cyto}$	1.0	50.0, 75.0, 100.0, 150.0	Single-exponential
CC(b)PlexinA1$_{cyto}$	5.0	50.0, 75.0, 100.0, 150.0	Linear
CC(c)PlexinA1$_{cyto}$	5.0	50.0, 75.0, 100.0, 150.0	Linear
CC(d)PlexinA1$_{cyto}$	1.0	50.0, 75.0, 100.0, 150.0	Single-exponential
CC(e)PlexinA1$_{cyto}$	5.0	50.0, 75.0, 100.0, 150.0	Single-exponential
CC(f)PlexinA1$_{cyto}$	5.0	50.0, 75.0, 100.0, 150.0	Linear
CC(g)PlexinA1$_{cyto}$	1.0	50.0, 75.0, 100.0, 150.0	Single-exponential
Monomer PlexinC1$_{cyto}$	2.0	25.0, 50.0, 75.0, 100.0, 150.0	Linear
CC(a)PlexinC1$_{cyto}$	2.0	50.0, 75.0, 100.0, 150.0	Single-exponential
CC(b)PlexinC1$_{cyto}$	2.0	25.0, 50.0, 75.0, 100.0, 150.0	Linear
CC(d)PlexinC1$_{cyto}$	2.0	50.0, 75.0, 100.0, 150.0	Single-exponential
CC(g)PlexinC1$_{cyto}$	2.0	25.0, 50.0, 75.0, 100.0, 150.0	Linear

* The plexin concentrations were chosen in order for the reaction rates to be within the dynamic range of the assay.

** Linear fitting: k_{cat}/K_M determined by fitting data to $V_0 = (k_{cat}/K_M)\,[E][S]$;

Single-exponential fitting: k_{cat}/K_M determined by fitting data to $A(t) = (A_{max} - A_{min})(1 - \exp(-kt)) + A_{min}$, in which $k = k_{cat}/K_M[E]$ and was fitted as a global parameter.

CHAPTER FOUR

Crystal structure of a pre-formed inhibitory dimer of plexin

Crystal structure of PlexinA4$_{cyto}$ reveals a pre-formed dimer mediated by a new conformation of the juxtamembrane helix

We obtained crystals of mouse PlexinA4$_{cyto}$ and determined the structure to 2.8 Å resolution (Table 4-1). The overall structure of the GAP domain and RBD of PlexinA4 superimposes well with previously determined monomeric plexins$_{cyto}$ structures (Figure 4-1A). Unexpectedly, the juxtamembrane helix of PlexinA4 assumes a new conformation (Figure 4-1B). In previously determined structures of plexins the juxtamembrane helix adopts a kinked conformation and wraps around the GAP domain (Figure 4-1B) (He et al., 2009). In a more recent PlexinB1/Rac1 complex structure this segment appears to be disordered (Bell et al., 2011). In the PlexinA4 structure, nevertheless, the orientation of the juxtamembrane helix is rotated by ~200º with respect to that observed in previous structures. The helix assumes a straight conformation and loses all the interactions with the GAP domain (Figure 4-1B). Analysis of the crystal packing revealed that the juxtamembrane helix detached conformation of plexin is stabilized by interactions with its symmetry mate in the crystal, leading to the formation of a crystallographic dimer (Figure 4-1C).

In the dimer the two juxtamembrane helices forms an antiparallel coiled-coil, stabilized by extensive hydrophobic interactions between the two helices (Figure 4-2B). The coiled-coil is an unusual right-handed supercoil, which exhibits a pattern of 11-residue repeat (residue positions designated from a to k) with hydrophobic residues occupying a, d and h positions (Figure 4-2A) (Parry et al., 2008). The N-terminal portion of the juxtamembrane helix (residues 1268-1279) from one monomer packs against a hydrophobic pocket in the RBD of the other monomer, effectively interlocking the two monomers together (Figure 4-2, C and D). The center of the hydrophobic pocket is formed by Ile1535 and Phe1536 on helix 10 in RBD and Val1514 on the adjacent beta sheets, flanked by loop segments containing hydrophobic residues Pro1506, Val1539 and Pro1545 (Figure 4-2, C and D). Met1275 in the juxtamembrane helix is inserted deeply into this pocket, directly contacting Val1514 and Ile1535, whereas Gln1276 makes Van der Waals interaction with Phe1536 and Val1539. Arg1272, on the other hand, appears to face the C-terminal end of helix 10 to interact with the helix dipole (Figure 4-2, C and D). About 3500 $Å^2$ of solvent accessible area is buried by dimer formation.

The asymmetric unit of the crystal contains two copies of PlexinA4$_{cyto}$, both of which form the same type of crystallographic dimer with their respective symmetry mates. In one of the dimers (refereed to as dimer A), the antiparallel coiled-coil formed by juxtamembrane helices appears to be slightly bent, clearly revealing the right-handed supercoil, where as in the other (referred to as dimer B) the two juxtamembrane helices are almost straight (Figure 4-3). Despite these conformational differences, the dimer

interface remains unchanged. The conformational difference between the two dimers suggests that the flexibility in the juxtamembrane helix, the RBD and the GAP domains enables the dimer to tolerate structural variations, which may allow the plexin family members under different conditions to adopt the same dimer mode.

The GAP domain does not seem to contribute to dimer interface formation, neither does it undergo any conformational change compared to previously determined $plexin_{cyto}$ monomer structures (Figure 4-1A). Although they do not interact with each other, the relative orientation of the two GAP domains is restrained by the dimer interactions. The two GAP domains in the dimer are arranged to embrace each other with their concaved active sites, which renders them inaccessible to the substrates Rap (Figure 4-4). We will refer to this crystallographic dimer as the inhibitory dimer hereafter, since formation of this dimer would lead to the inhibition of the GAP activity of plexin. In the inhibitory dimer the N-termini of the two antiparallel juxtamembrane helices are separated by ~70 Å, in stark contrast with the active dimer structure in which the juxtamembrane helices align in parallel and the N-termini are very close to each other (Figure 4-5). This suggests a mechanism by which the pre-formed inhibitory dimer is disrupted by the binding of semaphorin, which brings together the N-termini of the juxtamembrane helices to induce active dimer formation (Figure 4-5). Moreover, this model agrees with a recent structure of the plexin extracellular region, which showed that the Sema domain of plexin homodimerizes in *apo* state and becomes separated when bound to semaphorin (Figure 4-5).

Residues in the dimer interface are highly conserved among all plexins, suggesting that other family members could potentially also form the inhibitory dimer (Figure 4-2A). Many of the residues in juxtamembrane helix mediating the formation of the antiparallel coiled-coil, such as Met1277, Leu1280 and Val1284, are also involved in stabilizing the juxtamembrane helix-GAP domain interactions in previously determined plexin monomer structures. In addition, the C-terminal portion of the juxtamembrane helix (residues 1284-1306) also constitutes part of the active dimer interface (Figure 4-2A). Therefore the sequence conservation of these residues may be due to multiple functional constraints. Nevertheless, the N-terminal portion of the juxtamembrane helix (residues 1268-1279) only seems to be involved in formation of the inhibitory dimer (Figure 4-2A).

Crystal structure of GCN4 coiled-coil fused PlexinA4$_{cyto}$ shows the same inhibitory dimer

In an attempt to determine the structural basis for dimerization induced activation of plexins$_{cyto}$, we crystallized the GCN4 coiled-coil fused PlexinA4$_{cyto}$ with a three residue flexible linker (GSG) in-between. The growth of the crystal requires a small percentage (3-4%) of the organic solvent 2,2,2-Trifluoroethanol, a reagent well-known for its ability to stabilize α-helix. The initial crystal diffracted poorly, but was improved by a series of truncations of loop regions and removal of the first 6 residues (VKQLED) in the GCN4 coiled-coil (see Material and methods). The structure was solved to 3.3 Å

resolution with experimental phase determined through single-wavelength anomalous diffraction (Table 4-1). Although the coiled-coil fusion construct exists as exclusive dimers in solution, the asymmetric unit of the crystal contains a tightly packed PlexinA4$_{cyto}$ tetramer (Figure 4-6A). Close examination of the structure revealed that the tetramer could be viewed as two copies of inhibitory dimers clamped together by the coiled-coil moieties (Figure 4-6A). The two monomers that constitute the inhibitory dimer are not connected to the same GCN4 coiled-coil (Figure 4-6A). Conversely, the two fused to the same GCN4 coiled-coil actually remain separated from each other with no interactions in-between (Figure 4-2B). The tetrameric structure is held together by the GCN4-coiled coil, and stabilized by interactions observed in the inhibitory dimer. All the interfaces mediating inhibitory dimer formation remain virtually unchanged in the GCN4 coiled-coil fused PlexinA4$_{cyto}$ structure.

This conformation of GCN4 coiled-coil fused PlexinA4$_{cyto}$ is drastically different from that of the GCN4 fused PlexinC1$_{cyto}$ described in Chapter 3. In addition, the GAP active sites are blocked by inhibitory dimer formation, in contrast to the robust GAP activity this construct exhibited in solution (Wang et al., 2012). Finally, modeling the crystal structure under the plasma membrane showed that it is impossible for all four plexin protomers in the tetramer to be connected to their transmembrane regions simultaneously. Therefore we conclude that this tetramer structure of GCN4 coiled-coil fused PlexinA4$_{cyto}$ is not the native state of the protein. We speculate that the flexible linker between the GCN4 moiety and PlexinA4$_{cyto}$ may allow the two monomers in the

active dimer to disengage from each other and assemble the inhibitory dimer during the crystallization processes. Consistent with this, the GCN4 coiled-coil fused PlexinA4$_{cyto}$ constructs without the flexible linker or with a more rigid linker (Ala-Ala) failed to crystallize in the same condition. Despite this, the structure showed that the inhibitory dimer can be crystallized using two different constructs (native and GCN4 fused PlexinA4$_{cyto}$), which seems to indicate that the dimer readily forms in solution.

Examine the formation of the inhibitory dimer in solution

PlexinA4$_{cyto}$ and other plexins$_{cyto}$ are mainly monomeric in solution. During purification processes, a higher molecular weight peak is often observed on gel filtration chromatography, suggesting that plexins$_{cyto}$ could also exist as oligomers. The peak is usually small and only visible when a large amount of protein is loaded to the column, indicating a low affinity for oligomerization (Figure 4-7, A and B). First we suspected that this reflects a basal level of active dimer formation. PlexinA1$_{cyto}$ with mutations on the active dimer interface still forms similar amount of oligomers on gel filtration, suggesting that this oligomer peak is not the active dimer (Figure 4-7A).

We speculated that the oligomer in solution may correspond to the inhibitory dimer observed in the crystal structure. To test this we mutated residue Arg1272, which resides in the center of the dimer interface between the juxtamembrane helix and RBD and is highly conserved in the plexin family (Figure 4-2). Mutating Arg1272 to a glutamate would place a negative charge against the C-terminal end of helix 10, which is

energetically unfavorable due to the orientation of the helix dipole (Figure 4-2C). Gel filtration experiment showed that this mutation abolished the formation of the higher molecular weight peak, suggesting that Arg1272 is indeed important for in-solution oligomer formation (Figure 4-7B).

We also attempted to use non-denaturing PAGE to examine the oligomerization state of PlexinA4$_{cyto}$. PlexinA4$_{cyto}$ in native condition migrated on the gel as two distinct bands (Figure 4-7C). Nevertheless, the R1272E mutation did not affect the migration pattern of plexin (Figure 4-7C), suggesting that the upper band is not the inhibitory dimer observed in the crystal structure. We found that adding reducing agent (2 mM DTT) into the gel running buffer resulted in the disappearance of the upper band, suggesting that the band corresponds to disulfide-bond crosslinked species (Figure 4-7D). Although 50 mM 2-mercaptoethanol was included in the sample loading buffer, during the extended electrophoresis process (~8 hours) the cysteine residues in the protein could still be gradually oxidized to form disulfide bond.

Finally, we also used analytical ultracentrifugation to examine the oligomeric state of PlexinA4$_{cyto}$. Sedimentation velocity experiments showed that PlexinA4$_{cyto}$ is completely monomeric in solution up to 30 μM, which is the highest concentration we could use while avoiding hydrodynamic non-ideality (Figure 4-8). This indicates that if the inhibitory dimer indeed forms in solution, the affinity of the dimer is extremely weak.

Use disulfide cross-linking to trap the inhibitory dimer

In the inhibitory dimer interface, Cys1288 on the juxtamembrane helix is located right near the two-fold symmetry axis of the dimer, directly facing the same cysteine from the other monomer (Figure 4-9A). This observation and the results from the native PAGE experiments led us to hypothesize that the inhibitory dimer could be stabilized by inducing disulfide bond formation between the two cysteine residues. We engineered a construct of PlexinA4$_{cyto}$ with surface cysteine mutated to serine except for Cys1288. The protein was purified and exchanged into a non-reducing buffer. We then added the catalyst Cu^{2+}-o-phenanthroline to promote disulfide bond formation (Kobashi, 1968). Non-reducing SDS-PAGE showed that within two hours, PlexinA4$_{cyto}$ could be efficiently cross-linked to form dimers. Without Cu^{2+}-o-phenanthroline as disulfide catalyst, a weak dimer band was also visible but remained unchanged during the two hours (Figure 4-9B). As we expected, mutating the Cys1288 completely abolished the disulfide crosslinked dimer formation (Figure 4-9B). However, the crosslinking efficiency of Cys1288, as judged by the fraction of the crosslinked species over time, was not affected by the R1272E mutation that is predicted to destabilize the inhibitory dimer. This suggests that the crosslinking process does not require inhibitory dimer formation (Figure 4-9C).

We isolated the crosslinked dimer of PlexinA4$_{cyto}$ by using gel filtration chromatography. In vitro GAP activity assay showed that, surprisingly, the crosslinked dimer has higher activity than that of PlexinA4$_{cyto}$ monomer, although still lower than

that of the GCN4 coiled-coil induced active dimer of PlexinA4 (Figure 4-9E). Adding DTT to reduce the disulfide bond eliminated the increase of GAP activity (Figure 4-9E), supporting that the activation effect is due to crosslinking rather than mutations of the surface cysteine. This indicates that the Cys1288 crosslinked dimer has similar conformation with the active dimer of plexin$_{cyto}$. Based on the structure of PlexinC1$_{cyto}$ active dimer described Chapter 3, the two Cys1288 residues from the two monomers in the active dimer of PlexinA4$_{cyto}$ are likely to be located close to each other at the center of the dimer interface. This potentially allows them to be crosslinked once the active dimer forms (Figure 4-9D). The GAP activity of the disulfide crosslinked dimer is much lower than that of the GCN4 induced active dimer, suggesting that disulfide bridge formation induces certain structural changes unfavorable for GAP activation. Although plexins$_{cyto}$ does not seem to spontaneously form active dimers in solution, it is possible that transient formation of the active dimer could be trapped by crosslinking of the Cys1288 in the dimer interface. We could not rule out the possibility that the disulfide stabilized dimeric species is a mixture of active dimer and inhibitory dimer. However the result that R1272E mutation had no effect on crosslinking efficiency indicates that the inhibitory dimer did not form or was not able to be crosslinked.

Use structural scaffolding to promote inhibitory dimer formation

Our results collectively suggest that the affinity of the PlexinA4$_{cyto}$ inhibitory dimer is very weak. The extracellular region of plexin has been suggested to form a Sema

domain mediated pre-formed dimer, which potentially could hold the cytoplasmic regions in proximity to increase their local concentration for inhibitory dimer formation (Figure 4-10A) (Nogi et al., 2010). We decided to test this hypothesis by replacing the extracellular region of plexin with an alternative structural scaffold, analogous to our previous effort of using the GCN4 coiled-coil to induce the formation of the active dimer of $plexin_{cyto}$.

We searched through the PDB database, looking for an antiparallel coiled-coil structure that potentially could be fused with $PlexinA4_{cyto}$ to stabilize the inhibitory dimer. We found that the C-terminal domain of the bovine F1-ATPase inhibitor IF1 forms a stable antiparallel coiled-coil spanning the distance of ~70 Å (Gordon-Smith et al., 2001), which matches the distance between the N-termini of the two monomers in the inhibitory dimer (Figure 4-10B). IF1 normally undergoes a dimer-tetramer transition modulated by pH (Cabezon et al., 2000). However a mutant IF1 (IF1-H49K) identified previously exists exclusively as dimers in all pH conditions (Cabezon et al., 2000). We therefore connected the C-terminus of IF1-H49K with the N-terminus of $PlexinA4_{cyto}$. A 6-residue flexible linker (GSGGSG) is included between them to avoid steric clashes. The H49K-$PlexinA4_{cyto}$ fusion construct was expressed and purified, and indeed formed stable dimers as judged by its gel filtration profile. However, the fusion protein exhibited identical GAP activity as that of the native $PlexinA4_{cyto}$, suggesting that the inhibitory dimer were not induced to form as we expected (Figure 4-10C). Although this could be

due to problems in the design of the fusion construct such as a non-optimal flexible linker length, it also raised the possibility that the inhibitory dimer may not exist in solution.

Examine inhibitory dimer formation on lipid vesicles

As described above, our efforts in detecting the existence of the inhibitory dimer in solution have largely failed. We wondered whether this was due to a lack of lipid membrane in our reconstituted system. Modeling the inhibitory dimer formation under the plasma membrane indicated that the membrane-facing side of the antiparallel juxtamembrane helices displays neutral or positively charged residues, whereas the other side of the coiled-coil is highly enriched in negatively charged amino acids (Figure 4-11, A and B). This asymmetric charge distribution would allow the coiled-coil to interact favorably with the cytosolic side of plasma membrane, which has high concentration of negatively charged lipids such as phosphatidylserine and $PI(4,5)P_2$ (Figure 4-11A) (van Meer et al., 2008). A similar observation has been made for the juxtamembrane helix of EGFR, which was shown to homodimerize and interact with the negatively charged plasma membrane to promote the dimerization of the kinase domain (Jura et al., 2009).

We fused a 10-histidine tag to the N-terminus of $PlexinA4_{cyto}$, allowing it to be recruited to the surface of liposomes containing lipids with a nickel-nitrilotriacetate head group (1,2-dioleoyl-sn-glycero-3-[(N-(5-amino-1-carboxypentyl)iminodiacetic acid)succinyl] nickel salt, DOGS-NTA-Ni). Our model liposomes were prepared with 1,2-Dioleoyl-sn-Glycero-3- Phosphocholine (DOPC) as the major lipid component,

supplemented with 1% DOGS-NTA-Ni for binding of His-tagged protein. In addition, we also included 1,2-Dioleoyl-sn-Glycero-3-Phosphoserine (DOPS) at 30%, which is the estimated molar percentage of DOPS in the inner leaflet of plasma membrane (van Meer et al., 2008). Due to the low basal GAP activity of PlexinA4$_{cyto}$, we had to use high concentration of the protein for the assay, which greatly affected liposome stability and caused heavy precipitation. We therefore generated His$_{10}$-tag fused PlexinB1, which has much higher basal activity and is likely able to form the inhibitory dimer since the residues in dimer interface are highly conserved (Figure 4-2A). However, our result showed that localizing PlexinB1$_{cyto}$ to DOPC/DOPS vesicles did not change its GAP activity, suggesting that the inhibitory dimer does not form spontaneously on the liposome we prepared (Figure 4-11C). One caveat in the experiment was the oversimplified lipid composition of the liposome, which did not contain lipids such as cholesterol and PI(4,5)P_2 (van Meer et al., 2008). It is also unclear if the low affinity of His-tag and the curvature of the liposome have negative impacts on inhibitory dimer formation.

Determine the functional significance of the inhibitory dimer structure

We decided to use the well-established COS7 cell collapse assay to test the functional relevance of the inhibitory dimer structure. COS7 cells respond to semaphorin and collapse when plexin is transfected (Takahashi et al., 1999). Previous result showed that deletion of the Sema domain renders plexin constitutively active in inducing COS7

collapse (Takahashi and Strittmatter, 2001). We speculated that this is due to the disassembly of the pre-formed inhibitory dimer, the formation of which may depend on the homodimerization of the plexin Sema domain (Nogi et al., 2010). Loss of the inhibitory dimer could result in spontaneous formation of the active dimer due to high local concentration of plexin on cell membrane, leading to constitutive collapse of COS7 cells. If that is the case, mutation of the inhibitory dimer interface will have a similar effect. We mutated several residues mediating interactions between the N-terminal portion of the juxtamembrane helix from one monomer and the RBD from the other monomer (R1272E, Q1276R, S1505E, V1539R). These residues are conserved but are not involved in stabilizing the active dimer or the juxtamembrane helix-GAP domain interaction in the monomer structure, neither does any of them interact with the substrate Rap (Figure 4-2A). The result showed that none of the mutations significantly raised the percentage of COS7 cells undergoing collapse above the level of wildtype PlexinA4 (Figure 4-12B). The mutation Q1276R even further diminished the basal collapse, the reason for which is not known (Figure 4-12B).

In the above experiment, if the extracellular dimer mediated by the Sema domain persists despite the disruption of the cytosolic inhibitory dimer, the spontaneous transition to the active dimer may still be hindered, which would explain the lack of constitutive activation of plexin. We introduced mutations to the Sema domain pre-formed dimer interface (Figure 4-12A), and tested if disrupting both the extracellular and cytosolic inhibitory dimer results in plexin activation. Surprisingly, we did not observe constitutive

collapse for the mutant, neither did mutations of the Sema domain dimer only have any effect (Figure 4-12B). This result suggest that the autoinhibited state of plexin does not depend on the cytosolic dimer crystallized by us or the Sema domain dimer crystallized by Nogi et al (Nogi et al., 2010).

Determine the oligomerization state of plexin on cell surface

Two-color pulsed-interleaved excitation fluorescence cross-correlation spectroscopy (PIE-FCCS) is a new technique developed to analyze the oligomerization states of membrane proteins on cell surface (Endres et al., 2013; Larson et al., 2005). In collaboration with Dr. Adam. W. Smith's lab in University of Arkon, we used PIE-FCCS to determine whether or not full-length PlexinA4 in cells indeed exists as preformed dimers. In the experiment, two PlexinA4 constructs with either mGFP or mCherry tag were co-transfected into COS7 cells. The fluorescent proteins were excited alternatively with laser pulses (Muller et al., 2005). The fluorescence intensity fluctuates due to fluorescent protein tagged PlexinA4 diffusing in and out of the laser focus spot. The cross-correlation of the mGFP and mCherry intensities were then calculated to evaluate the amount of co-diffusing molecules which corresponds to pre-formed oligomers (Endres et al., 2013; Larson et al., 2005). The strength of this technique is that it is not affected by random collisions and molecular crowding effects, which usually plague cell based FRET assays.

We found that the correlation value of wildtype PlexinA4 is close to that of membrane localized GCN4 coiled-coil dimer, and significantly higher than that of membrane anchored fluorescent proteins alone (Figure 4-13). This result strongly suggests that PlexinA4 indeed homodimerizes on cell surface. However, the correlation was not affected by mutations on the interface of the cytosolic inhibitory dimer. Mutating the Sema domain pre-formed dimer had no effect either (Figure 4-13). Nevertheless, deletion of the whole Sema domain strongly diminished dimer formation, an effect not enhanced by additional mutations of the cytosolic inhibitory dimer (Figure 4-13). These results together with our previous analysis suggest that neither of the two crystallographic dimers represents the actual pre-formed dimers of plexin in cells.

Discussions and future directions

While much has been revealed for the ligand-bound, active state of plexin, the state of the unliganded receptor has remained elusive. It was suggested that plexin dimerizes on the cell surface prior to semaphorin binding, although no experimental evidence has been reported to support this claim (Antipenko et al., 2003; Tong et al., 2007). Our FCCS result represents the first direct examination of the oligomerization state of full-length plexin in cells, which clearly reveals the presence of pre-formed dimers. Unexpectedly, this dimer is not related to the PlexinA2 Sema domain dimer crystallized previously (Nogi et al., 2010), or the inhibitory dimer of the PlexinA4$_{cyto}$ presented in this chapter. Our cell base assay showed that neither of these dimer

structures is relevant for the autoinhibition of plexin, suggesting that they are probably artifacts due to crystal lattice formation. Protein crystallization processes strongly select for conformations most prone to form ordered lattices. Therefore the structure captured in a crystal is not necessarily the major or physiologically relevant state of the protein. Driven by crystal packing and high local concentrations, proteins in the crystal may appear to form high order oligomers, which may not exist in solution and should be interpreted with caution.

While our result confirmed the existence of a pre-formed dimer of plexin, the precise nature of this dimer awaits further study. Given that deletion of the Sema domain abolished dimer formation and also led to constitutive activation of plexin, this pre-formed dimer may indeed function to maintain the autoinhibition of plexin prior to ligand binding. Intriguingly, the constitutive collapse caused by Sema domain deletion of PlexinA1 could be inhibited by isolated Sema domain added *in trans* (Takahashi and Strittmatter, 2001). Based on this it was proposed that the Sema domain associates with other domains in the extracellular region of plexin and induces an autoinhibited state (Antipenko et al., 2003; Takahashi and Strittmatter, 2001). Our result suggest that such an autoinhibited conformation of plexin may be stabilized by homodimerization (Figure 4-14), the basis for which requires structural studies of the full-length extracellular region of plexins.

Both PlexinA4$_{cyto}$ alone and coiled-coil fused PlexinA4$_{cyto}$ crystallized in low pH conditions. We surveyed all the structures of plexins$_{cyto}$ and their crystallization buffers,

which revealed a very interesting trend (Table 4-2). Crystallization conditions with pH above 7.0 produced structures with the juxtamembrane helix of plexin docked to the GAP domain. In contrast, plexin crystallized in low pH buffers either has the juxtamembrane helix completely disordered, or visible but detached from the GAP domain. The juxtamembrane helix-GAP interface does not contain conserved a histidine which becomes protonated below pH 6.0. It is possible that the kinked conformation of the juxtamembrane helix is metastable, which relaxes to a straight conformation and detaches from the GAP domain at low pH due to increased protonation of the acidic residues mediating electrostatic interactions that anchors the juxtamembrane helix to the GAP domain (Figure 4-15).

Could this be a biologically relevant mechanism for altering the conformation of the juxtamembrane helix? It is tempting to speculate that when the juxtamembrane helix-GAP domain interaction is disrupted by low pH, the newly exposed surface serves as the docking site for regulatory proteins or downstream signaling molecules. pH-dependent conformational shifts are well documented for viral fusion proteins, which are expected to experience the acidic environment of endosomes after the virus is endocytosed by host cells (Harrison, 2008). The transmembrane topology of plexins determines that even after endocytosis, their intracellular regions remain exposed to the cytosol, which maintains a constant, slightly basic pH (Casey et al., 2010). Local pH changes near plasma membrane could be generated by ion transporters or hydrolysis events (Huang et al., 2010; Ludwig et al., 2013). For example, the release of protons from $PI(4,5)P_2$ hydrolysis catalyzed by

phospholipase C (PLC) has been suggested to alter the conformation of the scaffold protein INAD (Liu et al., 2011). Future study may reveal similar mechanisms for regulating semaphorin/plexin signaling.

Materials and methods

Protein expression and purification

The coding sequence for the cytoplasmic domain of mouse PlexinA4 (1263-1893) (provided by Dr. Masahiko Taniguchi) were amplified by PCR. The cDNA was sub-cloned into a modified pET28 vector (Novagen) that contains a recognition site for the human rhinovirus C3 protease following the His6-tag (His-tagged). To generate the GCN4-PlexinA4$_{cyto}$ construct, The GCN4 coiled-coil sequence (VKQLEDKVEELLSKNAHLENEVARLKKLV) with a 3-residue linker (GSG) was fused with PlexinA4$_{cyto}$ by PCR and subcloned into the same expression vectors. To generate IF1-H94K-PlexinA4$_{cyto}$ construct to encourage inhibitory dimer formation, the sequence of the antiparallel coile-coil portion of IF1 with the H94K mutation (LKKHKENEISHHAKEIERLQKEIERHKQSIKKLKQSED) with a 6-residue linker (ASGGSG) at the C-terminus was fused to the N-terminus of PlexinA4$_{cyto}$ by PCR extension with a series of overlapping primers. To localize PlexinA4$_{cyto}$ to Ni-NTA contain liposomes, a His$_{10}$-tag vector was generated by QuikChange PCR based on the above mentioned His$_6$ vector. The protease site was replaced with a Ser-Gly linker by QuikChange PCR.

Plexins were expressed using the ArcticExpress (Agilent) E. coli cells by following the manufacture's instructions. The proteins were first purified using a 1ml HisTrap column (GE Healthcare). After cleavage of the affinity tags, proteins were purified by using ion exchange chromatography (1 ml resource Q, GE Healthcare)

followed by gel filtration chromatography. The oligomerization states of the proteins were assessed by gel filtration chromatography using Superdex 200 10/300 GL columns (GE healthcare).

Crystallization and structural determination of PlexinA4$_{cyto}$ and GCN4 coiled-coil fused PlexinA4$_{cyto}$

The initial hit of PlexinA4$_{cyto}$ crystals was found in a condition of 20% PEG6,000, 2 M NaCl with no pH buffer reagent. The protein concentration used in crystallization was 3 mg/ml. Efforts of reproducing the crystal all failed, including directly purchasing pre-mixed crystallization condition from Hampton Research. Measurement of the pH of the initial condition showed that it was very acidic (pH < 6.0), possibly due to gradual degradation of PEG6,000 during prolonged storage. We therefore screened for crystals using the initial condition supplemented with 0.1M MMT buffer from pH 4.0 to pH 7.0 (MMT buffer is a 1:2:2 molar ratio mixture of DL-malic acid, MES and Tris base, which enables buffering over a pH range of 4.0 to 9.0. The ratio of mixture is selected so that the final buffer has a near-linear pH variation, so that the desired pH could be easily achieved by mixing high- and low-pH stock solutions proportionally). The crystals were successfully reproduced at pH 5.0 -6.0, and grew to large size at pH 5.1. However the crystals diffracted only to 4.5Å and has high mosiacity. Truncation of internal loops in the RBD domain was attempted but did not lead to higher quality crystals. Finally we

were able to improve the crystals by growing them at 4ºC at 20 mg/ml protein concentration. The crystals diffracted to ~ 2.8Å with low mosiacity.

Diffraction data were collected at 100 K on beamline 19ID at the Advanced Photon Source (Argonne National Laboratory). Data were indexed, integrated and scaled by using HKL2000 (Otwinowski and Minor, 1997). A 2.8 Å dataset in the $C222_1$ space group was collected. The structure of the GAP domain of mouse PlexinA3 (PDB ID: 3IG3) was used as the molecular replacement search model using the Phaser module in the Phenix package (Adams et al., 2002; Mccoy et al., 2007). The solution revealed serious steric clashes between the juxtamembrane helix of plexin and GAP domain from a neighboring plexin monomer in the crystal, suggesting that while the overall structure of the GAP domain and RBD remain unchanged, the juxtamembrane helix assumed a new conformation in the PlexinA4$_{cyto}$ crystal. Molecular replacement and structural refinement were then performed using PlexinA3$_{cyto}$ structure without the juxtamembrane helix as search model, which revealed strong positive density for the juxtamembrane helix in a new conformation.

GCN4-PlexinA4$_{cyto}$ was initially crystallized at 20ºC in 0.1M MES, pH 6.0, 20% PEG6,000, 0.2 M $MgCl_2$ with 4 mg/ml protein concentration. The crystals were tiny and did not diffract in the beginning, but was dramatically improved by adding 4% of the organic solvent 2,2,2-Trifluoroethanol, which was identified by using the additive screening kit (Hampton Research). The crystal grew to a size of ~200 μm diameter and diffracted to ~6Å after modifying the construct to remove these regions: 1) a long

disordered loop in the RBD (residue 1606-1628); 2) three "high-entropy" residues with long side chain in a short loop (QKE, residues 1662-1664); 3) a small loop on the back of the GAP domain (residues 1702-1707). The crystal was further improved to ~ 3Å by removing the first six residues in the GCN4-coiled coil region, which are reported to have modest effect on the dimerization affinity of the coiled-coil (Lumb et al., 1994). Selenomethoinine labeled GCN4-PlexinA4 was expressed in the same bacterial strain using a previously established protocol (Van Duyne et al., 1993). SAD dataset was collected in at 100 K on beamline 19ID at the Advanced Photon Source (Argonne National Laboratory). Data were indexed, integrated and scaled by using HKL2000 (Otwinowski and Minor, 1997). A 3.3 Å dataset in the $P2_12_12_1$ space group was collected. The Autosol module in Phenix was used to determine the phase using the SAD dataset.

For all the structures Coot was used for manual model building and refinement, followed by computational refinement using Phenix (Adams et al., 2002). Comprehensive model validation was performed by using MolProbity (Chen et al., 2010). Detailed statistics of data collection and refinement are listed in Table 1. Structure figures were prepared in PyMOL (the PyMOL Molecular Graphics System, Schrodinger). Sequences were aligned by using T-Coffee (Notredame et al., 2000) and rendered with ESPript (Gouet et al., 1999). Molecular surface area was calculated using the get_area function in PyMOL.

Native PAGE of PlexinA4$_{cyto}$

Ready Gel Tris-HCl Pre-cast gels (Bio-Rad) were used for native PAGE. 20 µg of purified PlexinA4$_{cyto}$ was mixed with native loading dye (10 mM Tris-HCl, pH 8.0, 150 mM NaCl, 10% Glycerol, 0.01% Bromophenol blue, 5 mM DTT) and loaded on to the gel. Running buffer and the gel are all pre-chilled in ice-water bath. The electrophoresis was conducted for 10 hrs with a constant voltage of 80 V in cold room, with the gel cassette immersed in ice-water bath. Gels were stained by Coomassie blue staining.

Analytical ultracentrifugation

Sedimentation velocity analytical ultracentrifugation experiments were performed with purified PlexinA4$_{cyto}$. Protein samples were prepared in Centrifugation Buffer (10 mM Tris pH 8, 50 mM NaCl, 2 mM TCEP). Samples at 0.5, 1, and 30 µM were used for the experiments. All samples were equilibrated overnight at 4 °C, then approximately 400 µL of the samples were loaded into the "sample" sides of dual-sectored charcoal-filled Epon centerpieces that were sandwiched between sapphire windows in a cell housing; the "reference" sectors were filled with the same volume of Centrifugation Buffer. Filled cells were placed in an An50Ti rotor and equilibrated for 2.5 hours under vacuum in the centrifuge at 20 °C prior to centrifugation. Experiments were conducted using a Beckman Optima XL-I analytical ultracentrifuge at 42,000 RPM at 20 °C. Absorbance data at 280 nm were collected using the Beckman control software until all components had fully sedimented. Protein partial-specific volume, solvent viscosity, and density

values were calculated using the program Sednterp (Laue et al., 1992). The data were analyzed using the *c*(*s*) distribution in the program SEDFIT (Schuck, 2000). A regularization level of 0.68 was routinely employed.

Disulfide crosslinking assay

Disulfide crosslinking was performed by using the (*o*-phenanthroline)$_2$-Cu^{2+} complex method (Kobashi, 1968). The reaction was carried out by mixing O-Phenanthroline, $CuSO_4$ and PlexinA4 proteins at final concentration of 5 μM, 2.5 μM, 100 μM, respectively in gel filtration buffer (10 mM Tris-HCl pH 8.0, 150 mM NaCl, 10% Glycerol). Reaction was performed in room temperature and stopped by flash freezing the mixture in liquid nitrogen. Non-reducing SDS-PAGE was used to monitor the reaction progression. The disulfide crosslinked species was purified by using gel filtration chromatography in non-reducing buffer.

Lipid vesicle assay

Small unilamellar vesicles were prepared using the extrusion method. The synthetic phospholipids 1,2-di-(9Z-octadecenoyl)-*sn*-glycero-3-phosphocholine (DOPC), 1,2-dioleoyl-*sn*-glycero-3-phospho-L-serine (DOPS) and 1,2-dioleoyl-*sn*-glycero-3-[(N-(5-amino-1-carboxypentyl)iminodiacetic acid)succinyl] (Ni-NTA-DOGS) were all purchased from Avanti Polar Lipids, Inc. DOPC, DOPS and Ni-NTA-DOGS were mixed in a molar percentage of 69%, 30% and 1%, respectively. The chloroform in the lipid

mixture was first removed by nitrogen flow and then by applying vacuum overnight. The dried lipid was rehydrated by adding 1x GAP activity buffer (100 mM Tris-HCl, pH 7.6, 50 mM NaCl, 1 mM $MgCl_2$, 10% Glycerol) followed by vigorous votexing. Extrusion was performed using the mini-extruder from Avanti with a 200 nm diameter membrane. The rehydrated lipids were extruded through the membrane for 50 times to yield a homogeneous liposome suspension. 10 μM of His_{10}-tagged $PlexinA4_{cyto}$ was incubated with the liposome with 20 μM total Ni-NTA-DOGS concentration for 20 min in room temperature. GAP activity was measured as described in the method section of the previous chapter.

COS7 cell collapse assay

The full-length PlexinA4 construct with a C-terminal Myc tag in pcDNA3.1 vector was obtained from Dr. Masahiko Taniguchi. Mutations on the dimer interfaces were introduced by using QuikChange. COS7 cells were plated on a 4-well Nunc Lab-Tek II chamber slide (Thermo Scientific) at 4.0 x 10^4 cells per well. The next day cells were transfected by using Fugene 6 transfection reagent (Promega). 0.8 ug PlexinA4 DNA was transfected with a DNA: Fugene ration of 1: 3. 48 hours post-transfection, the cells were washed once with Phosphate-Buffered Saline (PBS) and fixed with 4% paraformaldehyde in PBS at room temperature for 15 min. After fixation, cells were washed three times with PBS and permeabilized for 2 min with 0.1% Triton X-100 in PBS (PBSTx). 3% bovine serum albumin (BSA) in PBSTx was incubated with the cells

for 30 min in room temperature to block non-specific absorption of the antibody. Anti-Myc antibody from Cell Signaling (9B11) was diluted 1:1000 in PBSTx with 3% BSA and added to each well. After overnight incubation at 4ºC without agitation, the slides were washed with Tris-Buffered Saline, 0.05% Tween 20 (TBST) for 3 times, 10 min incubation with gentle shaking each time. Cells were then incubated with Cy3 conjugated goat anti-mouse IgG was diluted 1:500 in PBSTx with 3% BSA for 1 hours at room temperature. After removal of the secondary antibody, cells were incubated with 0.5 μg/ml 4',6-diamidino-2-phenylindole (DAPI) diluted in TBST for 1 min, followed by 2 times washing with TBST and 1 time with PBS. The slides were then rinsed once with water and mounted using the Aqua-Poly/Mount coverslip mounting medium (Polysciences). Nail polish was applied to seal the edge of the slide.

Cells were imaged using a DeltaVision epifluorescence microscope with 10x objective lens and a cooled CCD camera. Fore each well, 100-200 cells expressing plexin were scored calculate the percentage of collapse. Immunostaining, imaging and cell counting were conducted in a blind fashion.

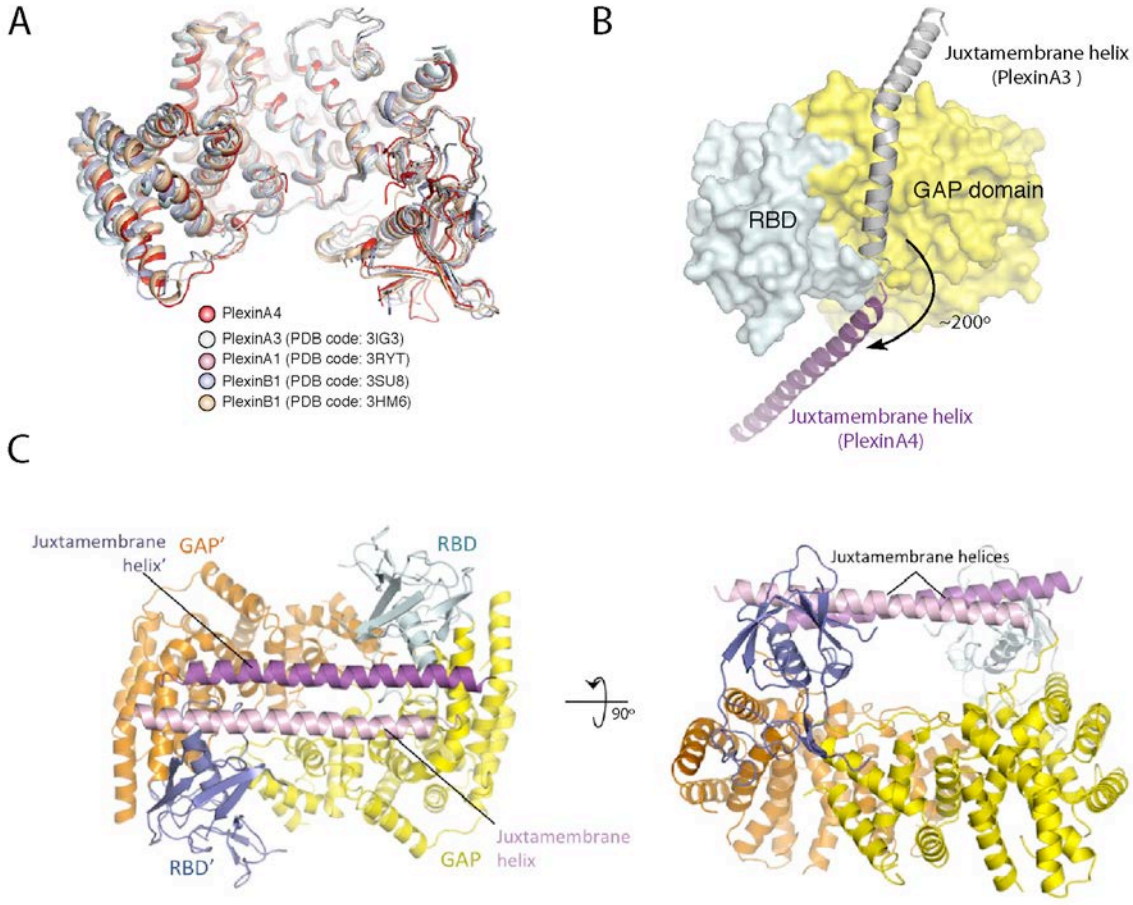

Figure 4-1. Crystal structure of PlexinA4$_{cyto}$ pre-formed dimer

(A) Superimposition of GAP domain and RBD in PlexinA4$_{cyto}$ structure and those in previously solved monomeric plexins$_{cyto}$ structures.

(B) Conformational change of the juxtamembrane helix. One monomer in the PlexinA4$_{cyto}$ pre-formed dimer is superimposed onto the monomeric PlexinA3$_{cyto}$ structure (PDB code: 3IG3). The GAP domain and RBD of PlexinA3$_{cyto}$ are shown in surface representation.

(C) The structure of the PlexinA4$_{cyto}$ crystallographic dimer.

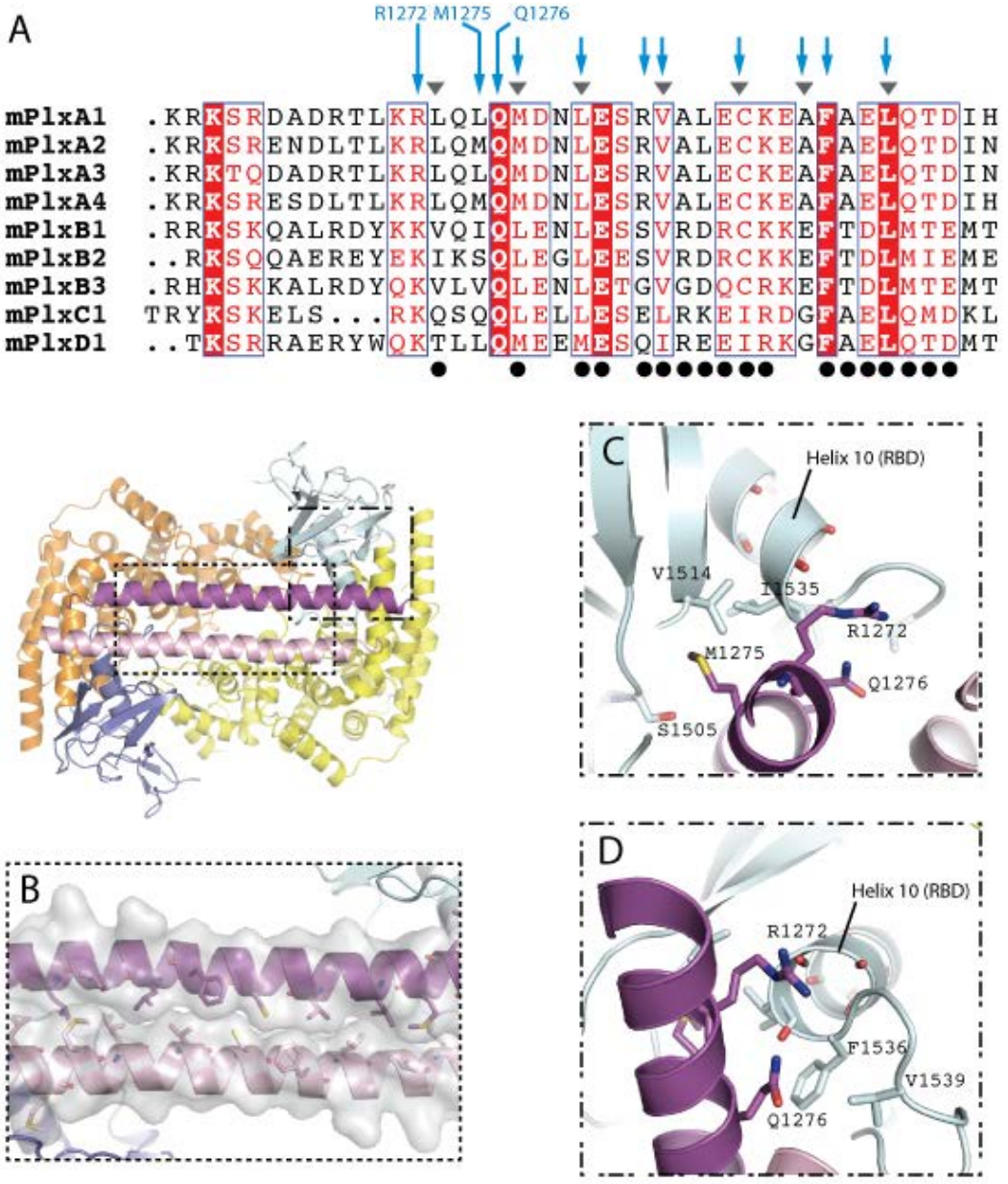

Figure 4-2. Interface of the pre-formed dimer of PlexinA4$_{cyto}$

(A) Sequence alignment of the juxtamembrane helix of plexins. Solid circles: residues involved in the active dimer interface and/or the juxtamembrane helix-GAP interface in plexin monomer. Solid triangles: hydrophobic residues located in a, d and h positions of

the antiparallel coiled-coil formed by the juxtamembrane helices. Blue arrows: residues in the pre-formed dimer interface.

(B) The antiparallel coiled-coil formed by the juxtamembrane helices.

(C) and (D) Dimer interface formed between the N-terminal portion of the juxtamembrane helix from one monomer and the hydrophobic pocket in RBD from the other monomer.

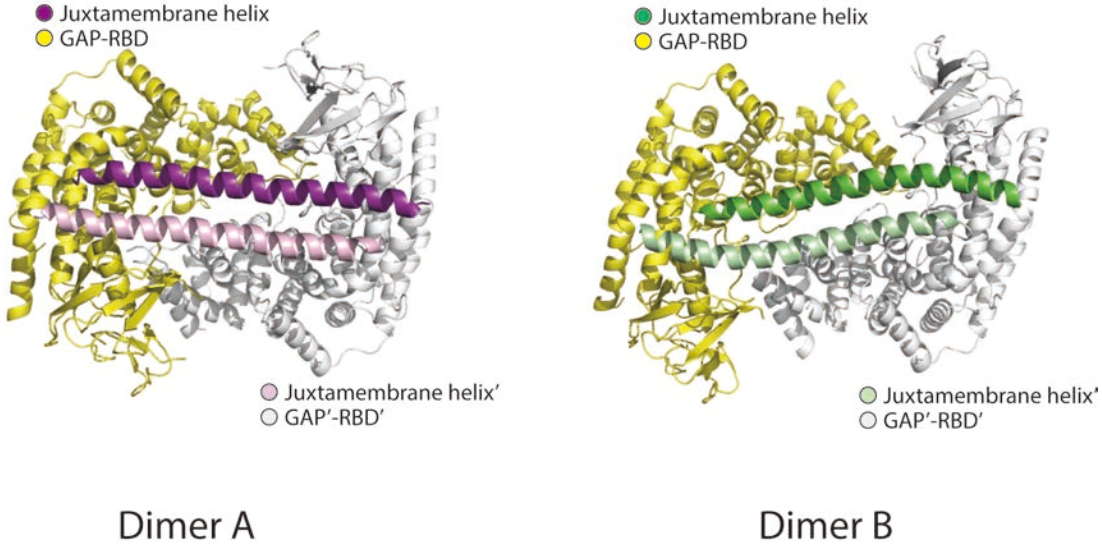

Figure 4-3. Conformational variation of the pre-formed dimer observed in the PlexinA4$_{cyto}$ crystal.

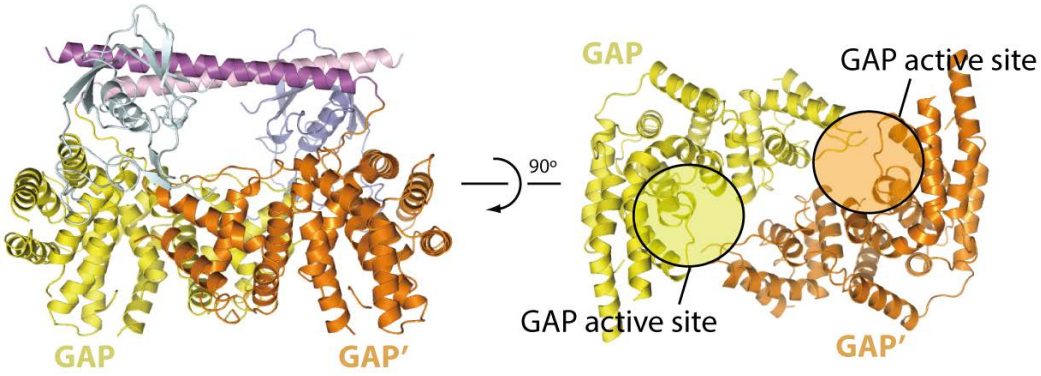

Figure 4-4. The GAP active sites are blocked in the inhibitory dimer of PlexinA4$_{cyto.}$

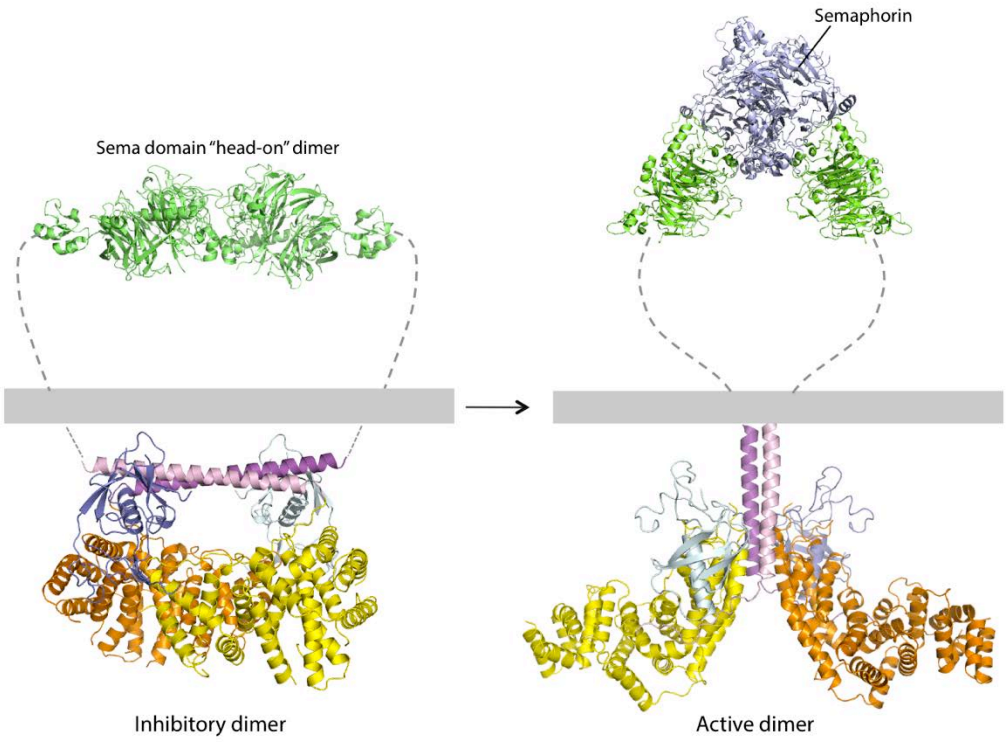

Figure 4-5. A model for semaphorin induced conformational transition of plexin.

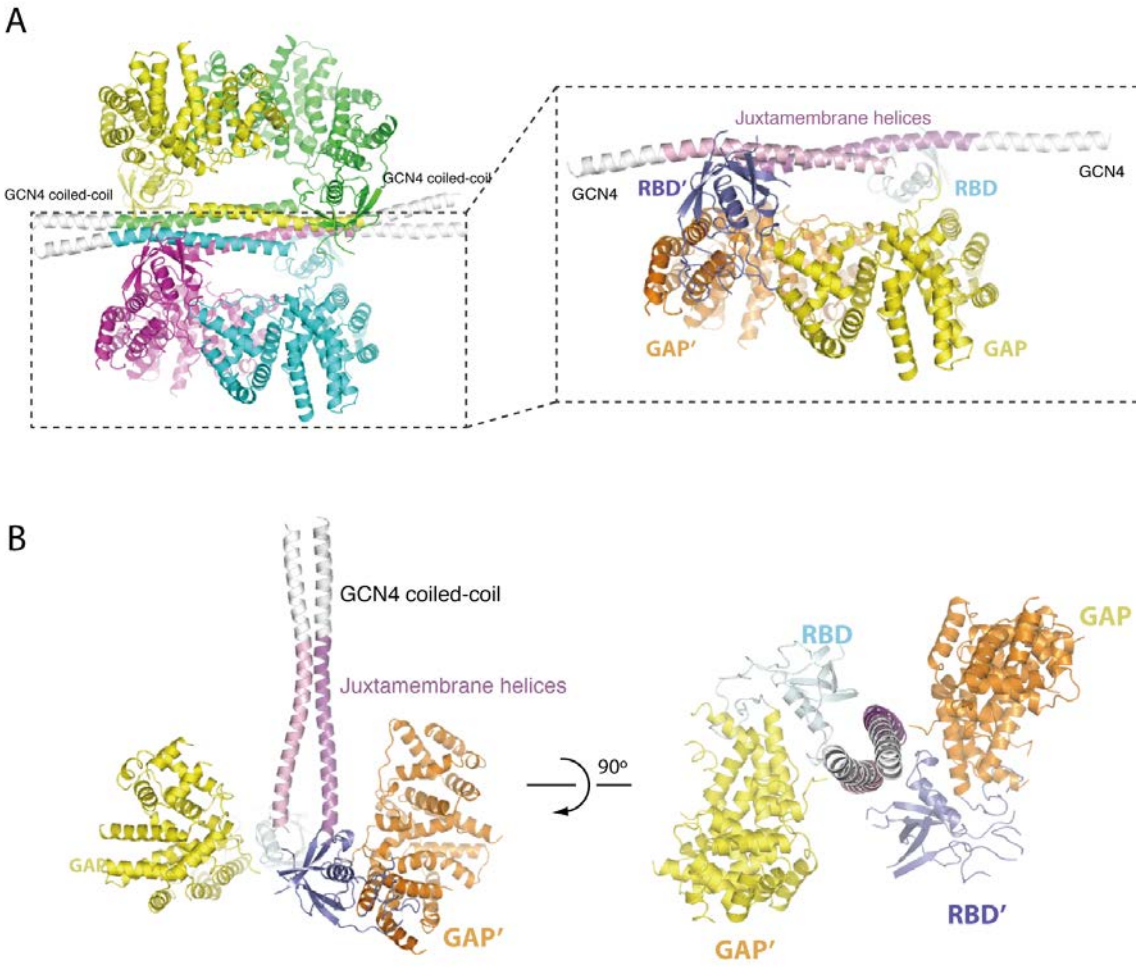

Figure 4-6. Crystal structure of GCN4 coiled-coil fused PlexinA4$_{cyto}$.

(A) Overall structure of the GCN4 coiled-coil-PlexinA4$_{cyto}$, with the four protomers in the tetramer colored differently. GCN4 coiled-coil moiety is colored white. The tetramer consists of two copies of the inhibitory dimer (shown on the right).

(B) The two monomers fused to the same GCN4 coiled-coil do not interact.

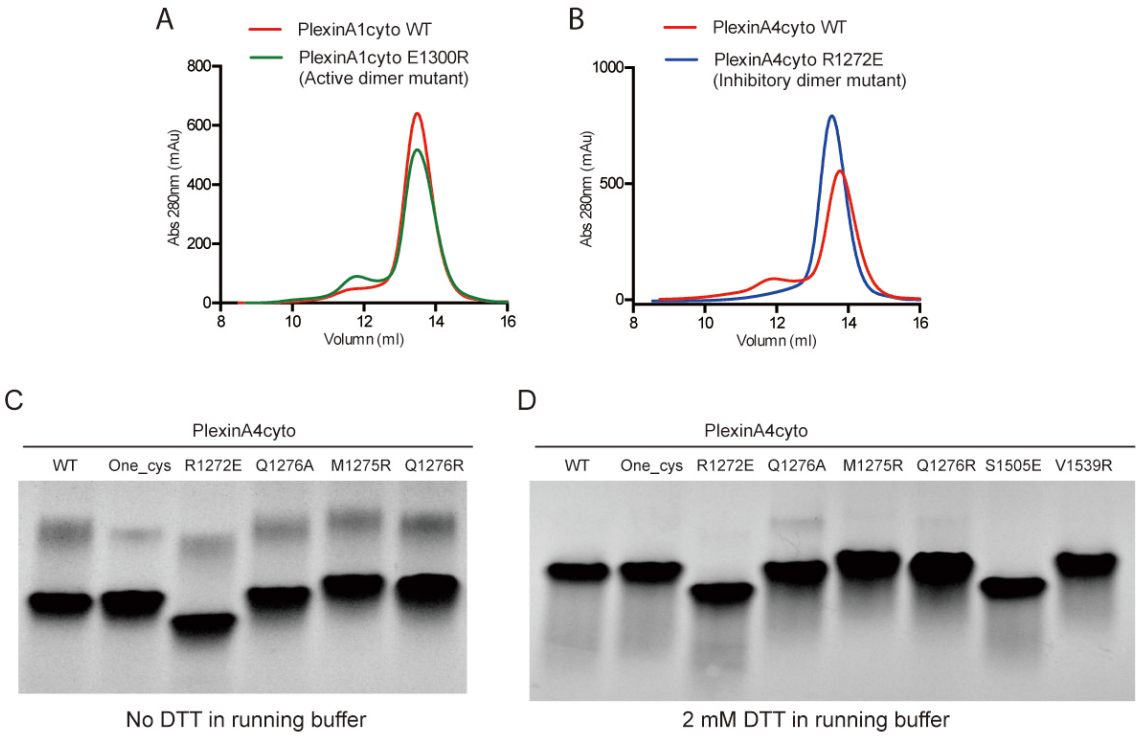

Figure 4-7. Analysis of inhibitory dimer formation in solution

(A) Gel filtration profiles of PlexinA1$_{cyto}$ wildtype and active dimer interface mutant (E1300R). The proteins are not fused to GCN4 coiled-coil.

(B) Gel filtration profiles of PlexinA4$_{cyto}$ wildtype and inhibitory dimer interface mutant (R1272E).

(C) and (D) Native PAGE of PlexinA4$_{cyto}$ wildtype and inhibitory dimer interface mutants. "One_cys" mutant has all the surface cysteines mutated to serine except for Cys1288.

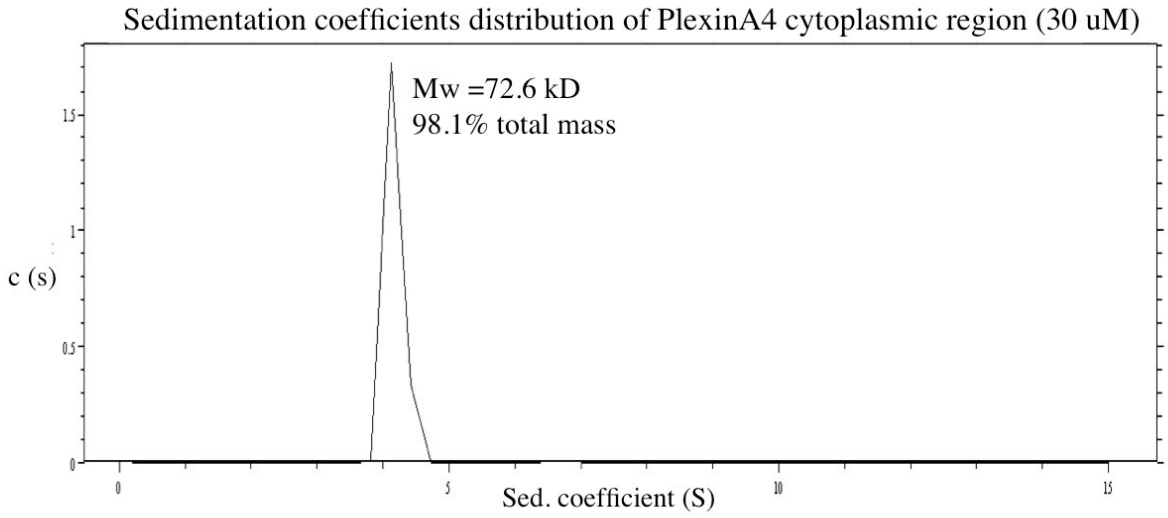

Figure 4-8. Analytical ultracentrifugation analysis of the oligomerization state of PlexinA4$_{cyto}$.

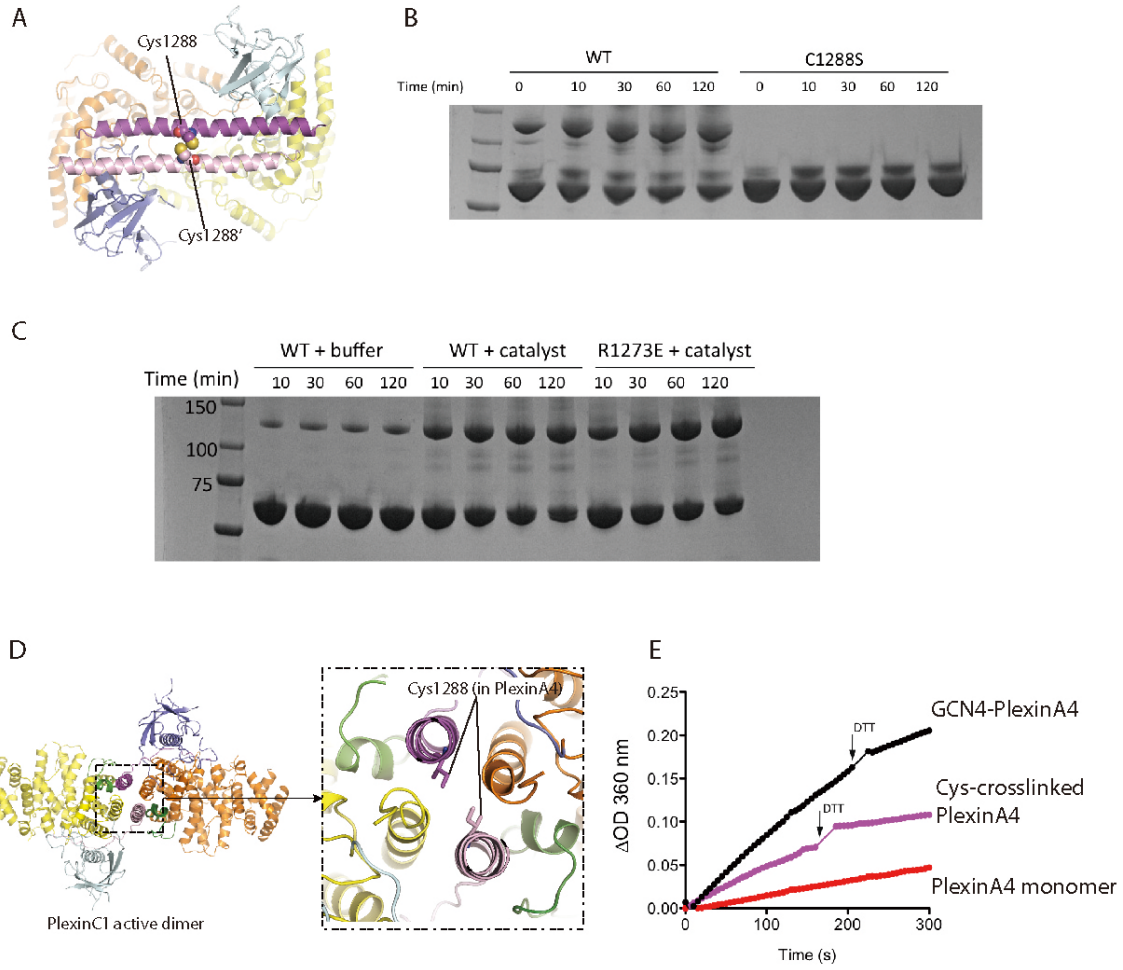

Figure 4-9. Disulfide crosslinking of the inhibitory dimer

(A) Cys1288 and its symmetry mate locate next to each other in the inhibitory dimer structure.
(B) and (C) Non-reducing SDS PAGE showing the progression of disulfide crosslinking of PlexinA4$_{cyto}$. All the proteins already have surface cysteines mutated to serine except for Cys1288.
(D) The predicted location of Cys1288 in PlexinA4 active dimer, based on sequence alignment of PlexinA4 and PlexinC1.
(E) In vitro GAP activity assay of disulfide crosslinked PlexinA4$_{cyto}$ dimer

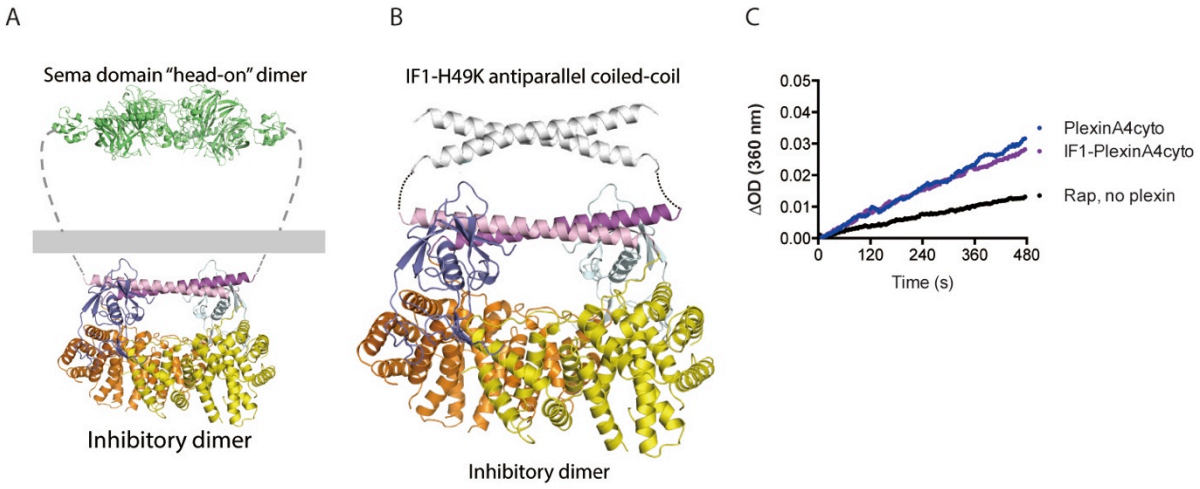

Figure 4-10. Use structural scaffold to stabilize the inhibitory dimer.

(A) A model showing that the cytosolic inhibitory dimer is stabilized by the extracellular Sema domain dimer.

(B) A structural model of IF1-H49K fused inhibitory dimer of PlexinA4$_{cyto}$.

(C) Comparison of the GAP activities of native and IF1-H49K fused PlexinA4$_{cyto}$.

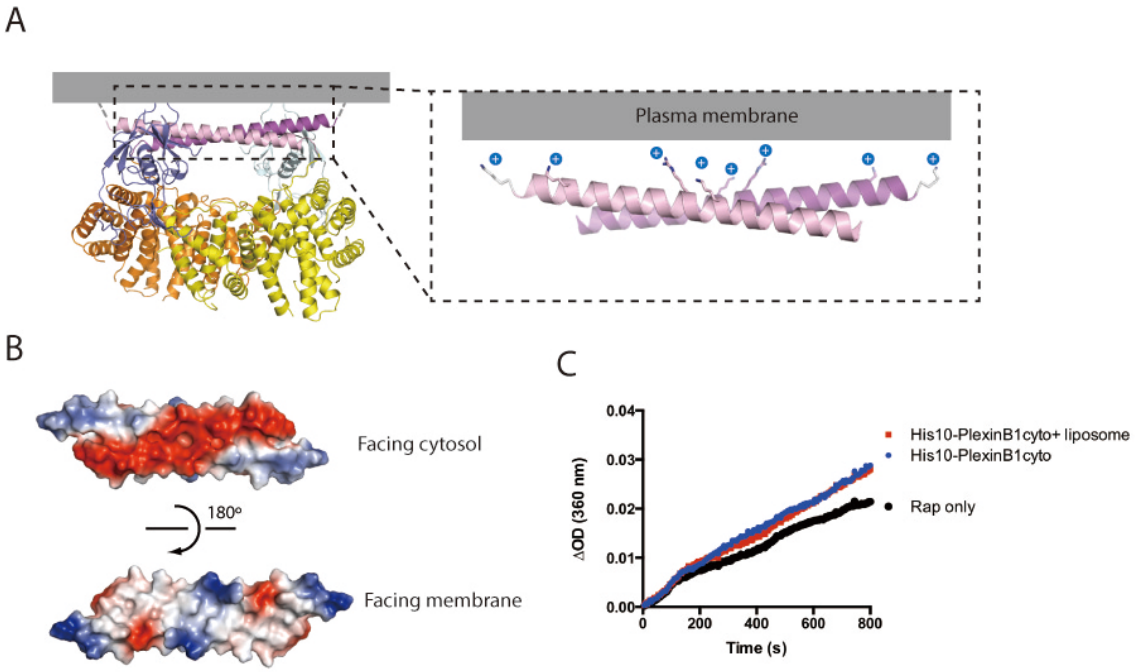

Figure 4-11. Examine inhibitory dimer formation on lipid membrane

(A) The inhibitory dimer may be stabilized by favorable interactions with negatively charged lipids on cell membrane. The antiparallel coiled-coil formed by PlexinB1 juxtamembrane helices are modeled based on the PlexinA4 structure, and positively charged residues are shown.

(B) Electrostatic potential of the antiparallel coiled-coil formed by PlexinB1 juxtamembrane helices.

(C) In vitro GAP activity assay of $PlexinB1_{cyto}$ in solution and on DOPC/DOPS lipid vesicles

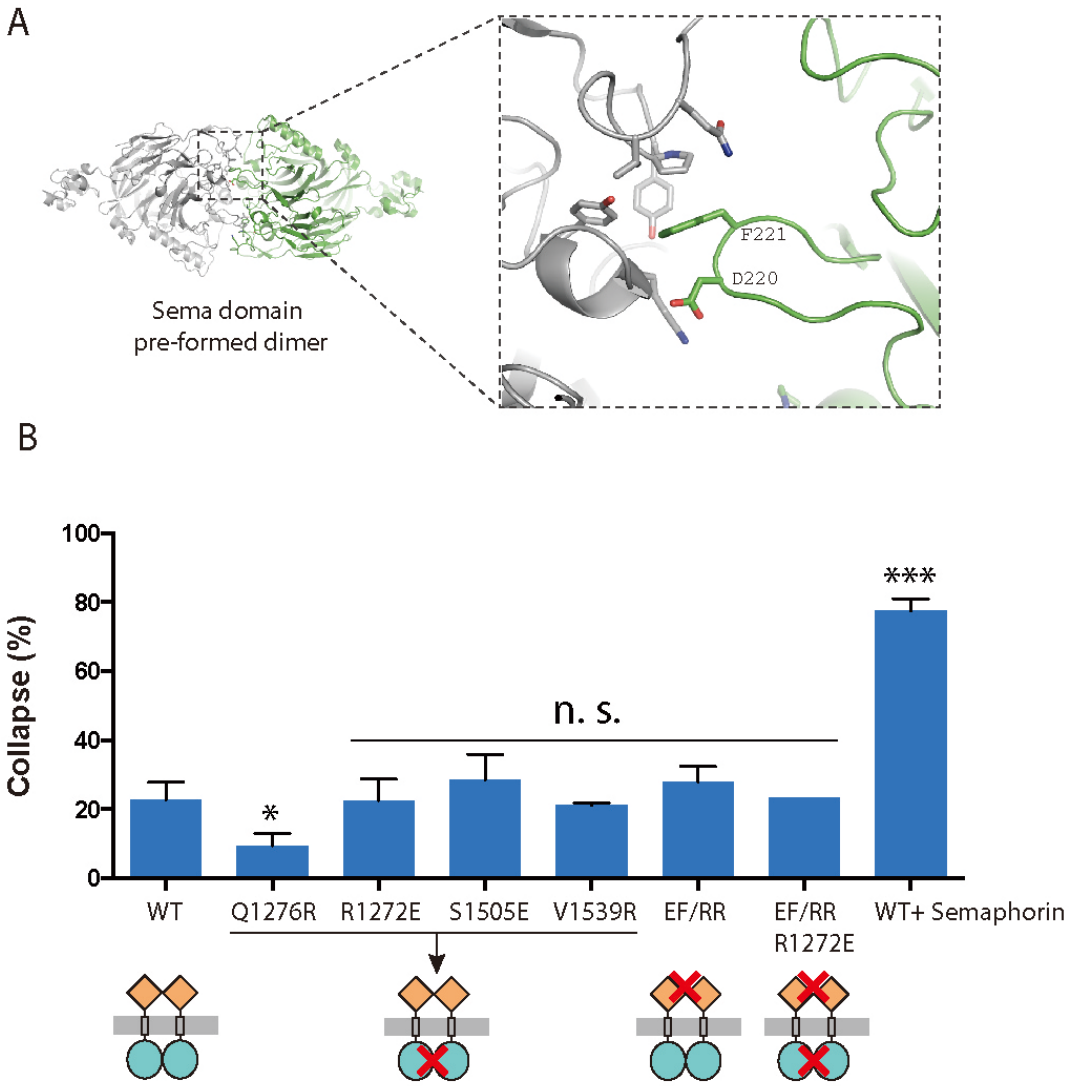

Figure 4-12. Collapse assay of PlexinA4 wildtype and inhibitory dimer mutants

(A) Interface of the PlexinA2 Sema domain pre-formed dimer solved by Nogi et al (Nogi et al., 2010).

(B) COS7 collapse assay of inhibitory dimer interface mutants. EFRR: residues Asp220 and Phe221 in (A) (Glu220/Phe221 in PlexinA4) are mutated to arginine to disrupt the

Sema domain dimer. Cartoon diagrams indicate the location of the mutation. Brown square: Sema domain of plexin. Blue circle: cytoplasmic region of plexin.

Statistical significance is determined by a two-tailed student t test. (n.s. $p > 0.05$. not significant; * $p < 0.05$; *** $p < 0.001$)

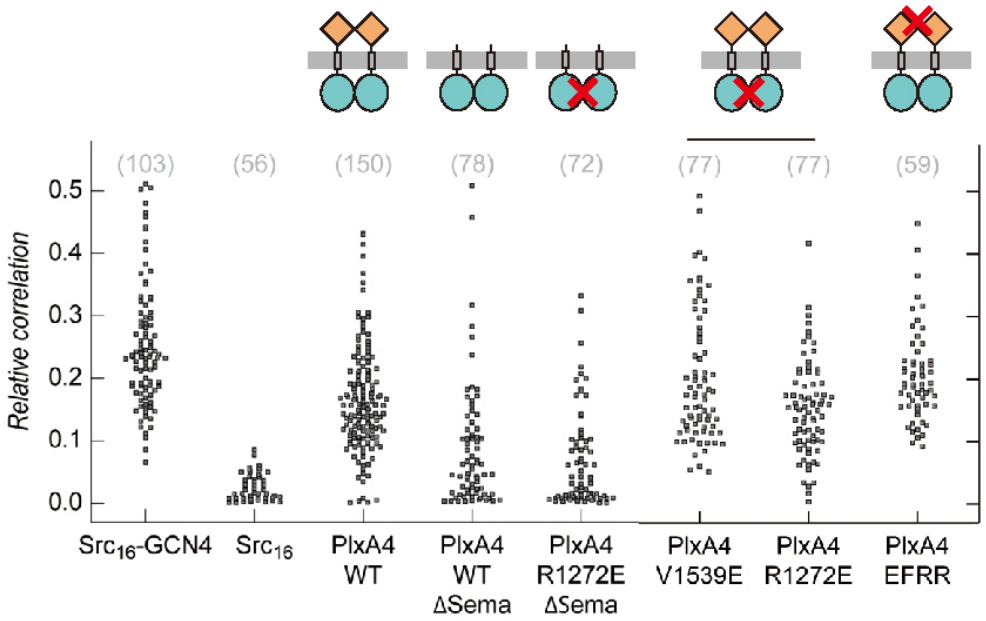

Figure 4-13. FCCS assay of PlexinA4 wildtype and inhibitory dimer mutants

Each dot represents the correlation value determined for one transfected cell. The numbers in parenthesis are the number of cells examined for each construct. Src_{16}-GCN4: Src myristoylation sequence fused to GCN4 coiled-coil, which constitutively dimerizes on cell membrane. $Src1_6$: Src myristoylation sequence only, which is monomeric on cell membrane.

Cartoon diagrams indicate the location of the mutation for the PlexinA4 constructs. Brown square: Sema domain of plexin. Blue circle: cytoplasmic region of plexin.

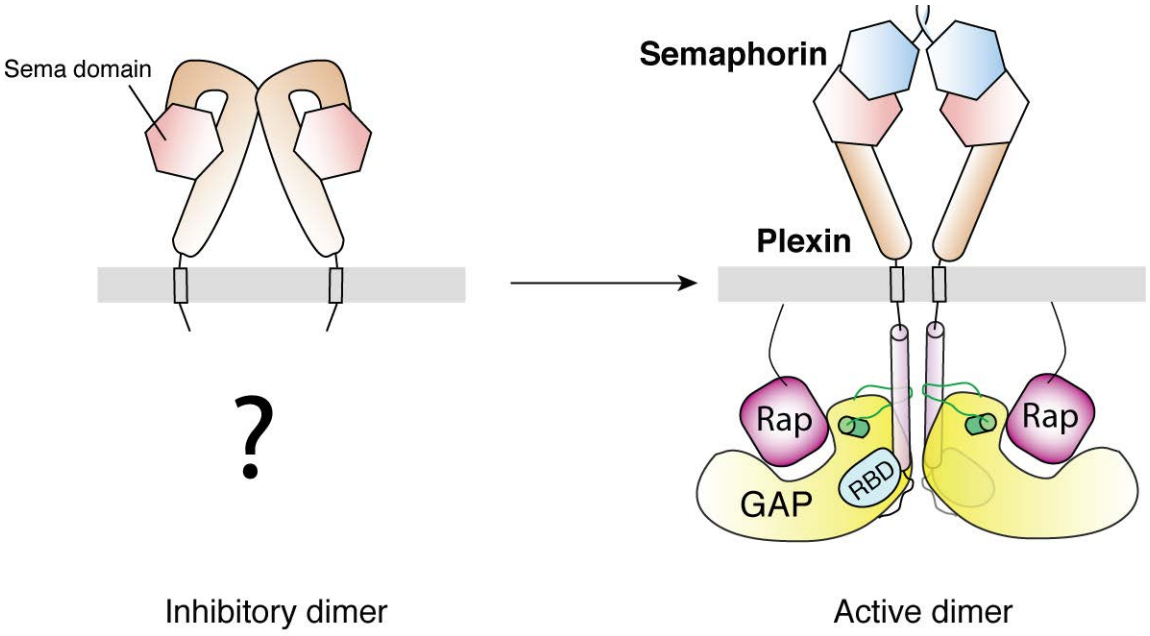

Figure 4-14. A hypothetical model showing the state of plexin before and after semaphorin binding.

The model illustrates that prior to semaphorin binding plexin exists as pre-formed dimers, which could be responsible for suppression the basal activity of the receptor. Semaphorin induces the formation of the active dimer. The exact conformation of the pre-formed inhibitory dimer is unknown and drawn for illustration purpose only.

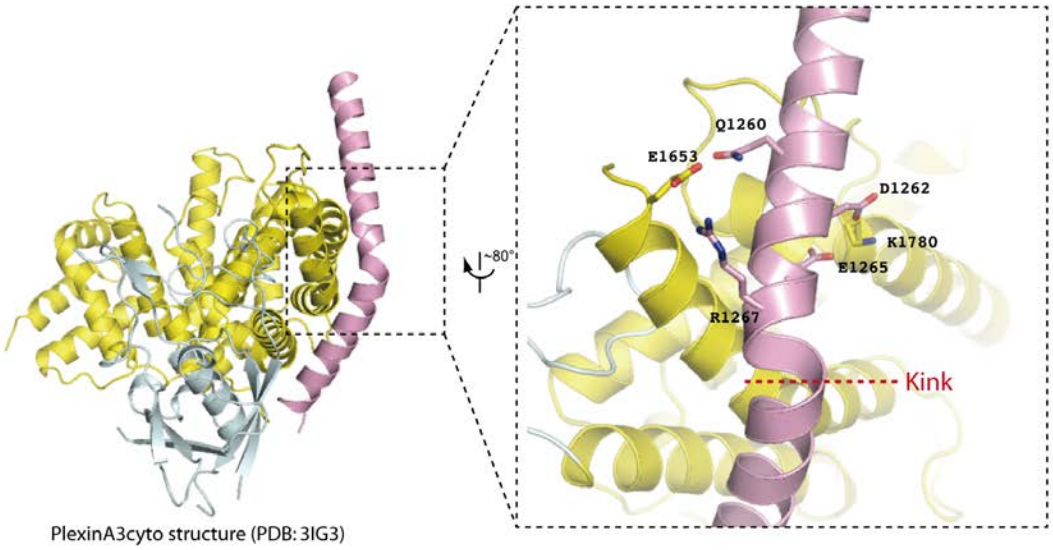

Figure 4-15. Electrostatic interactions that anchors the kinked juxtamembrane helix on to the GAP domain.

Table 4-1. Data collection and refinement statistics

Data collection		
Crystal	PlexinA4$_{cyto}$	GCN4 coiled-coil PlexinA4$_{cyto}$
Space group	C 222_1	P $2_12_12_1$
Cell dimensions		
a, *b*, *c* (Å)	20.793 188.425 143.49	87.683 151.984 251.481
α, β, γ (°)	90, 90, 90	90, 90, 90
Resolution (Å)	50.0-2.78 (2.88-2.78)*	50.0-3.30(3.4-3.30)*
R_{sym}	6.8 (78.4)	10.0 (65.3)
$I/\sigma I$	25.4(1.9)	30.1 (1.5)
Completeness (%)	99.2(99.0)	99.5(95.1)
Redundancy	4.7(4.6)	7.0(4.9)
Refinement		
Resolution (Å)	2.78	3.30
No. reflections	39697	50861
Completeness(%)	99.2	99.5
$R_{work/}$ R_{free} (%)	21.0/25.8	22.2/27.8
No. atoms	8555	16674
Protein	8496	16674
Ligand/ion	6	0
Water	53	0
B-factors		
Protein	97.8	137.6
Ligand/ion	102.0	-
Water	66.0	-
R.m.s deviations		
Bond lengths (Å)	0.003	0.013
Bond angles (°)	0.61	0.83
Ramanchandran plot		
Favored (%)	96.0	94.0
Allowed (%)	3.7	5.5
Disallowed (%)	0.3	0.5

*Highest resolution shell is shown in parenthesis.

Table 4-2. Buffer pH in crystallization condition of plexins$_{cyto}$ and the state of the juxtamembrane helix in the structures.

	Crystallization pH	Juxtamembrane helix
PlexinA3 (PDB: 3IG3)	7.75	Docked to GAP
PlexinA1 (PDB: 3RYT)	7.0	Docked to GAP
PlexinB1 (PDB: 3HM6)	8.0	Docked to GAP
PlexinB1 (PDB: 3SUA)	5.6	Disordered
PlexinA4 (unpublished)	5.1	Detached from GAP
GCN4-PlexinA4 (unpublished)	6.0	Detached from GAP
PlexinB2 (unpublished)	5.6	Disordered
PlexinC1 (unpublished)	6.0	Disordered

Bibliography

Abramoff, M.D., Magelhaes, P.J., and Ram, S.J. (2004). Image Processing with ImageJ. Biophotonics International *11*, 36-42.

Adams, P.D., Grosse-Kunstleve, R.W., Hung, L.W., Ioerger, T.R., McCoy, A.J., Moriarty, N.W., Read, R.J., Sacchettini, J.C., Sauter, N.K., and Terwilliger, T.C. (2002). PHENIX: building new software for automated crystallographic structure determination. Acta crystallographica *58*, 1948-1954.

Antipenko, A., Himanen, J.P., van Leyen, K., Nardi-Dei, V., Lesniak, J., Barton, W.A., Rajashankar, K.R., Lu, M., Hoemme, C., Puschel, A.W*., et al.* (2003). Structure of the semaphorin-3A receptor binding module. Neuron *39*, 589-598.

Aurandt, J., Vikis, H.G., Gutkind, J.S., Ahn, N., and Guan, K.L. (2002). The semaphorin receptor plexin-B1 signals through a direct interaction with the Rho-specific nucleotide exchange factor, LARG. Proc Natl Acad Sci U S A *99*, 12085-12090.

Bell, C.H., Aricescu, A.R., Jones, E.Y., and Siebold, C. (2011). A dual binding mode for RhoGTPases in plexin signalling. PLoS Biol *9*, e1001134.

Beranger, F., Goud, B., Tavitian, A., and de Gunzburg, J. (1991). Association of the Ras-antagonistic Rap1/Krev-1 proteins with the Golgi complex. Proc Natl Acad Sci U S A *88*, 1606-1610.

Biddlecome, G.H., Berstein, G., and Ross, E.M. (1996). Regulation of phospholipase C-beta1 by Gq and m1 muscarinic cholinergic receptor. Steady-state balance of receptor-mediated activation and GTPase-activating protein-promoted deactivation. The Journal of biological chemistry *271*, 7999-8007.

Boccaccio, C., and Comoglio, P.M. (2006). Invasive growth: a MET-driven genetic programme for cancer and stem cells. Nature reviews Cancer *6*, 637-645.

Bos, J.L., Rehmann, H., and Wittinghofer, A. (2007). GEFs and GAPs: critical elements in the control of small G proteins. Cell *129*, 865-877.

Brinkmann, T., Daumke, O., Herbrand, U., Kuhlmann, D., Stege, P., Ahmadian, M.R., and Wittinghofer, A. (2002). Rap-specific GTPase activating protein follows an alternative mechanism. The Journal of biological chemistry *277*, 12525-12531.

Cabezon, E., Arechaga, I., Jonathan, P., Butler, G., and Walker, J.E. (2000). Dimerization of bovine F1-ATPase by binding the inhibitor protein, IF1. The Journal of biological chemistry *275*, 28353-28355.

Carmeliet, P. (2003). Blood vessels and nerves: common signals, pathways and diseases. Nature reviews Genetics *4*, 710-720.

Casey, J.R., Grinstein, S., and Orlowski, J. (2010). Sensors and regulators of intracellular pH. Nature reviews *11*, 50-61.

Catalano, A., Lazzarini, R., Di Nuzzo, S., Orciari, S., and Procopio, A. (2009). The plexin-A1 receptor activates vascular endothelial growth factor-receptor 2 and nuclear factor-kappaB to mediate survival and anchorage-independent growth of malignant mesothelioma cells. Cancer research *69*, 1485-1493.

Chen, G., Sima, J., Jin, M., Wang, K.Y., Xue, X.J., Zheng, W., Ding, Y.Q., and Yuan, X.B. (2008). Semaphorin-3A guides radial migration of cortical neurons during development. Nature neuroscience *11*, 36-44.

Chen, V.B., Arendall, W.B., 3rd, Headd, J.J., Keedy, D.A., Immormino, R.M., Kapral, G.J., Murray, L.W., Richardson, J.S., and Richardson, D.C. (2010). MolProbity: all-atom structure validation for macromolecular crystallography. Acta crystallographica *66*, 12-21.

Cheng, H.J., Bagri, A., Yaron, A., Stein, E., Pleasure, S.J., and Tessier-Lavigne, M. (2001). Plexin-A3 mediates semaphorin signaling and regulates the development of hippocampal axonal projections. Neuron *32*, 249-263.

Clackson, T., Yang, W., Rozamus, L.W., Hatada, M., Amara, J.F., Rollins, C.T., Stevenson, L.F., Magari, S.R., Wood, S.A., Courage, N.L.*, et al.* (1998). Redesigning an FKBP-ligand interface to generate chemical dimerizers with novel specificity. Proc Natl Acad Sci U S A *95*, 10437-10442.

Conrotto, P., Valdembri, D., Corso, S., Serini, G., Tamagnone, L., Comoglio, P.M., Bussolino, F., and Giordano, S. (2005). Sema4D induces angiogenesis through Met recruitment by Plexin B1. Blood *105*, 4321-4329.

Cowan, C.W., Shao, Y.R., Sahin, M., Shamah, S.M., Lin, M.Z., Greer, P.L., Gao, S., Griffith, E.C., Brugge, J.S., and Greenberg, M.E. (2005). Vav family GEFs link activated Ephs to endocytosis and axon guidance. Neuron *46*, 205-217.

Dai, Y., Walker, S.A., De Vet, E., Cook, S., Welch, H.C., and Lockyer, P.J. (2011). Ca2+-dependent monomer and dimer formation switches capri between RasGAP and RapGAP activities. The Journal of biological chemistry.

Driessens, M.H., Hu, H., Nobes, C.D., Self, A., Jordens, I., Goodman, C.S., and Hall, A. (2001). Plexin-B semaphorin receptors interact directly with active Rac and regulate the actin cytoskeleton by activating Rho. Curr Biol *11*, 339-344.

Driessens, M.H., Olivo, C., Nagata, K., Inagaki, M., and Collard, J.G. (2002). B plexins activate Rho through PDZ-RhoGEF. FEBS letters *529*, 168-172.

Emsley, P., and Cowtan, K. (2004). Coot: model-building tools for molecular graphics. Acta crystallographica *60*, 2126-2132.

Endres, N.F., Das, R., Smith, A.W., Arkhipov, A., Kovacs, E., Huang, Y., Pelton, J.G., Shan, Y., Shaw, D.E., Wemmer, D.E.*, et al.* (2013). Conformational coupling across the plasma membrane in activation of the EGF receptor. Cell *152*, 543-556.

Fujisawa, H. (2002). From the discovery of neuropilin to the determination of its adhesion sites. Advances in experimental medicine and biology *515*, 1-12.

Fukuyama, T., Ogita, H., Kawakatsu, T., Fukuhara, T., Yamada, T., Sato, T., Shimizu, K., Nakamura, T., Matsuda, M., and Takai, Y. (2005). Involvement of the c-Src-Crk-C3G-Rap1 signaling in the nectin-induced activation of Cdc42 and formation of adherens junctions. The Journal of biological chemistry *280*, 815-825.

Gherardi, E., Love, C.A., Esnouf, R.M., and Jones, E.Y. (2004). The sema domain. Curr Opin Struct Biol *14*, 669-678.

Giordano, S., Corso, S., Conrotto, P., Artigiani, S., Gilestro, G., Barberis, D., Tamagnone, L., and Comoglio, P.M. (2002). The semaphorin 4D receptor controls invasive growth by coupling with Met. Nature cell biology *4*, 720-724.

Gloerich, M., and Bos, J.L. (2011). Regulating Rap small G-proteins in time and space. Trends Cell Biol *21*, 615-623.

Gordon-Smith, D.J., Carbajo, R.J., Yang, J.C., Videler, H., Runswick, M.J., Walker, J.E., and Neuhaus, D. (2001). Solution structure of a C-terminal coiled-coil domain from bovine IF(1): the inhibitor protein of F(1) ATPase. J Mol Biol *308*, 325-339.

Gouet, P., Courcelle, E., Stuart, D.I., and Metoz, F. (1999). ESPript: analysis of multiple sequence alignments in PostScript. Bioinformatics *15*, 305-308.

Gu, C., and Giraudo, E. (2013). The role of semaphorins and their receptors in vascular development and cancer. Exp Cell Res *319*, 1306-1316.

Gu, C.H., Rodriguez, E.R., Reimert, D.V., Shu, T.Z., Fritzsch, B., Richards, L.J., Kolodkin, A.L., and Ginty, D.D. (2003). Neuropilin-1 conveys semaphorin and VEGF signaling during neural and cardiovascular development. Developmental cell *5*, 45-57.

Guan, K.L., and Rao, Y. (2003). Signalling mechanisms mediating neuronal responses to guidance cues. Nature reviews Neuroscience *4*, 941-956.

Gui, Y., Guo, G., Huang, Y., Hu, X., Tang, A., Gao, S., Wu, R., Chen, C., Li, X., Zhou, L.*, et al.* (2011). Frequent mutations of chromatin remodeling genes in transitional cell carcinoma of the bladder. Nat Genet *43*, 875-878.

Hall, A., and Lalli, G. (2010). Rho and Ras GTPases in Axon Growth, Guidance, and Branching. Cold Spring Harbor perspectives in biology *2*.

Harrison, S.C. (2008). Viral membrane fusion. Nature structural & molecular biology *15*, 690-698.

He, H., Yang, T., Terman, J.R., and Zhang, X. (2009). Crystal structure of the plexin A3 intracellular region reveals an autoinhibited conformation through active site sequestration. Proc Natl Acad Sci U S A *106*, 15610-15615.

He, X., Kuo, Y.C., Rosche, T.J., and Zhang, X. (2013). Structural basis for autoinhibition of the guanine nucleotide exchange factor FARP2. Structure *21*, 355-364.

Hirotani, M., Ohoka, Y., Yamamoto, T., Nirasawa, H., Furuyama, T., Kogo, M., Matsuya, T., and Inagaki, S. (2002). Interaction of plexin-B1 with PDZ domain-containing Rho guanine nucleotide exchange factors. Biochemical and biophysical research communications *297*, 32-37.

Hu, H., Marton, T.F., and Goodman, C.S. (2001). Plexin B mediates axon guidance in Drosophila by simultaneously inhibiting active Rac and enhancing RhoA signaling. Neuron *32*, 39-51.

Huang, J., Liu, C.H., Hughes, S.A., Postma, M., Schwiening, C.J., and Hardie, R.C. (2010). Activation of TRP channels by protons and phosphoinositide depletion in Drosophila photoreceptors. Curr Biol *20*, 189-197.

Hung, R.J., Pak, C.W., and Terman, J.R. (2011). Direct redox regulation of F-actin assembly and disassembly by Mical. Science *334*, 1710-1713.

Hung, R.J., and Terman, J.R. (2011). Extracellular inhibitors, repellents, and semaphorin/plexin/MICAL-mediated actin filament disassembly. Cytoskeleton (Hoboken) *68*, 415-433.

Huse, M., and Kuriyan, J. (2002). The conformational plasticity of protein kinases. Cell *109*, 275-282.

Janssen, B.J., Malinauskas, T., Weir, G.A., Cader, M.Z., Siebold, C., and Jones, E.Y. (2012). Neuropilins lock secreted semaphorins onto plexins in a ternary signaling complex. Nature structural & molecular biology *19*, 1293-1299.

Janssen, B.J.C., Robinson, R.A., Pérez-Brangulí, F., Bell, C.H., Mitchell, K.J., Siebold, C., and Jones, E.Y. (2010). Structural basis of semaphorin–plexin signalling. Nature *467*, 1118-1122.

Jeon, C.Y., Kim, H.J., Lee, J.Y., Kim, J.B., Kim, S.C., and Park, J.B. (2010). p190RhoGAP and Rap-dependent RhoGAP (ARAP3) inactivate RhoA in response to nerve growth factor leading to neurite outgrowth from PC12 cells. Exp Mol Med *42*, 335-344.

Jura, N., Endres, N.F., Engel, K., Deindl, S., Das, R., Lamers, M.H., Wemmer, D.E., Zhang, X., and Kuriyan, J. (2009). Mechanism for activation of the EGF receptor catalytic domain by the juxtamembrane segment. Cell *137*, 1293-1307.

Kikutani, H., Suzuki, K., and Kumanogoh, A. (2007). Immune semaphorins: increasing members and their diverse roles. Advances in immunology *93*, 121-143.

Klostermann, A., Lohrum, M., Adams, R.H., and Puschel, A.W. (1998). The chemorepulsive activity of the axonal guidance signal semaphorin D requires dimerization. The Journal of biological chemistry *273*, 7326-7331.

Kobashi, K. (1968). Catalytic oxidation of sulfhydryl groups by o-phenanthroline copper complex. Biochimica et biophysica acta *158*, 239-245.

Koppel, A.M., and Raper, J.A. (1998). Collapsin-1 covalently dimerizes, and dimerization is necessary for collapsing activity. The Journal of biological chemistry *273*, 15708-15713.

Koyano, Y., Kawamoto, T., Kikuchi, A., Shen, M., Kuruta, Y., Tsutsumi, S., Fujimoto, K., Noshiro, M., Fujii, K., and Kato, Y. (2001). Chondrocyte-derived ezrin-like domain containing protein (CDEP), a rho guanine nucleotide exchange factor, is inducible in chondrocytes by parathyroid hormone and cyclic AMP and has transforming activity in NIH3T3 cells. Osteoarthritis Cartilage *9 Suppl A*, S64-68.

Kruger, R.P., Aurandt, J., and Guan, K.L. (2005). Semaphorins command cells to move. Nature reviews *6*, 789-800.

Kubo, T., Yamashita, T., Yamaguchi, A., Sumimoto, H., Hosokawa, K., and Tohyama, M. (2002). A novel FERM domain including guanine nucleotide exchange factor is involved in Rac signaling and regulates neurite remodeling. J Neurosci *22*, 8504-8513.

Kumanogoh, A., Watanabe, C., Lee, I., Wang, X.S., Shi, W., Araki, H., Hirata, H., Iwahori, K., Uchida, J., Yasui, T.*, et al.* (2000). Identification of CD72 as a lymphocyte receptor for the class IV semaphorin CD100: A novel mechanism for regulating B cell signaling. Immunity *13*, 621-631.

Kupzig, S., Bouyoucef-Cherchalli, D., Yarwood, S., Sessions, R., and Cullen, P.J. (2009). The ability of GAP1IP4BP to function as a Rap1 GTPase-activating protein (GAP) requires its Ras GAP-related domain and an arginine finger rather than an asparagine thumb. Molecular and cellular biology *29*, 3929-3940.

Kupzig, S., Deaconescu, D., Bouyoucef, D., Walker, S.A., Liu, Q., Polte, C.L., Daumke, O., Ishizaki, T., Lockyer, P.J., Wittinghofer, A.*, et al.* (2006). GAP1 family members constitute bifunctional Ras and Rap GTPase-activating proteins. The Journal of biological chemistry *281*, 9891-9900.

Larson, D.R., Gosse, J.A., Holowka, D.A., Baird, B.A., and Webb, W.W. (2005). Temporally resolved interactions between antigen-stimulated IgE receptors and Lyn kinase on living cells. J Cell Biol *171*, 527-536.

Laue, T.M., Shah, B.D., Ridgeway, T.M., and Pelletier, S.L. (1992). Computer-aided interpretation of analytical sedimentation data for proteins. In Analytical ultracentrifugation in biochemistry and polymer science, H.e. al., ed. (Cambridge United Kingdom: Royal Society of Chemistry).

Liu, H., Juo, Z.S., Shim, A.H., Focia, P.J., Chen, X., Garcia, K.C., and He, X. (2010). Structural basis of semaphorin-plexin recognition and viral mimicry from Sema7A and A39R complexes with PlexinC1. Cell *142*, 749-761.

Liu, W., Wen, W., Wei, Z., Yu, J., Ye, F., Liu, C.H., Hardie, R.C., and Zhang, M. (2011). The INAD scaffold is a dynamic, redox-regulated modulator of signaling in the Drosophila eye. Cell *145*, 1088-1101.

Love, C.A., Harlos, K., Mavaddat, N., Davis, S.J., Stuart, D.I., Jones, E.Y., and Esnouf, R.M. (2003). The ligand-binding face of the semaphorins revealed by the high-resolution crystal structure of SEMA4D. Nature structural biology *10*, 843-848.

Lowery, L.A., and Van Vactor, D. (2009). The trip of the tip: understanding the growth cone machinery. Nat Rev Mol Cell Bio *10*, 332-343.

Ludwig, F.T., Schwab, A., and Stock, C. (2013). The Na+ /H+ -exchanger (NHE1) generates pH nanodomains at focal adhesions. J Cell Physiol *228*, 1351-1358.

Lumb, K.J., Carr, C.M., and Kim, P.S. (1994). Subdomain folding of the coiled coil leucine zipper from the bZIP transcriptional activator GCN4. Biochemistry *33*, 7361-7367.

Mccoy, A.J., Grosse-Kunstleve, R.W., Adams, P.D., Winn, M.D., Storoni, L.C., and Read, R.J. (2007). Phaser crystallographic software. Journal of Applied Crystallography *40*, 658-674.

Merajver, S.D., and Usmani, S.Z. (2005). Multifaceted role of Rho proteins in angiogenesis. J Mammary Gland Biol *10*, 291-298.

Messersmith, E.K., Leonardo, E.D., Shatz, C.J., Tessier-Lavigne, M., Goodman, C.S., and Kolodkin, A.L. (1995). Semaphorin III can function as a selective chemorepellent to pattern sensory projections in the spinal cord. Neuron *14*, 949-959.

Miyamoto, Y., Yamauchi, J., and Itoh, H. (2003). Src kinase regulates the activation of a novel FGD-1-related Cdc42 guanine nucleotide exchange factor in the signaling pathway from the endothelin A receptor to JNK. The Journal of biological chemistry *278*, 29890-29900.

Mochizuki, N., Yamashita, S., Kurokawa, K., Ohba, Y., Nagai, T., Miyawaki, A., and Matsuda, M. (2001). Spatio-temporal images of growth-factor-induced activation of Ras and Rap1. Nature *411*, 1065-1068.

Muller, B.K., Zaychikov, E., Brauchle, C., and Lamb, D.C. (2005). Pulsed interleaved excitation. Biophysical journal *89*, 3508-3522.

Murakami, Y., Suto, F., Shimizu, M., Shinoda, T., Kameyama, T., and Fujisawa, H. (2001). Differential expression of plexin-A subfamily members in the mouse nervous system. Dev Dyn *220*, 246-258.

Murata, T., Ohnishi, H., Okazawa, H., Murata, Y., Kusakari, S., Hayashi, Y., Miyashita, M., Itoh, H., Oldenborg, P.A., Furuya, N.*, et al.* (2006). CD47 promotes neuronal development through Src- and FRG/Vav2-mediated activation of Rac and Cdc42. J Neurosci *26*, 12397-12407.

Murray, A.J., and Shewan, D.A. (2008). Epac mediates cyclic AMP-dependent axon growth, guidance and regeneration. Mol Cell Neurosci *38*, 578-588.

Murray, A.J., Tucker, S.J., and Shewan, D.A. (2009). cAMP-dependent axon guidance is distinctly regulated by Epac and protein kinase A. J Neurosci *29*, 15434-15444.

Nakamura, F., Kalb, R.G., and Strittmatter, S.M. (2000). Molecular basis of semaphorin-mediated axon guidance. Journal of neurobiology *44*, 219-229.

Nakamura, T., and Matsuda, M. (2009). In vivo imaging of signal transduction cascades with probes based on Forster Resonance Energy Transfer (FRET). Curr Protoc Cell Biol *Chapter 14*, Unit 14 10.

Network, T.C.G.A.R. (2012). Comprehensive molecular characterization of human colon and rectal cancer. Nature *487*, 330-337.

Nobes, C.D., Lauritzen, I., Mattei, M.G., Paris, S., Hall, A., and Chardin, P. (1998). A new member of the Rho family, Rnd1, promotes disassembly of actin filament structures and loss of cell adhesion. J Cell Biol *141*, 187-197.

Nogi, T., Yasui, N., Mihara, E., Matsunaga, Y., Noda, M., Yamashita, N., Toyofuku, T., Uchiyama, S., Goshima, Y., Kumanogoh, A.*, et al.* (2010). Structural basis for semaphorin signalling through the plexin receptor. Nature *467*, 1123-1127.

Nomura, K., Kanemura, H., Satoh, T., and Kataoka, T. (2004). Identification of a novel domain of Ras and Rap1 that directs their differential subcellular localizations. The Journal of biological chemistry *279*, 22664-22673.

Notredame, C., Higgins, D.G., and Heringa, J. (2000). T-Coffee: A novel method for fast and accurate multiple sequence alignment. J Mol Biol *302*, 205-217.

O'donnell, M., Chance, R.K., and Bashaw, G.J. (2009). Axon Growth and Guidance: Receptor Regulation and Signal Transduction. Annu Rev Neurosci *32*, 383-412.

O'Shea, E.K., Klemm, J.D., Kim, P.S., and Alber, T. (1991). X-ray structure of the GCN4 leucine zipper, a two-stranded, parallel coiled coil. Science *254*, 539-544.

Ohba, Y., Kurokawa, K., and Matsuda, M. (2003). Mechanism of the spatio-temporal regulation of Ras and Rap1. Embo J *22*, 859-869.

Oinuma, I., Ishikawa, Y., Katoh, H., and Negishi, M. (2004a). The Semaphorin 4D receptor Plexin-B1 is a GTPase activating protein for R-Ras. Science *305*, 862-865.

Oinuma, I., Katoh, H., and Negishi, M. (2004b). Molecular dissection of the semaphorin 4D receptor plexin-B1-stimulated R-Ras GTPase-activating protein activity and neurite remodeling in hippocampal neurons. J Neurosci *24*, 11473-11480.

Oinuma, I., Katoh, H., and Negishi, M. (2006). Semaphorin 4D/Plexin-B1-mediated R-Ras GAP activity inhibits cell migration by regulating beta(1) integrin activity. J Cell Biol *173*, 601-613.

Otwinowski, Z., and Minor, W. (1997). Processing of X-ray Diffraction Data Collected in Oscillation Mode. Methods in enzymology *276*, 307-326.

Parry, D.A., Fraser, R.D., and Squire, J.M. (2008). Fifty years of coiled-coils and alpha-helical bundles: a close relationship between sequence and structure. J Struct Biol *163*, 258-269.

Pena, V., Hothorn, M., Eberth, A., Kaschau, N., Parret, A., Gremer, L., Bonneau, F., Ahmadian, M.R., and Scheffzek, K. (2008). The C2 domain of SynGAP is essential for stimulation of the Rap GTPase reaction. EMBO reports *9*, 350-355.

Perrot, V., Vazquez-Prado, J., and Gutkind, J.S. (2002). Plexin B regulates Rho through the guanine nucleotide exchange factors leukemia-associated Rho GEF (LARG) and PDZ-RhoGEF. The Journal of biological chemistry *277*, 43115-43120.

Pizon, V., Desjardins, M., Bucci, C., Parton, R.G., and Zerial, M. (1994). Association of Rap1a and Rap1b proteins with late endocytic/phagocytic compartments and Rap2a with the Golgi complex. Journal of cell science *107 (Pt 6)*, 1661-1670.

Richter, M., Murai, K.K., Bourgin, C., Pak, D.T., and Pasquale, E.B. (2007). The EphA4 receptor regulates neuronal morphology through SPAR-mediated inactivation of Rap GTPases. J Neurosci *27*, 14205-14215.

Ridley, A.J. (2001). Rho family proteins: coordinating cell responses. Trends in Cell Biology *11*, 471-477.

Rohm, B., Ottemeyer, A., Lohrum, M., and Puschel, A.W. (2000a). Plexin/neuropilin complexes mediate repulsion by the axonal guidance signal semaphorin 3A. Mechanisms of development *93*, 95-104.

Rohm, B., Rahim, B., Kleiber, B., Hovatta, I., and Puschel, A.W. (2000b). The semaphorin 3A receptor may directly regulate the activity of small GTPases. FEBS letters *486*, 68-72.

Saito, Y., Oinuma, I., Fujimoto, S., and Negishi, M. (2009). Plexin-B1 is a GTPase activating protein for M-Ras, remodelling dendrite morphology. EMBO reports *10*, 614-621.

Sakurai, A., Gavard, J., Annas-Linhares, Y., Basile, J.R., Amornphimoltham, P., Palmby, T.R., Yagi, H., Zhang, F., Randazzo, P.A., Li, X.*, et al.* (2010). Semaphorin 3E initiates antiangiogenic signaling through plexin D1 by regulating Arf6 and R-Ras. Molecular and cellular biology *30*, 3086-3098.

Sakurai, A., Jian, X., Lee, C.J., Manavski, Y., Chavakis, E., Donaldson, J., Randazzo, P.A., and Gutkind, J.S. (2011). Phosphatidylinositol-4-phosphate 5-kinase and GEP100/Brag2 protein mediate antiangiogenic signaling by semaphorin 3E-plexin-D1 through Arf6 protein. The Journal of biological chemistry *286*, 34335-34345.

Scheffzek, K., Ahmadian, M.R., Kabsch, W., Wiesmuller, L., Lautwein, A., Schmitz, F., and Wittinghofer, A. (1997). The Ras-RasGAP complex: structural basis for GTPase activation and its loss in oncogenic Ras mutants. Science *277*, 333-338.

Schlessinger, J. (2000). Cell signaling by receptor tyrosine kinases. Cell *103*, 211-225.

Schmidt, E.F., Shim, S.O., and Strittmatter, S.M. (2008). Release of MICAL autoinhibition by semaphorin-plexin signaling promotes interaction with collapsin response mediator protein. J Neurosci *28*, 2287-2297.

Schuck, P. (2000). Size-distribution analysis of macromolecules by sedimentation velocity ultracentrifugation and lamm equation modeling. Biophysical journal *78*, 1606-1619.

Scrima, A., Thomas, C., Deaconescu, D., and Wittinghofer, A. (2008). The Rap-RapGAP complex: GTP hydrolysis without catalytic glutamine and arginine residues. Embo J *27*, 1145-1153.

Serini, G., Valdembri, D., Zanivan, S., Morterra, G., Burkhardt, C., Caccavari, F., Zammataro, L., Primo, L., Tamagnone, L., Logan, M.*, et al.* (2003). Class 3

semaphorins control vascular morphogenesis by inhibiting integrin function. Nature *424*, 391-397.

Siebold, C., and Jones, E.Y. (2013). Structural insights into semaphorins and their receptors. Seminars in cell & developmental biology *24*, 139-145.

Song, H., Ming, G., He, Z., Lehmann, M., McKerracher, L., Tessier-Lavigne, M., and Poo, M. (1998). Conversion of neuronal growth cone responses from repulsion to attraction by cyclic nucleotides. Science *281*, 1515-1518.

Sot, B., Kotting, C., Deaconescu, D., Suveyzdis, Y., Gerwert, K., and Wittinghofer, A. (2010). Unravelling the mechanism of dual-specificity GAPs. EMBO J *29*, 1205-1214.

Sternweis, P.C., Carter, A.M., Chen, Z., Danesh, S.M., Hsiung, Y.F., and Singer, W.D. (2007). Regulation of Rho guanine nucleotide exchange factors by G proteins. Advances in protein chemistry *74*, 189-228.

Suzuki, K., Okuno, T., Yamamoto, M., Pasterkamp, R.J., Takegahara, N., Takamatsu, H., Kitao, T., Takagi, J., Rennert, P.D., Kolodkin, A.L.*, et al.* (2007). Semaphorin 7A initiates T-cell-mediated inflammatory responses through alpha 1 beta 1 integrin. Nature *446*, 680-684.

Swiercz, J.M., Kuner, R., Behrens, J., and Offermanns, S. (2002). Plexin-B1 directly interacts with PDZ-RhoGEF/LARG to regulate RhoA and growth cone morphology. Neuron *35*, 51-63.

Takahashi, T., Fournier, A., Nakamura, F., Wang, L.H., Murakami, Y., Kalb, R.G., Fujisawa, H., and Strittmatter, S.M. (1999). Plexin-neuropilin-1 complexes form functional semaphorin-3A receptors. Cell *99*, 59-69.

Takahashi, T., and Strittmatter, S.M. (2001). Plexina1 autoinhibition by the plexin sema domain. Neuron *29*, 429-439.

Takamatsu, H., and Kumanogoh, A. (2012). Diverse roles for semaphorin-plexin signaling in the immune system. Trends Immunol *33*, 127-135.

Tamagnone, L. (2012). Emerging Role of Semaphorins as Major Regulatory Signals and Potential Therapeutic Targets in Cancer. Cancer Cell *22*, 145-152.

Tamagnone, L., Artigiani, S., Chen, H., He, Z., Ming, G.I., Song, H., Chedotal, A., Winberg, M.L., Goodman, C.S., Poo, M.*, et al.* (1999). Plexins are a large family

of receptors for transmembrane, secreted, and GPI-anchored semaphorins in vertebrates. Cell *99*, 71-80.

Tata, A., Stoppel, D.C., Hong, S., Ben-Zvi, A., Xie, T., and Gu, C. (2014). An image-based RNAi screen identifies SH3BP1 as a key effector of Semaphorin 3E-PlexinD1 signaling. J Cell Biol.

Terman, J.R., Mao, T., Pasterkamp, R.J., Yu, H.H., and Kolodkin, A.L. (2002). MICALs, a family of conserved flavoprotein oxidoreductases, function in plexin-mediated axonal repulsion. Cell *109*, 887-900.

Tong, Y., Chugha, P., Hota, P.K., Alviani, R.S., Li, M., Tempel, W., Shen, L., Park, H.W., and Buck, M. (2007). Binding of Rac1, Rnd1, and RhoD to a Novel Rho GTPase Interaction Motif Destabilizes Dimerization of the Plexin-B1 Effector Domain. The Journal of biological chemistry *282*, 37215-37224.

Tong, Y., Hota, P.K., Penachioni, J.Y., Hamaneh, M.B., Kim, S., Alviani, R.S., Shen, L., He, H., Tempel, W., Tamagnone, L.*, et al.* (2009). Structure and function of the intracellular region of the plexin-b1 transmembrane receptor. The Journal of biological chemistry *284*, 35962-35972.

Toyofuku, T., Yoshida, J., Sugimoto, T., Zhang, H., Kumanogoh, A., Hori, M., and Kikutani, H. (2005). FARP2 triggers signals for Sema3A-mediated axonal repulsion. Nature neuroscience *8*, 1712-1719.

Toyofuku, T., Zhang, H., Kumanogoh, A., Takegahara, N., Suto, F., Kamei, J., Aoki, K., Yabuki, M., Hori, M., Fujisawa, H.*, et al.* (2004a). Dual roles of Sema6D in cardiac morphogenesis through region-specific association of its receptor, Plexin-A1, with off-track and vascular endothelial growth factor receptor type 2. Genes & development *18*, 435-447.

Toyofuku, T., Zhang, H., Kumanogoh, A., Takegahara, N., Yabuki, M., Harada, K., Hori, M., and Kikutani, H. (2004b). Guidance of myocardial patterning in cardiac development by Sema6D reverse signalling. Nature cell biology *6*, 1204-1211.

Tran, T.S., Kolodkin, A.L., and Bharadwaj, R. (2007). Semaphorin regulation of cellular morphology. Annual review of cell and developmental biology *23*, 263-292.

Turner, L.J., Nicholls, S., and Hall, A. (2004). The activity of the plexin-A1 receptor is regulated by Rac. The Journal of biological chemistry *279*, 33199-33205.

Uesugi, K., Oinuma, I., Katoh, H., and Negishi, M. (2009). Different requirement for Rnd GTPases of R-Ras GAP activity of Plexin-C1 and Plexin-D1. The Journal of biological chemistry *284*, 6743-6751.

Van Duyne, G.D., Standaert, R.F., Karplus, P.A., Schreiber, S.L., and Clardy, J. (1993). Atomic structures of the human immunophilin FKBP-12 complexes with FK506 and rapamycin. J Mol Biol *229*, 105-124.

van Meer, G., Voelker, D.R., and Feigenson, G.W. (2008). Membrane lipids: where they are and how they behave. Nature reviews *9*, 112-124.

Vikis, H.G., Li, W., and Guan, K.L. (2002). The plexin-B1/Rac interaction inhibits PAK activation and enhances Sema4D ligand binding. Genes & development *16*, 836-845.

Wang, Y., He, H., Srivastava, N., Vikarunnessa, S., Chen, Y.B., Jiang, J., Cowan, C.W., and Zhang, X. (2012). Plexins are GTPase-activating proteins for Rap and are activated by induced dimerization. Sci Signal *5*, ra6.

Wang, Y., Pascoe, H.G., Brautigam, C.A., He, H., and Zhang, X. (2013). Structural basis for activation and non-canonical catalysis of the Rap GTPase activating protein domain of plexin. eLife *2*, e01279.

Webb, M.R., and Hunter, J.L. (1992). Interaction of GTPase-activating protein with p21ras, measured using a continuous assay for inorganic phosphate release. The Biochemical journal *287 (Pt 2)*, 555-559.

Wennerberg, K., Forget, M.A., Ellerbroek, S.M., Arthur, W.T., Burridge, K., Settleman, J., Der, C.J., and Hansen, S.H. (2003). Rnd proteins function as RhoA antagonists by activating p190 RhoGAP. Curr Biol *13*, 1106-1115.

Winberg, M.L., Noordermeer, J.N., Tamagnone, L., Comoglio, P.M., Spriggs, M.K., Tessier-Lavigne, M., and Goodman, C.S. (1998). Plexin A is a neuronal semaphorin receptor that controls axon guidance. Cell *95*, 903-916.

Wong, A.W., Brickey, W.J., Taxman, D.J., van Deventer, H.W., Reed, W., Gao, J.X., Zheng, P., Liu, Y., Li, P., Blum, J.S.*, et al.* (2003). CIITA-regulated plexin-A1 affects T-cell-dendritic cell interactions. Nature immunology *4*, 891-898.

Worzfeld, T., Swiercz, J.M., Senturk, A., Genz, B., Korostylev, A., Deng, S., Xia, J., Hoshino, M., Epstein, J.A., Chan, A.M.*, et al.* (2014a). Genetic dissection of plexin signaling in vivo. Proc Natl Acad Sci U S A *111*, 2194-2199.

Worzfeld, T., Swiercz, J.M., Senturk, A., Genz, B., Korostylev, A., Deng, S.H., Xia, J.J., Hoshino, M., Epstein, J.A., Chan, A.M.*, et al.* (2014b). Genetic dissection of plexin signaling in vivo. P Natl Acad Sci USA *111*, 2194-2199.

Yamada, T., Sakisaka, T., Hisata, S., Baba, T., and Takai, Y. (2005). RA-RhoGAP, Rap-activated Rho GTPase-activating protein implicated in neurite outgrowth through Rho. The Journal of biological chemistry *280*, 33026-33034.

Yaron, A., and Zheng, B. (2007). Navigating their way to the clinic: emerging roles for axon guidance molecules in neurological disorders and injury. Developmental neurobiology *67*, 1216-1231.

Yazdani, U., and Terman, J.R. (2006). The semaphorins. Genome biology *7*, 211.

Zanata, S.M., Hovatta, I., Rohm, B., and Puschel, A.W. (2002). Antagonistic effects of Rnd1 and RhoD GTPases regulate receptor activity in Semaphorin 3A-induced cytoskeletal collapse. J Neurosci *22*, 471-477.

Zhuang, B., Su, Y.S., and Sockanathan, S. (2009). FARP1 promotes the dendritic growth of spinal motor neuron subtypes through transmembrane Semaphorin6A and PlexinA4 signaling. Neuron *61*, 359-372.

Zwartkruis, F.J., Wolthuis, R.M., Nabben, N.M., Franke, B., and Bos, J.L. (1998). Extracellular signal-regulated activation of Rap1 fails to interfere in Ras effector signalling. EMBO J *17*, 5905-5912.